Project number: 101111888
Project acronym: SHIMMER
Project duration: 09/2023 – 08/2026
Project Coordinator:
Diana González, SINTEF AS – Institute SINTEF Industry

Co-funded by the European Union

Clean Hydrogen Partnership

HORIZON 2020: Horizon Europe Framework Programme (HORIZON)

HORIZON-JTI-CLEANH2-2022-05-03

Safe hydrogen injection management at network-wide level: towards European gas sector transition

Shimmer

Safe Hydrogen Injection Modelling and Management for European gas network Resilience

D3.3 Report on recommendation and guidelines for inspection of pipelines for H-NG blends

VERSION	DATE	TYPE	DISSEMINATION LEVEL
Version 02	27-02-2026	Report	Public

ABSTRACT

This deliverable provides recommendations and guidelines for the inspection of pipelines intended for the transport of H2-NG mixtures. Its purpose is to define methods, tools, and technologies for managing multi-gas networks and quality monitoring, including simulation, forecasting, and managing safe network operation in the context of the widespread use of hydrogen injection throughout Europe. The main objective of this document is to propose best practices for hydrogen safety in natural gas infrastructure and managing the risks associated with blending natural gas with hydrogen in gas transmission and distribution networks. Risk management requires recognizing the source and extent of the risk, accurately identifying the causes, defining methods, and implementing preventative measures. In response to these requirements, this report attempts to address these issues. The document summarizes standards for various methods commonly used for the inspection and condition assessment of steel structures, including steel pipelines, using non-destructive testing (NDT). The next step was to analyse the results of a review of current measurement techniques for pingable and non-pigable steel gas pipelines. The goal was to understand gas operators' attitude and experiences regarding pipelines unsuitable for pig cleaning, assess the history of using different NDT methods, and determine whether there are similarities between pipeline infrastructure operators in Europe.

The project included initial pipeline inspections using MFL and geometry tools, acoustic emission (AE) testing, stress concentration tomography (SCT), and magnetic metal memory testing (MMM). As a complementary investigation, which did not directly indicate material or corrosion defects but was related to corrosion risk, a direct current voltage gradient (DCVG) steel pipeline insulation test was conducted, and a gas network inspection was conducted using the system with a hyperspectral camera to identify potential sources of methane leakage and emissions (iDiaGaSys). Field inspections were conducted using AE, SCT, and DCVG, and the results were then compared with the MFL and geometry tests. Tests of individual methods were conducted on a section of a DN 700 high-pressure steel pipeline.

Based on the conducted tests and comparisons, the report developed a protocol and recommendations for hydrogen management, identifying the risks and extent of damage that may result from the presence of hydrogen, or it blends. The report analyses the impact of hydrogen on the durability of materials and components used in natural gas transmission and distribution infrastructure, the types of damage caused

by hydrogen, and the degradation mechanisms of steel pipes exposed to hydrogen. The project verified existing methods and identified and tested alternative methods for steel pipelines inspections.

AUTHORSHIP AND APPROVAL INFORMATION

AUTHOR(S)	**DATE / SIGN**
Dorota Polak, Jakub Cybulski, Piotr Paszylk, Łukasz Piwoda, Radosław Rolf / GAZ-SYSTEM	Dorota Polak Dorota Polak (Mar 6, 2026 11:50:06 GMT+1)
REVIEWED BY WP-LEADER	**DATE / SIGN**
Nevena Marinova/ TECNALIA	Nevena Marinova Nevena Marinova (Mar 6, 2026 12:02:10 GMT+1)
APPROVED BY COORDINATOR	**DATE / SIGN**
Diana González / SINTEF	Diana González Diana González (Mar 6, 2026 12:21:58 GMT+1)

FUNDED BY THE EUROPEAN UNION. VIEWS AND OPINIONS EXPRESSED ARE HOWEVER THOSE OF THE AUTHOR(S) ONLY AND DO NOT NECESSARILY REFLECT THOSE OF THE EUROPEAN UNION OR THE CLEAN HYDROGEN JOINT UNDERTAKING. NEITHER THE EUROPEAN UNION NOR THE GRANTING AUTHORITY CAN BE HELD RESPONSIBLE FOR THEM.

Release history

VERSION	DATE	VERSION DESCRIPTION
01	16/02/2026	First version for review with WP3 partners
02	25/02/2026	Final version

The research leading to these results has received funding from Horizon 2020, the European Union's Framework Programme for Research and Innovation (H2020) under grant agreement n° 101111888.

Table of contents

The research leading to these results has received funding from Horizon 2020, the European Union's Framework Programme for Research and Innovation (H2020) under grant agreement n° 101111888.

The research leading to these results has received funding from Horizon 2020, the European Union's Framework Programme for Research and Innovation (H2020) under grant agreement n° 101111888.

Table of Figures

The research leading to these results has received funding from Horizon 2020, the European Union's Framework Programme for Research and Innovation (H2020) under grant agreement n° 101111888.

The research leading to these results has received funding from Horizon 2020, the European Union's Framework Programme for Research and Innovation (H2020) under grant agreement n° 101111888.

The research leading to these results has received funding from Horizon 2020, the European Union's Framework Programme for Research and Innovation (H2020) under grant agreement n° 101111888.

List of Tables

The research leading to these results has received funding from Horizon 2020, the European Union's Framework Programme for Research and Innovation (H2020) under grant agreement n° 101111888.

The research leading to these results has received funding from Horizon 2020, the European Union's Framework Programme for Research and Innovation (H2020) under grant agreement n° 101111888.

List of Abbreviations

Table 1: List of abbreviations

Term	Explanation
TSO	Transmission System Operator
DSO	Distribution System Operator
NDT	Non-Destructive Testing
ILI	In-Line Inspection
ACVG	Alternating Current Voltage Gradient
DCVG	Direct Current Voltage Gradient
UT	Ultrasonic Tests
UTT	Ultrasonic Thickness Testing
RT	Radiographic Testing
LDAR	Leak Detection and Repair
ECDA	External Corrosion Direct Assessment
MMM	Metal Magnetic Memory Method
NACE	National Association of Corrosion Engineers
MFL	Magnetic Flux Leakage
AE	Acoustic Emission
LEV	Localized Events
HE	Hydrogen Embrittlement
SSRT	Slow Strain Rate Tests
SEM	Scanning Electron Microscopy
RAAE	Risk Assessment and Analysis Evaluation
ASL	Average Signal Level
RMS	Root Mean Square
SCT™	Stress Concentration Tomography
GNSS	Global Navigation Satellite System
NCMD	Non-Contact Magnetometric Diagnostics
SCZ	Stress Concentration Zones
MP	Magnetic Particle
MFG	Manufacturing Defects

The research leading to these results has received funding from Horizon 2020, the European Union's Framework Programme for Research and Innovation (H2020) under grant agreement n° 101111888.

Term	Explanation
ERF	Estimated Repair Factors
ART	Atmospheric Radiative Transfer Modeling
GIS	Geographic Information System
AMF	Adaptive Matched Filter
CMF	Matched Filter For Clutter
SAM	Spectral Angle Mapper
DEF	Deformation Tool
MOP	Maximum Operating Pressure
DMAOHS	Design Maximum Allowable Operating Hoop Stress
HIC	Hydrogen Induced Cracking
SCC	Stress Corrosion Cracks
EMAT	Electromagnetic And Acoustic Transduction Technology
FCGR	Fatigue Crack Growth Rate

The research leading to these results has received funding from Horizon 2020, the European Union's Framework Programme for Research and Innovation (H2020) under grant agreement n° 101111888.

Executive Summary

The European natural gas infrastructure provides the opportunity to accept hydrogen (H_2), as a measure to integrate low-carbon gases while leveraging the existing gas network and contributing to decarbonisation. However, there are technical and regulatory gaps that should be closed, adaptations and investments to be made to ensure that multi-gas networks across Europe will be able to operate in a reliable and safe way while providing a highly controllable gas quality and required energy demand. Aspects such as material integrity of pipelines and components, as well as the lack of harmonisation of gas quality requirements at European level must be addressed in order to facilitate the injection of H_2 in the natural gas network.

In this context, the SHIMMER project (Safe Hydrogen Injection Modelling and Management for European gas network Resilience, aims to enable a higher integration of low-carbon gases and safer H_2 injection management in multi-gas networks by strengthening the knowledge base and improving the understanding of risks and opportunities in H_2 projects. This report contains recommendations and guidelines for the inspection of pipelines intended for the transport of H-NG mixtures. Its purpose is to define methods, tools and technologies for managing multi-gas networks and monitoring quality, including simulation, forecasting and safe network operation management in the context of the widespread use of hydrogen injection on a European scale. The aim of the work is to propose best practices for hydrogen safety in natural gas infrastructure and for managing the risks associated with blending natural gas and hydrogen in the gas transmission and distribution network. Proper risk management requires recognition of the source and scope of risk, accurate identification of causes, methods of identification and preventive measures. In response to this, the report attempts to take these aspects into account.

H_2 is a more challenging medium than natural gas due to phenomena commonly referred to as hydrogen corrosion. The action of hydrogen intensifies the negative effects present in natural gas, so we are not dealing with new risks, but rather an extension of existing risks with additional ones caused by H_2. For this reason, it is necessary to verify the current methods of technical condition verification and check to what extent they are sufficient for the additional identified risks caused by H_2. The first section of the document summarises the standards relating to various methods commonly used to inspect and assess the condition of steel structures, including steel pipelines, using non-destructive testing (NDT) methods, in particular ultrasonic testing (UT), radiographic testing (RT), acoustic emission (AE), magnetic particle testing (MP).

In the next step, the conclusions from the survey on the currently used measurement techniques for gas pipelines that can be tested with pigs and those that are unpiggable were analysed. The reason for conducting the survey was to inquire about the gas operators' attitude and experience with the unpiggable pipelines. Another important point was to check the application's history of several listed NDT inspection methods. The idea behind conducting the survey was to check whether there are similarities in these fields across different operators in Europe as well as to compare the attitude towards the unpiggable pipelines. A survey conducted among gas distribution and transmission system operators confirms that pipelines that cannot be cleaned and then tested using pigs are part of every operator's infrastructure and will continue to be used throughout Europe for some time to come. The basic tests that are required and give the best results are ILI inspections carried out using measuring pigs. the survey confirms the widespread use of MFL tools for testing steel gas pipelines, based on measuring leakage and interference in the generated magnetic field. However, a range of methods used by operators for non-pigging infrastructure has been identified. These conclusions were then used in selecting the methods tested in the project. As part of the project, alternative methods of field measurement and analysis of the condition of steel pipelines were selected. Since it is assumed that testing using MFL tools is the commonly used method, proven in practice, recognised by pipeline operators and having extensive data interpretation systems, this fact cannot be overlooked. For this reason, it was decided that MFL inspection should be used as a reference measurement against which the effectiveness of other methods tested within the project will be compared. MFL inspection is most often supplemented by pipeline geometry inspection, also performed using pipeline pigs. For this reason, a DN 700 high-pressure gas pipeline was selected for testing,

The research leading to these results has received funding from Horizon 2020, the European Union's Framework Programme for Research and Innovation (H2020) under grant agreement n° 101111888.

which was recently subjected to current ILI testing of both types. And the complete report from the inspection was available for those working on this report.

For verification in the project, reference tests of the pipeline with MFL and geometry tools were selected, in addition to the Acoustic Emission Method (AE) test, Stress Concentration Tomography (SCT) testing, Metal Magnetic Memory Method (MMM) testing, and as a supplement, testing not directly indicating material and corrosion defects but related to the risk of corrosion, testing of the technical condition of steel pipeline insulation using the Direct Current Voltage Gradient (DCVG) test, and inspection of the gas network and verification of possible sources of methane leakage and emissions using the iDiaGaSys System with a hyperspectral camera. Field tests were performed using AE, SCT, and DCVG methods, and their results were then compared with the MFL and geometry inspection. Tests of individual methods used in the research were carried out on a section of a DN 700 high-pressure steel pipeline, which had been inspected the previous year using the MFL and DEF methods to detect material defects in the pipeline. The defects detected during this pipeline inspection were expressed as ERF in accordance with ASME B31G, including defects with an ERF value greater than 0.85. At one location, the MFL inspection revealed a defect with an ERF value ≥ 1. The location of the defect was excavated by the pipeline operator and verified by non-destructive radiographic testing (RT). This direct inspection was consistent with the MFL results, although the depth of material loss indicated by the MFL was slightly overestimated compared to the RT results. The reference test results were compared with the results obtained using other non-destructive testing (NDT) methods used in the project in order to compare and establish possible correlations between the measurement results.

The detected pipeline damage was then verified to determine the feasibility, suitability, defects, and limitations of the methods used to inspect the steel pipeline. The purpose of pipeline inspection is to detect damage and material loss. It is important to identify the types of material damage occurring in steel pipelines. These damages have various causes, as they may originate from the pipe production phase, the pipeline construction phase, and may be the result of negative phenomena occurring during the operation of the infrastructure, including negative impacts on the pipeline and corrosion, as well as those aided by possible hydrogen admixtures. All these types of defects and hazards have been identified and described, along with how to identify them using tested inspection methods.

Based on the research and comparisons conducted, an H_2 management protocol and recommendations were developed in the raport, indicating the risks and extent of damage that may arise as a result of the presence of hydrogen or hydrogen additives in transport pipelines. Attention was drawn to the continuous development of pipeline testing techniques using MFL tools and various modifications allowing for better detection of defects oriented in directions relative to the pipeline axis or steel pipe wall cross-section, highlighting the directions of development of measurement techniques and currently available measurement techniques. The possibility of detecting material defects characteristic of hydrogen corrosion in the form of developing cracks was analyzed by examining the possibility of using UT testing, which is the most reliable and effective method of identifying this type of defect, in relation to modifications to equipment that allow such defects to be detected, currently being implemented, including the e-MAT tool solution.

The next stage in the report refers to analyses of the impact of hydrogen on the strength of materials and components used in natural gas transmission and distribution infrastructure. It analyses the types of damage caused by hydrogen and the mechanisms of degradation of metallic and non-metallic materials under the influence of hydrogen. This includes experimental data from scientific research, project results, and relevant standards that are used to assess the behaviour of materials in H_2 containing environments, particularly in the context of H_2 blending in the gas network. It also considers the compatibility of materials with hydrogen, providing the information needed to make decisions on the safe integration of H_2 into existing gas infrastructure. In this context, further steps have also been taken to evaluate complementary methods for ILI testing based on the use of measuring pigs. Such methods can be used as additional methods to extend the range of phenomena identified by ILI testing using measuring pigs and as methods for testing unpigable pipelines.

The research leading to these results has received funding from Horizon 2020, the European Union's Framework Programme for Research and Innovation (H2020) under grant agreement n° 101111888.

The report ends with conclusions. The project verified existing methods and identified and tested alternative ILI testing methods using measuring tools. The tested methods are designed to detect additional stresses in the pipeline that affect FE and FCGR phenomena, generating additional operational risks caused by the mixing of hydrogen and natural gas. Ensuring safety in the process of blending natural gas and hydrogen requires the implementation of appropriate pipeline inspection techniques to manage risk at the required level. Current steel pipeline inspection techniques focus on detecting material loss and pipeline shape defects such as dents. For this purpose, MFL pistons assisted by geometry measurement pistons are commonly used, and in recent years they have been supplemented by tools that detect geometry changes based on the position of the pipeline in space and terrain by integrating measurement pistons with inertial navigation systems (IMUs). This approach, widely used by gas infrastructure operators, is appropriate for natural gas, where the risk of fatigue corrosion during operation is relatively low. For gas pipelines transporting H_2 and its additives to natural gas, it is necessary to extend the scope of testing. In the case of hydrogen, which will be transported as an additive to natural gas or on its own, the adverse effects of hydrogen must be considered. In the context of assessing the susceptibility of steel pipe materials to hydrogen, issues related to hydrogen embrittlement (HE) and hydrogen-induced cracking (HIC) of ferritic steels used in the construction of pipelines, including natural gas pipelines, are important.

About the project: The European natural gas infrastructure provides the opportunity to accept hydrogen (H_2), as a measure to integrate low-carbon gases while leveraging the existing gas network and contributing to decarbonisation. However, there are technical and regulatory gaps that should be closed, adaptations and investments to be made to ensure that multi-gas networks across Europe will be able to operate in a reliable and safe way while providing a highly controllable gas quality and required energy demand. Aspects such as material integrity of pipelines and components, as well as the lack of harmonisation of gas quality requirements at European level must be addressed in order to facilitate the injection of H_2 in the natural gas network.

In this context, the SHIMMER project (Safe Hydrogen Injection Modelling and Management for European gas network Resilience) was selected for funding as part of the 2023 Clean Hydrogen Partnership programme. SHIMMER aims to enable a higher integration of low-carbon gases and safer H_2 injection management in multi-gas networks by strengthening the knowledge base and improving the understanding of risks and opportunities in H_2 projects.

It will do this by:

- Mapping and assessing European gas T&D infrastructure in relation to materials, components, technology, and their readiness for hydrogen blends.
- Defining methods, tools and technologies for multi-gas network management and quality tracking, including simulation, prediction, and safe management of network operation in view of widespread hydrogen injection in a European-wide context.
- Proposing best practice guidelines for handling the safety of hydrogen in the natural gas infrastructure and managing the risks.

The research leading to these results has received funding from Horizon 2020, the European Union's Framework Programme for Research and Innovation (H2020) under grant agreement n° 101111888.

1 Introduction

1.1 Purpose of the document

Regardless of the medium transmitted, the system operators' role is to ensure that the condition of the pipelines is on the satisfactory level. The addition of the hydrogen into the natural gas pipeline systems will result in new challenges for the system operators. The existing approach of using mainlu MFL technology may be not enough as the hydrogen existence results in new potential defects. Moreover, the existence of non-piggable pipelines requires looking for the techniques that enable checking the pipeline's condition without pigging. The aim of this document is to provide with the information about promising technologies, their weaknesses and strengths, together with their usefulness for the system with the hydrogen's presence. Moreover, ones of the conclusions intended for this deliverable are the proposed approach for the hydrogen-presents system together with the directions in which the existing technologies may be developed in order to handle the pipelines with hydrogen-natural gas blend.

1.2 Intended readership

The results presented in this deliverable may be interesting for the operators, both DSOs and TSOs, as the work done includes practical information about the different inspection techniques, including their advantages and disadvantages. What should also be of interest for operators are the conclusions from this report which include the proposition of how the systems containing hydrogen could be inspected, taking into account the differences from the natural gas system.

1.3 Structure of this document

The document is divided into several main sections. It starts with the overview of the documents and standards related to the various inspection techniques which is followed by the information about the survey on the non-piggable pipelines and the inspection techniques which was directed to the DSOs and TSOs. Next main part is the description of various technologies that may be used for the inspection of the condition of the pipelines. The part that comes afterwards is the description of the field surveys done within the project and their results. The last part of the document contains the information about the conclusions that comes from the comparison of selected inspection techniques, especially in the matter of its usefulness for hydrogen or blends together with the proposed recommendations.

1.4 Stakeholder involvement

The survey on the inspection techniques and the non-piggable pipelines was sent to operators (TSOs and DSOs) from the project's consortium and their input was then involved the deliverable's text.

1.5 Relationship with other deliverables

The conclusions on the identification of the challenges and defining key parameters with probable impact on the inspections presented in this document receives inputs from the following deliverables:

- D3.1 – Identification of critical material properties and component factors.

The research leading to these results has received funding from Horizon 2020, the European Union's Framework Programme for Research and Innovation (H2020) under grant agreement n° 101111888.

2 Documents and standards

This section of the Deliverable provides the overview of the standards that relates to various methods and can be used for the inspections and assessment of the condition of the pipelines. In particular, the methods for which the standards are described are:

- Ultrasonic Testing (UT)
- Radiographic Testing (RT)
- Acoustic Emmission (AE)
- Magnetic Particle (MP).

1. CEN/TR 14748 - Non-destructive testing - Methodology for qualification of non-destructive tests

Scope of the Standard:

This document sets out basic principles and provides recommendations and general guidelines for carrying out qualification of non-destructive tests.

The document deals with methods for qualifying non-destructive tests to determine whether they can attain their objectives. It applies to all aspects of tests which influence their effectiveness. The parties involved decide in their own responsibility on the need for a qualification of a non-destructive test. This includes identification of the qualification-team and its technical competence. There may be a need for qualification when there is a deviation from a European NDT Standard, or when new techniques or methods are to be implemented for which, there are no European Standards. Table 1 summarises when qualification is required.

Ultrasonic Testing Standards

1. EN ISO 16810:2025 – Non-destructive testing - Ultrasonic testing - General principles

Scope of the Standard:

Document specifies the general principles for the ultrasonic testing of industrial products that permit the transmission of ultrasound.

The specific conditions of application and use of ultrasonic testing, which depend on the type of product to be tested, are described in documents which can include:

— product standards;

— specifications;

— Standards;

— contractual documents;

— written procedures.

Document specifies the minimum applicable requirements, unless otherwise specified in the referencing documents.

Document does not specify:

— extent of testing and scan plans;

— acceptance criteria.

The research leading to these results has received funding from Horizon 2020, the European Union's Framework Programme for Research and Innovation (H2020) under grant agreement n° 101111888.

Document describes only conventional probes, however, the general principles for ultrasonic testing also apply to ultrasonic testing using array techniques. If array techniques are used, then additional steps or verifications can be needed.

2. **EN ISO 16811:2025-09 – Non-destructive testing - Ultrasonic testing - Sensitivity and range setting**
   Scope of the Standard:

   Document specifies the general rules for setting the time-base range and sensitivity (i.e. gain adjustment) of a manually operated ultrasonic instrument with A-scan display in order that reproducible determinations can be made of the location and echo height of a reflector.

   Document is applicable to contact techniques employing a single probe with either a single transducer or dual transducers. This document does not apply to the immersion technique and techniques employing more than one probe.

3. **EN ISO 16823:2025-07 – Non-destructive testing - Ultrasonic testing - Through-transmission technique**
   Scope of the Standard:

   Document specifies the principles of ultrasonic through-transmission techniques.

   Through-transmission techniques can be used for:

   — detection of discontinuities;

   — determination of sound attenuation.

   The general principles required for the use of ultrasonic testing of industrial products are described in ISO 16810.

   The through-transmission technique is used for the testing of fiat products, e.g. plates and sheets.

   Further, it can be used for tests, for example:

   — where the shape, dimensions or orientation of possible discontinuities are unfavourable for direct reflection;

   — of materials with high sound attenuation;

   — on thin test objects.

4. **EN ISO 16826:2025-09 – Non-destructive testing - Ultrasonic testing - Testing for discontinuities perpendicular to the surface**
   Scope of the Standard:

   Document specifies principles for the tandem technique and the longitudinal-longitudinal-transverse wave (LLT) technique for detection of discontinuities perpendicular to the surface or almost perpendicular to the surface.

   The general principles for ultrasonic testing of industrial products are described in ISO 16810.

   The tandem or LLT techniques can be used for the detection of embedded planar discontinuities.

   Document gives guidelines for the testing of metallic materials with a thickness between 40 mm and 500 mm with parallel or concentric surfaces.

   The procedures provided in this document can be used for testing of other materials or smaller thickness if special measures are taken according to a written testing procedure.

   Phased array techniques can also be applied for the tandem technique and the LLT technique, but additional steps or verifications can be needed.

The research leading to these results has received funding from Horizon 2020, the European Union's Framework Programme for Research and Innovation (H2020) under grant agreement n° 101111888.

5. **EN ISO 16827:2014 – Non-destructive testing — Ultrasonic testing — Characterization and sizing of discontinuities**

   Scope of the Standard:

   Document specifies the general principles and techniques for characterization and sizing of previously detected discontinuities on order to ensure their evaluation against applicable acceptance criteria. It is applicable, in general terms, to discontinuities in those materials and applications covered by ISO 16810.

6. **EN ISO 16828:2014 – Non-destructive testing -- Ultrasonic testing -- Time-of-flight diffraction technique as a method for detection and sizing of discontinuities**

   Scope of the Standard:

   Document defines the general principles for the application of the time-of-flight diffraction (TOFD) technique for both detection and sizing of discontinuities in low alloyed carbon steel components. It can also be used for other types of materials, provided the application of the TOFD technique is performed with necessary consideration of geometry, acoustical properties of the materials, and the sensitivity of the examination.

   Although it is applicable, in general terms, to discontinuities in materials and applications covered by SO 16810, it contains references to the application on welds. This approach has been chosen for reasons of clarity as to the ultrasonic probe positions and directions of scanning.

7. **EN ISO 5577:2017-04 – Non-destructive testing -- Ultrasonic testing -- Vocabulary**

   Scope of the Standard:

   Document defines the terms used in ultrasonic non-destructive testing and forms a common basis for standards and general use. It does not cover terms used in ultrasonic testing with phased array.

8. **EN ISO 23243:2021 – Non-destructive testing -- Ultrasonic testing with arrays -- Vocabulary**

   Scope of the Standard:

   Document defines terms used in ultrasonic testing with arrays. It includes phased array technology and signal processing technology using arrays, e.g. the full-matrix capture (FMS) and total focusing technique (TFM).

9. **EN 1330-1 - Non-destructive testing -- Terminology -- Part 1: List of general terms**

   Scope of the Standard

   This part of the Standard specifies general terms used in non-destructive testing that originate from other technical fields (such as electricity, vacuum technology, metrology, etc.).

10. **EN 1330-2 - Non-destructive testing -- Terminology – Part 2: Terms common to the non-destructive testing methods.**

    Scope of the Standard

    Seventeen common terms used in two or more non-destructive testing methods have been defined. The terms are given in Polish, English, German and French.

11. **EN ISO 18563-1:2023-02 Non-destructive testing -- Characterization and verification of ultrasonic phased array equipment -- Part 1: Instruments**

    Scope of the Standard

    Document specifies the functional characteristics of multi-channel ultrasonic phased array instruments used for array probes and provides methods for their measurement and verification.
    It also gives the extent of the verification and defines acceptance criteria within a frequency range of 0,5 MHz to 10 MHz.

The research leading to these results has received funding from Horizon 2020, the European Union's Framework Programme for Research and Innovation (H2020) under grant agreement n° 101111888.

12. EN ISO 18563-2:2025-04 - Non-destructive testing — Characterization and verification of ultrasonic phased array equipment — Part 2: Probes

Scope of the Standard

Document specifies characterization tests to be performed at the end of the fabrication of an array probe. It defines both methodology and acceptance criteria.
Document is applicable to the following array probes used for ultrasonic non-destructive testing [phased array technique or signal processing technique, e.g. full-matrix capture (FMC) and total-focusing technique (TFM)] in contact technique (with or without a wedge or delay line) or in immersion technique, with centre frequencies in the range 0,5 MHz to 10 MHz:
a) array probes with elements in one direction:
— 1-D-linear array (linear array);
— 1-D-curved array;
— annular array;
b) array probes with elements in two directions:
— 2-D-array (matrix array);
— sectorial annular array;
— partial sectorial annular array.
This document does not give methods and acceptance criteria to characterize the performance of an ultrasonic phased array instrument or the performance of a complete system, which are given in ISO 18563-1 and in ISO 18563-3.

13. EN ISO 18563-3:2024-11 - Non-destructive testing - Characterization and verification of ultrasonic phased array equipment - Part 3: Complete systems

Scope of the Standard

Document addresses ultrasonic test systems implementing array probes, for contact technique (with or without wedge) or for immersion technique, with centre frequencies in the range of 0,5 MHz to 10 MHz.
Document provides methods and acceptance criteria for determining the compliance of the complete system. Its purpose is for the verification of the correct operation of the system prior to testing or verification of the absence of degradation of the system.
The methods are not intended to prove the suitability of the system for particular applications but are intended to prove the capability of the complete system (used for an application) to operate correctly according to the settings used.
However, document does not cover the sensitivity setting of the system for a specific application. Nor does it apply to the characterization or verification of the mechanical scanning equipment. It is intended that these items will be covered by the test procedure.
Document also does not address the phased array technique using tandem technique.
Document (in annex) gives characterization of beams, as recommended in case of dead elements.

14. EN ISO 17640:2019-01 – Non-destructive testing of welds -- Ultrasonic testing -- Techniques, testing levels, and assessment

Scope of the Standard:

Document specifies techniques for the manual ultrasonic testing of fusion-welded joints in metallic materials of thickness ≥ 8 mm, which exhibit low ultrasonic attenuation (especially that due to scatter), at object temperatures from 0 °C to 60 °C. It is primarily intended for use on full penetration welded joints where both the welded and parent material are ferritic.

Where material-dependent ultrasonic values are specified, they are based on steels having an ultrasonic sound velocity of (5 920 ± 50) m/s for longitudinal waves and (3 255 ± 30) m/s for transverse waves.

Document specifies four testing levels, each corresponding to a different probability of detection of imperfections. Guidance on the selection of testing levels A, B, and C is given in Annex A.

The research leading to these results has received funding from Horizon 2020, the European Union's Framework Programme for Research and Innovation (H2020) under grant agreement n° 101111888.

Testing level D is intended for special applications and can only be used when defined by specification. This includes: tests of non-ferritic metals, tests of partial penetration welds, tests with automated testing and testing at temperatures outside the range 0 °C to 60 °C.

Standard can be used for the assessment of discontinuities for acceptance purposes by either:

a) evaluation based on length and echo amplitude

b) evaluation based on characterization and sizing using probe movement techniques

15. EN ISO 11666 :2018-04 – Non-destructive testing of welds -- Ultrasonic testing -- Acceptance levels

Scope of the Standard:

This document specifies two ultrasonic acceptance levels known as acceptance level 2 (AL 2] and acceptance level 3 (AL 3) for full penetration welded joints in ferritic steels, which correspond to ISO 5817:2014, quality levels B and C. An acceptance level corresponding to ISO 5817:2014, quality level D is not included in this document, as ultrasonic testing is generally not requested for this weld quality.

These acceptance levels are applicable to testing carried out in accordance with ISO 17640.

This document applies to the testing of full penetration ferritic Steel welds, with thicknesses from 8 mm to 100 mm. It can also be used for other types of welds, materials and thicknesses, provided the tests have been performed with necessary consideration of the geometry and acoustic properties of the component, and an adequate sensitivity can be employed to enable the acceptance levels of this document to be applied. The nominal frequency of probes used in this document is between 2 MHz and 5 MHz, unless attenuation or requirements for higher resolution call for other frequencies. It is important to consider the use of these acceptance levels in conjunction with frequencies outside this range carefully.

16. EN ISO 23279:2017– Non-destructive testing of welds. Ultrasonic testing. Characterization of discontinuities in welds

Scope of the Standard:

Document specifies how to characterize indications from discontinuities by classifying them as originating from planar or non-planar embedded discontinuities. This procedure is also suitable for indications from discontinuities that break the surface after removal of the weld reinforcement.

17. EN ISO 22825:2017-12 – Non-destructive testing of welds—Ultrasonic testing— Testing of welds in austenitic steels and nickel-based alloys

Scope of the Standard:

Document specifies the approach to be followed when developing procedures for the ultrasonic testing of the following welds:

— welds in stainless steels;

— welds in nickel-based alloys;

— welds in duplex steels;

— dissimilar metal welds;

— austenitic welds.

The purposes of the testing can be very different, for example:

— for the assessment of quality level (manufacturing);

— for the detection of specific discontinuities induced in service.

The research leading to these results has received funding from Horizon 2020, the European Union's Framework Programme for Research and Innovation (H2020) under grant agreement n° 101111888.

Acceptance levels are not included in this document but can be applied in accordance with the scope of the testing.

The requirements of this document are applicable to both manual and mechanized testing.

18. EN ISO 13588:2019-04 – Non-destructive testing of welds -- Ultrasonic testing -- Use of automated phased array technology

Scope of the Standard:

Document specifies two ultrasonic acceptance levels known as acceptance level 2 (AL 2] and acceptance level 3 (AL 3) for full penetration welded joints in ferritic steels, which correspond to ISO 5817:2014, quality levels B and C. An acceptance level corresponding to ISO 5817:2014, quality level D is not included in this document, as ultrasonic testing is generally not requested for this weld quality. These acceptance levels are applicable to testing carried out in accordance with ISO 17640.

Document applies to the testing of full penetration ferritic Steel welds, with thicknesses from 8 mm to 100 mm. It can also be used for other types of welds, materials and thicknesses, provided the tests have been performed with necessary consideration of the geometry and acoustic properties of the component, and an adequate sensitivity can be employed to enable the acceptance levels of this document to be applied. The nominal frequency of probes used in this document is between 2 MHz and 5 MHz, unless attenuation or requirements for higher resolution call for other frequencies. It is important to consider the use of these acceptance levels in conjunction with frequencies outside this range carefully.

19. EN ISO 20601:2019-03 - Non-destructive testing of welds -- Ultrasonic testing -- Use of automated phased array technology for thin-walled steel components

Scope of the Standard:

Document specifies the application of phased array technology for the semi or fully automated ultrasonic testing of fusion-welded joints in steel parts with thickness values between 3,2 mm and 8,0 mm. This meets the typical range of tube wall thickness values in boilers, which is an important application of this testing technology. The minimum and maximum value of the wall thickness range can be exceeded, when testing level "D" of this document is applied. Document applies to full penetration welded joints of simple geometry in plates, tubes, pipes, and vessels, **where both the weld and parent material are low-alloy** and/or fine-grained steel.

NOTE "Semi-automated testing" encompasses a controlled movement of one or more probes on the surface of a component along a fixture (guidance strip, ruler, etc.), whereby the probe position is unambiguously measured with a position sensor. The probe is moved manually. "Fully automated testing" includes mechanized propulsion in addition,

Where material-dependent ultrasonic parameters arc specified in this document, they arc based on steels having a sound velocity of (5 920 ± 50) m/s for longitudinal waves, and (3 255 ± 30) m/s for transverse waves. It is necessary to take this fact into account when testing materials with a different velocity.

This document provides guidance on the specific capabilities and limitations of phased array technology for the detection, location, sizing and characterization of discontinuities in fusion-welded joints. Ultrasonic phased array technology can be used as a stand-alone technique or in combination with other non-destructive testing (NDT) methods nr techniques, during manufacturing and testing of new welds/repair welds (pre-service testing).

This document specifics two testing levels;

— level "C” for standard situations;

— level "D” for different situations/special applications.

This document describes assessment of discontinuities for acceptance purposes based on:

— height and length;

— amplitude (equivalent reflector size) and length;

— go/no-go decision.

Document does not include acceptance levels for discontinuities.

The research leading to these results has received funding from Horizon 2020, the European Union's Framework Programme for Research and Innovation (H2020) under grant agreement n° 101111888.

20. EN ISO 19285:2017-11 – Non-destructive testing of welds -- Phased array ultrasonic testing (PAUT) -- Acceptance levels

Scope of the Standard:

Document specifies acceptance levels for the phased array ultrasonic testing technique (PAUT) of full penetration welds in ferritic steels of minimum thickness of 6 mm which correspond to the quality levels of ISO 5817

21. EN ISO 4761:2023-06 – Non-destructive testing of welds -- Phased array ultrasonic testing (UT-PA) for thin-walled steel components -- Acceptance levels

Scope of the Standard:

Document specifies acceptance levels of phased array ultrasonic testing technique(UT-PA) of full penetration welds in low-alloy and/fine grained steels in the wall thickness range from 3,2 mm to 8 mm which correspond to quality levels of ISO 5817.

The acceptance levels are applicable to indications detected according to ISO 20601.

22. EN ISO 23864:2022-06 – Non-destructive testing of welds -- Ultrasonic testing -- Use of automated total focusing technique (TFM) and related technologies

Scope of the Standard:

Document specifics the application of the TFM technique and related technologies for semi or fully automated ultrasonic testing of fusion- welded joints in metallic materials of minimum thickness 3,2 mm.

Document is applicable to components with welds fabricated using metals which have isotropic (constant properties in all directions) and homogeneous conditions. This includes welds in low carbon alloy steels and common aerospace grade aluminium and titanium alloys, provided they are homogeneous and isotropic.

Document applies to full penetration welded joints of simple geometry in plates, pipes and vessels.

Document specifies four testing levels (A, B, C, D), each corresponding to a different probability of detection of imperfections. Guidance on the selection of testing levels is provided. Coarse-grained metals and austenitic welds can be tested when the provisions of this document have been considered.

Document gives provisions on the specific capabilities and limitations of the TFM technique for the detection, locating, sizing and characterization of discontinuities in fusion-welded joints. The TFM technique can be used as a stand-alone approach or in combination with other non-destructive testing methods for manufacturing, in-service and post-repair tests.

Document includes assessment of indications for acceptance purposes based on either amplitude (equivalent reflector size) and length or height and length.

Document does not include acceptance levels for discontinuities.

The following two typical testing techniques for welded joints are referred to in this document:

a) side scanning, where the probe(s) is (are) positioned adjacent to the weld cap, typically using

wedges. Side scanning can be performed from one side or both sides of the weld;

b) top scanning where the probe is positioned on top of weld cap with a flexible, conformable delay line or using immersion technique, or using contact technique after removing the weld cap.

Semi-automated testing encompasses a controlled movement of one or more probes along a fixture (guidance strip, ruler, etc.), whereby the probe position is measured with a position sensor. The scan is performed manually.

The research leading to these results has received funding from Horizon 2020, the European Union's Framework Programme for Research and Innovation (H2020) under grant agreement n° 101111888.

Tn addition, fully automated testing includes mechanized propulsion.

23. ISO 23865:2021 – Non-destructive testing. Ultrasonic testing. General use of full matrix capture/total focusing technique (FMC/ TFM) and related technologies

Scope of the Standard:

Document gives general provisions for applying ultrasonic testing with arrays using FMC/TFM techniques and related technologies. It is intended to promote the adoption of good practice either at the manufacturing stage or for in-service testing of existing installations or for repairs.

Some examples of applications considered in this document deal with characterization and sizing in damage assessment.

Materials considered are low-alloyed carbon steels and common aerospace grade aluminium and titanium alloys, provided they are homogeneous and isotropic, but some recommendations are given for other materials (e.g. austenitic ones).

This document does not include acceptance levels for discontinuities**.**

24. EN ISO 10893-1:2011 – Non-destructive testing of steel tubes - Part 1: Automated electromagnetic testing of seamless and welded (except submerged arc-welded) steel tubes for the verification of hydraulic leaktightness

Scope of the Standard:

Document is part of ISO 10893 and specifies requirements for automated electromagnetic testing of seamless and welded steel tubes, apart from submerged arc-welded (SAW) tubes, for verification of hydraulic leaktightness. It is applicable to the inspection of tubes with an outside diameter greater than or equal to 4 mm, when testing with eddy current, and greater than 10 mm when testing with flux leakage method.

This part of ISO 10893 can also be applicable to the testing of hollow sections.

NOTE: Electromagnetic inspection using magnetic flux leakage method is not applicable to austenitic stainless-steel tubes.

25. EN ISO 10893-8:2011 – Non-destructive testing of steel tubes - Part 8: Automated ultrasonic testing of seamless and welded steel tubes for the detection of laminar imperfections

Scope of the Standard:

Document is part of ISO 10893 and specifies requirements for automated ultrasonic testing for the detection of laminar imperfections:

a) in the pipe body (full peripheral testing) of seamless and welded, except submerged arc-welded (SAW), Steel tubes, or

b) in the area adjacent to the weld seam of welded steel tubes, and optionally

c) at the ends (full peripheral testing) of seamless and welded tubes.

This part of ISO 10893 can also be applicable to the testing of circular hollow sections.

NOTE: For welded tubes, see ISO 10893-9 for an alternative test method for the detection of laminar imperfections in steel strip/plate prior to tube forming.

26. EN ISO 10893-9:2011 - Non-destructive testing of steel tubes - Part 9: Automated ultrasonic testing for the detection of laminar imperfections in strip/plate used for the manufacture of welded steel tubes

Scope of the Standard:

This part of ISO 10893 specifies requirements for the automated ultrasonic testing of strip/plate used in the manufacture of welded tubes for the detection of laminar imperfections carried out in the pipe mill before or during pipe production.

27. EN ISO 10893-10:2011 – Non-destructive testing of steel tubes -- Part 10: Automated full peripheral ultrasonic testing of seamless and welded (except submerged arc-welded) steel tubes for the detection of longitudinal and/or transverse imperfections

Scope of the Standard:

The research leading to these results has received funding from Horizon 2020, the European Union's Framework Programme for Research and Innovation (H2020) under grant agreement n° 101111888.

Document is part of ISO 10893 and specifies requirements for automated full peripheral ultrasonic shear wave (generated by conventional or phased array technique) testing of seamless and welded [except submerged arc-welded
(SAW)] steel tubes, for the detection of longitudinal and/or transverse imperfections.
This part of ISO 10893 is applicable to the inspection of tubes with an outside diameter greater than or equal to 10 mm, normally with an outside diameter-to-thickness ratio greater than or equal to 5.
This part of ISO 10893 can also be applicable to the testing of circular hollow sections.

28. **EN ISO 10893-11:2011 – Non-destructive testing of steel tubes - Part 11: Automated ultrasonic testing of the weld seam of welded steel tubes for the detection of longitudinal and/or transverse imperfections**

Scope of the Standard:

This part of ISO 10893 specifies requirements for the automated ultrasonic shear wave (generated by conventional or phased array technique) testing of the weld seam of submerged arc-welded (SAW) or electric resistance and induction-welded (EW) steel tubes.
For SAW tubes, the test covers the detection of imperfections oriented predominantly parallel to or, by agreement, perpendicular to the weld seam or both.
For EW tubes, the test covers the detection of imperfections oriented predominantly parallel to the weld seam.
In the case of testing on longitudinal imperfections, Lamb wave testing can be applied at the discretion of the manufacturer.
For the detection of imperfections at the weld seam of EW tubes, full peripheral ultrasonic testing is possible.
This part of ISO 10893 can also be applicable to the testing of circular hollow sections.

29. **EN ISO 16809 – Non-destructive testing -- Ultrasonic thickness measurement**

Scope of the Standard:

Document specifies the principles for ultrasonic thickness measurement of metallic and non-metallic materials by direct contact, based on measurement of time of light of ultrasonic pulses only.

30. **EN 17290 - Non-destructive testing -- Ultrasonic testing -- Examination for loss of thickness due to erosion and/or corrosion using the TOFD technique**

Scope of the Standard:

Document specifics the application of the time-of-flight diffraction (TOFD) technique in testing of metals for quantifying loss of thickness due to erosion and/or corrosion. It applies to all types of corrosion and/or erosion damage, particularly those defined in EN ISO 16809.
Document applies to unalloyed or low-alloyed steels. It applies to components with a nominal thickness > 6 mm. For smaller thicknesses, feasibility tests are performed to validate the test technique. For other materials, feasibility tests are essential, too.
The TOFD technique can be used as a stand-alone technique or in combination with other non-destructive testing techniques, for in-service testing, in order to detect material loss caused by erosion and/or corrosion.
This technique is based on analysis of TOFD images using reflected and/or diffracted ultrasonic signals.
Document does not specify acceptance levels.

31. **EN ISO 10863:2020-12 - Non-destructive testing of welds -- Ultrasonic testing -- Use of time-of-flight diffraction technique (TOFD)**

Scope of the Standard:

Document specifies the application of the time-of-flight diffraction (TOFD) technique to the semi or fully automated ultrasonic testing of fusion-welded joints in metallic materials of minimum thickness 6 mm.
It applies to full penetration welded joints of simple geometry in plates, pipes, and vessels, where both the weld and the parent material are low-alloyed carbon Steel. Where specified and appropriate, TOFD can also be used on other types of materials that exhibit Iow ultrasonic attenuation (especially that due to scatter).

The research leading to these results has received funding from Horizon 2020, the European Union's Framework Programme for Research and Innovation (H2020) under grant agreement n° 101111888.

Where material-dependent ultrasonic parameters are specified in this document, they are based on steels having a sound velocity of (5 920 ± 50) m/s for longitudinal waves and (3 255 ± 30) m/s for transverse waves. It is necessary to take this fact into account when testing materials with a different velocity.
Document refers to ISO 16828 and provides guidance on the specific capabilities and limitations of TOFD for the detection, location, sizing and characterization of discontinuities in fusion-welded joints.
TOFD can be used as a stand-alone method or in combination with other non-destructive testing (NDT) methods or techniques, for manufacturing inspection, and for in-service inspection.
Document specifies four testing levels (A, B, C, D) in accordance with ISO 17635 and corresponding to an increasing level of testing reliability. Guidance on the selection of testing levels is provided.
Document permits assessment of TOFD indications for acceptance purposes. This assessment is based on the evaluation of transmitted, reflected and diffracted ultrasonic signals within a generated TOFD image.
Document does not include acceptance levels for discontinuities.

32. **EN 12732:2022-04 appendix C - Gas infrastructure - Welding steel pipework - Functional requirements**

Scope of the Standard:

Document contains requirements for the production and testing of weld joints for the installation and modification, including in-service welding, of onshore Steel pipelines and pipework used in gas infrastructure. This includes all pressure ranges and processes, non-toxic and non-corrosive natural gas according to EN ISO 13686 and non-conventional gases such as (injected biomethane and hydrogen, where:

- the pipeline elements arc made of unalloyed or low-alloyed carbon steel;
- the pipeline is not located within commercial or industrial premises as integral part of the industrial process on those premises except for any pipelines and facilities delivering gas to such premises;
- the pipework is not located within households or industrial installations according to EN 1775 or EN 15001;
- the design temperature of the system is between -40 °C up to and including 120 °C.

For injected biomethane or hydrogen a detailed technical evaluation of the functional requirements is required, ensuring there are no other constituents or properties of the gases that can affect the integrity of the pipeline. This document is not applicable to welds produced prior to the publication of this document. This document specific common basic principles for gas infrastructure. Users of this document are expected to be aware that there can exist more detailed national standards and/or Standards of practice in the CEN member countries This document is intended to be applied in association with these national standards and/or Standards of practice setting out the above-mentioned basic principles. In the event of conflicts in terms of more restrictive requirements in national legislation/regulation with the requirements of this document, the national legislation/regulation takes precedence as illustrated in CEN/TR 13737 (all parts).

NOTE: CEN/TR 13737 (all parts) contains:

- clarification of relevant legislation/regulations applicable in a country;
- if appropriate, more restrictive national requirements;
- national contact point for the latest Information.

33. **EN ISO 15626:2018-10 Non-destructive testing of welds -- Time-of-flight diffraction technique (TOFD) -- Acceptance levels**

Scope of the Standard:

Document specifies acceptance levels for the time-of-flight diffraction technique (TOFD) of fully penetration welds in ferritic steels from 6 mm up to 300 mm thickness which correspond to the quality levels of ISO 5817.
These acceptance levels are applicable to indications classified in accordance with ISO 10863.

34. **EN 12680-1:2005 – Founding - Ultrasonic examination - Part 1: Steel castings for general purposes**

Scope of the Standard:

The research leading to these results has received funding from Horizon 2020, the European Union's Framework Programme for Research and Innovation (H2020) under grant agreement n° 101111888.

Document specifies the requirements for the ultrasonic examination of steel castings (with ferritic structure) for general purposes and the methods for determining internal discontinuities by the pulse echo technique. It applies to the ultrasonic examination of steel castings which have usually received a grain refining heat treatment, and which have wall thicknesses up to and including 600 mm. For greater wall thicknesses, special agreements apply with respect to test procedure and recording levels.
Document does not apply to austenitic steels and joint welds.

35. **EN 12680-2:2005 – Founding - Ultrasonic examination - Part 2: Steel castings for highly stressed components**

Scope of the Standard:

Document specifies the requirements for the ultrasonic examination of steel castings (with ferritic structure) for highly stressed components and the methods for determining internal discontinuities by the pulse echo technique. It applies to the ultrasonic examination of steel castings which have usually received a grain refining heat treatment, and which have wall thicknesses up to and including 600 mm. For greater wall thicknesses, special agreements apply with respect to test procedure and recording levels.
Document does not apply to austenitic steels and joint welds.

36. **EN 12680-1:2005 – Founding - Ultrasonic testing - Part 3: Spheroidal graphite cast iron castings**

Scope of the Standard:

Document specifies the requirements for the ultrasonic examination of steel castings (with ferritic structure) of spheroidal graphite cast iron castings and the methods for determining internal discontinuities by the pulse echo technique. It does not apply to ultrasonic testing of the nodularity of spheroidal graphite cast irons.
Document does not apply to transmission technique.
NOTE The transmission technique has insufficient sensitivity to detect the discontinuities found in spheroidal graphite cast iron castings and is used in exceptional cases only.

37. **EN 10308:2002 – Non-destructive testing. Ultrasonic testing of steel bars**

Scope of the Standard:

Document describes the techniques to be used for manual, pulse-echo, ultrasonic testing of steel bars of diameter or equivalent thickness less or equal to 400 mm or equivalent section. Mechanised, semi-automatic or automatic techniques may be used but should be agreed between the purchaser and the supplier.

38. **EN 10228-3:2016– Non-destructive testing of steel forgings -- Part 3: Ultrasonic testing of ferritic or martensitic steel forgings**

Scope of the Standard:

Document describes techniques to be used for the manual, pulse-echo, ultrasonic testing of forgings manufactured from ferritic and martensitic steel. Mechanized scanning techniques, such as immersion testing, may be used but should be agreed between the purchaser and supplier.
This part of EN 10228 applies to four types of forgings, classified according to their shape and method of production. Types 1, 2 and 3 are essentially simple shapes. Type 4 covers complex shapes.
This part of EN 10228 does not apply to:
— closed die forgings;
— turbine rotor and generator forgings.

39. **EN 10228-4:2016 – Non-destructive testing of steel forgings—Part 4: Ultrasonic testing of austenitic and austenitic-ferritic stainless-steel forgings**

Scope of the Standard:

Document describes techniques for the manual, pulse-echo, ultrasonic testing of forgings manufactured from austenitic and austenitic-ferritic stainless steels. Mechanized scanning techniques, such as immersion testing, may be used but should he agreed between the purchaser and supplier.

The research leading to these results has received funding from Horizon 2020, the European Union's Framework Programme for Research and Innovation (H2020) under grant agreement n° 101111888.

This part of EN 10228 applies to four types of forgings, classified according to their shape and method of production. Types 1, 2 and 3 are essentially simple shapes. Type 4 covers complex shapes.
This part of EN 10228 does not apply to:
— closed die forgings;
— turbine rotor and generator forgings.

40. **EN 10160:2020 – Ultrasonic testing of steel flat product of thickness equal or greater than 6 mm (reflection method)**

Scope of the Standard:

Document describes method of ultrasonic testing of uncoated steel flat products aimed at detecting internal discontinuities is described. It applies to flat products with a nominal thickness range from 6 mm to 200 mm of non-alloy or alloy steel, excluding austenitic or austenitic-ferritic steels. The standard may also apply to the latter steels, however, provided that there is sufficient distance between the noise level and the level of registration.

41. **EN 10307:2002 – Non-destructive testing—Ultrasonic testing of austenitic and austenitic-ferritic stainless steels flat products of thickness equal to or greater than 6 mm (reflection method) – (the English version has been withdrawn, national versions may be valid)**

Scope of the Standard:

Document describes a method for the ultrasonic-testing of uncoated flat austenitic and austenitic-ferritic stainless-steel product for internal discontinuities. It is applicable to flat product in nominal thickness range of 6 mm to 200 mm. Mechanised, semi-automatic or automatic techniques may be used but should be agreed between the purchaser and the supplier.

Document also defines 3 quality classes for the flat product body (classes S_1, S_2 and S_3) and 4 quality classes (E_1 E_2, E_3, E_4) for the edges.

Radiographic Testing Standards

1. **EN ISO 17636-1:2023 - Non-destructive testing of welds -- Radiographic testing -- Part 1: X- and gamma-ray techniques with film**

Scope of the Standard:

Document specifies techniques of radiographic testing of fusion-welded joints in metallic materials using industrial radiographic film techniques with the object of enabling satisfactory and repeatable results. The techniques are based on generally recognized practice and fundamental theory of the subject.
It applies to the joints of plates and pipes in metallic materials. Besides its conventional meaning, "pipe" as used in this document covers other cylindrical bodies, such as tubes, penstocks, boiler drums and pressure vessels.
Document does not specify acceptance levels for any of the indications found on the radiographs. This is provided in ISO 10675 series.

2. **EN ISO 17636-2:2023 - Non-destructive testing of welds -- Radiographic testing -- Part 2: X- and gamma-ray techniques with digital detectors**

Scope of the Standard:

Document specifies techniques of digital radiography with the object of enabling satisfactory and repeatable results. The techniques are based on generally recognized practice and fundamental theory of the subject.
Document applies to the digital radiographic testing of fusion welded joints in metallic materials.
It applies to the joints of plates and pipes. Besides its conventional meaning, "pipe", as used in this document, covers other cylindrical bodies such as tubes, penstocks, boiler drums and pressure vessels.
Document specifies the requirements for digital radiographic X- and gamma-ray testing by either computed radiography (CR) or radiography with digital detector arrays (DDAs) of the welded joints

The research leading to these results has received funding from Horizon 2020, the European Union's Framework Programme for Research and Innovation (H2020) under grant agreement n° 101111888.

of metallic plates and tubes for the detection of imperfections. It includes manual and automated inspection with DDAs.
Digital detectors provide a digital grey value image which can be viewed and evaluated using a computer. This document specifies the recommended procedure for detector selection and radiographic practice. The procedure specified in this document provides the minimum requirements for radiographic practice which permits exposure and acquisition of digital radiographs with equivalent sensitivity for the detection of imperfections as film radiography.
This document does not specify acceptance levels for any of the indications found on the digital radiographs. This is provided in ISO 10675 series.
If contracting parties apply lower test criteria, it is possible that the quality achieved will be significantly lower than when this document is strictly applied.

3. **EN ISO 10675-1:2022 - Non-destructive testing of welds -- Acceptance levels for radiographic testing -- Part 1: Steel, nickel, titanium and their alloys**

Scope of the Standard:
Document specifies acceptance levels for indications from imperfections in butt welds of steel, nickel, titanium and their alloys detected by radiographic testing. If agreed, the acceptance levels can be applied to other types of welds (such as fillet welds, etc.) or materials.
The acceptance levels can be related to welding standards, application standards, specifications or Standards. This document assumes that the radiographic testing has been carried out in accordance with ISO 17636-1 for RT-F (F = film) or ISO 17636-2 for RT-S (S = radioscopy) and RT-D (D = digital detectors).

4. **EN ISO 5817:2023 - Welding -- Fusion-welded joints in steel, nickel, titanium and their alloys (beam welding excluded) -- Quality levels for imperfections**

Scope of the Standard:
Document specifies quality levels of imperfections in fusion-welded joints (except for beam welding) in all types of steel, nickel, titanium and their alloys. It applies to material thickness > 0,5 mm.
It covers fully penetrated butt welds and all fillet welds. Its principles can also be applied to partial penetration buttwelds.
Quality levels for beam-welded joints in steel are presented in ISO 13919-1.
Three quality levels are given in order to permit application to a wide range of welded fabrication. They are designated by symbols B, C and D. Quality level B corresponds to the highest requirement on the finished weld.
Several types of loads are considered, e.g. static load, thermal load, corrosion load, pressure load.

Document is applicable to:
a) non-alloy and alloy steels;
b) nickel and nickel alloys;
c) titanium and titanium alloys;
d) manual, mechanized and automatic welding;
c) all welding positions;
f) all types of welds, e.g. butt welds, fillet welds and branch connections;
g) the following welding processes and their sub-processes, as defined in ISO 4063:
— 11 metal arc welding without gas protection;
— 12 submerged arc welding;
— 13 gas-shielded metal arc welding;
— 14 gas-shielded arc welding with non-consumable tungsten electrode;
— 15 plasma arc welding;
— 31 oxyfuel gas welding (for steel only).
Metallurgical aspects, such as grain size and hardness, are not covered by this document.

5. **EN 12732:2022 - Gas infrastructure -- Welding steel pipework -- Functional requirements**

Scope of the Standard:
Document contains requirements for the production and testing of weld joints for the installation and modification, including in-service welding, of onshore steel pipelines and pipework used in gas

The research leading to these results has received funding from Horizon 2020, the European Union's Framework Programme for Research and Innovation (H2020) under grant agreement n° 101111888.

infrastructure. This includes all pressure ranges and processed, non-toxic and non-corrosive natural gas according to EN ISO 13686 and non-conventional gases such as (injected) biomethane and hydrogen, where:
• the pipeline elements are made of unalloyed or low-alloyed carbon steel;
• the pipeline is not located within commercial or industrial premises as integral part of the industrial process on those premises except for any pipelines and facilities delivering gas to such premises;
• the pipework is not located within households or industrial installations according to EN 1775 or EN 15001;
• the design temperature of the system is between -40 °C up to and including 120 °C.
For injected biomethane or hydrogen a detailed technical evaluation of the functional requirements is required, ensuring there are no other constituents or properties of the gases that can affect the integrity of the pipeline.
This document specifies common basic principles for gas infrastructure.
It is intended to be applied in association with these national standards and/or Standards of practice setting out the above-mentioned basic principles.

In the event of conflicts in terms of more restrictive requirements in national legislation/regulation with the requirements of this document, the national legislation/regulation takes precedence as illustrated in CEN/TR 13737 (all parts].
NOTE CEN/TR 1 3737 (all parts) contains:

- clarification of relevant legislation/regulations applicable in a country;
- if appropriate, more restrictive national requirements;
- national contact point for the latest information.

6. **EN ISO 19232:2013 - Non-destructive testing - Image quality of radiographs**

   Scope of the Standard:

   Part 1: Determination of the image quality value using wire-type image quality indicators. This part specifies a device and a method for the determination of the image quality of radiographs using wire - type image quality.
   Part 2: Determination of the image quality value using step/hole-type image quality indicators. This part specifies a device and a method for determination of the image quality of radiographs using step/hole-type image quality indicators.
   Part 3: Determination of the image quality value using step/hole-type image quality indicators. This part specifies the minimum image quality values to ensure a uniform radiographic quality. It applies to the two types of quality indicators as detailed in Part 1 and 2 of this Standard and for two techniques described in ISO 5579. Values are specified for the two classes of radiographic technique specified in ISO 5579.'
   Part 4: Experimental evaluation of image quality values and image quality tables. This part gives instructions for determination of image quality values and image quality tables.
   Part 5: Determination of the image unsharpness and basic spatial resolution value using duplex wire-type image quality indicators. This part specifies a method of determining the total image unsharpness and basic spatial resolution of radiographs and radioscopic images.

7. **EN ISO 9712:2022 - Non-destructive testing -- Qualification and certification of NDT personnel**

   Scope of the Standard:

   Document specifies requirements for the qualification and certification of personnel who perform industrial non-destructive testing (NDT) including radiographic testing.
   NOTE 2 CEN/TR 14748 provides guidance on the methodology for qualification of non-destructive tests.

8. **EN ISO 17635:2025 - Non-destructive testing of welds - General rules for metallic materials**

   Scope of the Standard:

   Document gives guidelines for the choice of non-destructive testing (NDT) methods for welds in metals and for the evaluation of the results for quality control purposes, based on quality requirements, material, weld thickness, welding process and extent of testing.
   It also specifies general rules and standards to be applied to the different types of testing, for the selection of the method, the techniques and the acceptance levels.

The research leading to these results has received funding from Horizon 2020, the European Union's Framework Programme for Research and Innovation (H2020) under grant agreement n° 101111888.

The requirements specified in this document for acceptance levels for NDT conform with quality levels stated in ISO 5817 or ISO 10042 (moderate, intermediate, stringent) only on a general basis and not in detail for each indication.
In annexes, correlations between quality levels, testing levels and acceptance levels for specific testing techniques are given, also an overview on specific testing techniques of standards linked to quality levels, acceptance levels and testing methods.

9. EN 12681-1:2018 - Founding -- Radiographic testing -- Part 1: Film techniques

Scope of the Standard:

Document gives specific procedures for industrial X-ray and gamma radiography for discontinuity detection purposes, using NDT (Non-destructive Testing) film techniques. This part of EN 12681 specifies the requirements for film radiographic testing of castings.
Films after exposure and processing become radiographs with different area of optical density.
Radiographs are viewed and evaluated using industrial radiographic illuminators.
This part of EN 12681 also specifies the recommended procedure for the choice of operating conditions and radiographic practice.
These procedures are applicable to castings produced by any casting process, especially for steel, cast iron, aluminium, cobalt, copper, magnesium, nickel, titanium, zinc and any alloys of them.

This part of this European Standard does not apply to:
— radiographic testing of castings for aerospace **applications (see prEN 2002-21);**
— radiographic testing of welded joints (see EN ISO 17636-1);
— radiography with digital detectors (see EN 12681-2);
— radioscopic testing (see EN 13068, all parts).

10. EN 12681-2:2017 - Founding -- Radiographic testing -- Part 2: Techniques with digital detectors

Scope of the Standard:

This European Standard gives specific procedures for industrial X-ray and gamma radiography for discontinuity detection purposes, using NDT (non-destructive testing) digital X-ray image detectors.
This part of EN 12681 specifies the requirements for digital radiographic testing by either computed radiography (CR) or radiography with digital detector arrays (DDA) of castings.
Digital detectors provide a digital grey value image which can be viewed and evaluated using a computer.
NOTE This part of EN 12681 complies with EN 14784-2 for CR. Some clauses and annexes are taken from EN ISO 17636-2.
This part of EN 12681 specifies the recommended procedure for detector selection and radiographic practice. Selection of computer, software, monitor, printer and viewing conditions are important hut are not the main focus of this standard. The procedure specified in this standard provides the minimum requirements for radiographic practice which permit exposure and acquisition of digital images with equivalent sensitivity for detection of imperfections as film radiography, as specified in Part 1 of this standard.
This standard does not consider radiographic or radioscopic fitness for purpose testing as applied for specific castings based on manufacturers internal requirements and procedures.
The requirements on image quality in class A and B testing of Annex A consider the good workmanship quality for general casting applications as also required in Part 1 of this standard for film radiography.
The classes A and By\ reflect the quality requirements of current automated and semi-automated radiographic testing systems with DDAs and computer or operator based image evaluation, and mini or micro focus tubes (spot size < 1 mm) with reduced requirements to the unsharpness, but unchanged requirements to contrast sensitivity as also required in Part 1 of this standard for film radiography.
The specified procedures are applicable to castings produced by any casting process, especially for steels, cast irons, aluminium, cobalt, copper, magnesium, nickel, titanium, zinc and any alloys of them.
This part of this European Standard does not apply to:
— the testing of welded joints (see EN ISO 17636-2);
— film radiography (see EN 12681-1:2017);
— real time testing with radioscopy (see EN 13068-1; radioscopy with image intensifiers).

The research leading to these results has received funding from Horizon 2020, the European Union's Framework Programme for Research and Innovation (H2020) under grant agreement n° 101111888.

11. **EN 5579:2014 - Non-destructive testing -- Radiographic testing of metallic materials using film and X- or gamma rays -- Basic rules**

    Scope of the Standard:

    Document outlines the general rules for industrial X- and gamma- radiography for flaw-detection purposes, using film techniques, applicable to the inspection of metallic products and materials.
    It does not give acceptance criteria of the imperfections.

12. **EN 10893-6:2019 - Non-destructive testing of steel tubes -- Part 6: Radiographic testing of the weld seam of welded steel tubes for the detection of imperfections**

    Scope of the Standard:

    Document specifies requirements for film based radiographic X-ray testing of the longitudinal or helical weld seams of automated fusion arc-welded steel tubes for detection of imperfections.
    It can also be applicable to testing of circular hollow sections.

Acoustic Emission Standards

1. **EN 13554:2011 - Non-destructive testing - Acoustic emission testing - General principles**

   Scope of the Standard:

   Document specifies the general principles required for the acoustic emission testing (AT) of industrial structures, components, and different materials under stress and for harsh environment, in order to provide a defined and repeatable performance. It includes guidelines for the preparation of application documents, which describe the specific requirements for the application of the AE method.

2. **EN 1330-9:2017 - Non-destructive testing -- Terminology -- Part 9: Terms used in acoustic emission testing**

   Scope of the Standard:

   This European Standard is concerned only with terms used specifically in acoustic emission testing (AT) and these fall into four parts:
   a) terms relating to the physical phenomenon;
   b) terms relating to the detection of the acoustic emission;
   c) terms relating to the measured characteristics of the signal(s);
   d) terms relating to acoustic emission applications.

3. **EN 17391:2022-11 - Non-destructive testing -- Acoustic emission testing -- In-service acoustic emission monitoring of metallic pressure equipment and structures -- General requirements**

   Scope of the Standard:

   Document specifies general requirements for in-service acoustic emission (AE) monitoring. It relates to detection, location and grading of AE sources with application to metallic pressure equipment and other structures such as bridges, bridge ropes, cranes, storage tanks, pipelines, wind turbine towers, marine applications, offshore structures. The monitoring can be periodic, temporary or continuous, on site or remote-controlled, supervised or automated. The objectives of AE monitoring are to define regions which are acoustically active because of damage or defect evolution.

4. **EN ISO 18081:2016-08 - Non-destructive testing - Acoustic emission testing (AT) - Leak detection by means of acoustic emission**

   Scope of the Standard:

   Document specifies the general principles required for leak detection by acoustic emission testing (AT). It is addressed to the application of the methodology on structures and components, where a leak flow because of pressure differences appears and generates acoustic emission (AE).
   It describes phenomena of the AE generation and influence of the nature of fluids, shape of the gap, wave propagation and environment.
   The different application techniques, instrumentation and presentation of AE results are discussed. Also included are guidelines for the preparation of application documents which describe specific requirements for the application of the acoustic emission testing.
   Document also gives procedures for some leak-testing applications.

5. **EN 14584:2013-07 - Non-destructive testing - Acoustic emission testing - Examination of metallic pressure equipment during proof testing - Planar location of AE sources**

The research leading to these results has received funding from Horizon 2020, the European Union's Framework Programme for Research and Innovation (H2020) under grant agreement n° 101111888.

Scope of the Standard:

This European Standard describes the method for conducting acoustic emission testing (AT) of metallic pressure equipment during acceptance pressure testing using a planar location method. This standard is applicable also for subsequent tests for requalification. General principles of Acoustic Emissions are described
in EN 13554.

The objectives of the AE testing are to provide 100 % volumetric testing to define regions of the structure which are acoustically active with burst type AE, e.g. as a result of evolution of sub-critical discontinuities, thus increasing the reliability of the acceptance test. The test provides a reference map for comparison with results of future tests.

6. **EN 13477-1:2022-03 - Non-destructive testing - Acoustic emission - Equipment characterisation - Part 1: Equipment description**

   Scope of the Standard:

   This European Standard describes the main components that constitute an acoustic emission (AE) monitoring system comprising:
   - Detection,
   - Signal conditioning,
   - Signal measurement,
   - Analysis and output of results.

7. **EN 13477-2:2022-03 - Non-destructive testing -- Acoustic emission testing -- Equipment characterisation -- Part 2: Verification of operating characteristics**

   Scope of the Standard:

   This document specifies test routines for the periodic verification of the performance of acoustic emission (AE) test equipment, i.e. sensors, pre-amplifiers, signal processors, external parametric inputs.

   It is intended for use by qualified personnel to implement an automated verification process.

   Safety aspects of equipment for use in potentially explosive zones are not considered in this document.

Magnetic Particle standards

1. **EN ISO 17638:2017 - Non-destructive testing of welds -- Magnetic particle testing**

   Scope of the Standard:

   Document specifies techniques for detection of surface imperfections in welds in ferromagnetic materials, including the heat affected zones, by means of magnetic particle testing. The techniques are suitable for most welding processes and joint configurations. Variations in the basic techniques that will provide a higher or lower test sensitivity are described in Annex A.

   However, document does not specify acceptance levels of the indications, that is decribed in ISO 23278 or in product or application standards.

2. **EN ISO 9934-1:2017 - Non-destructive testing -- Magnetic particle testing -- Part 1: General principles**

   Scope of the Standard:

   Document specifies general principles for the magnetic particle testing of ferromagnetic materials. Magnetic particle testing is primarily applicable to the detection of surface-breaking discontinuities, particularly cracks. It can also detect discontinuities just below the surface but its sensitivity diminishes rapidly with depth.

   Document specifies also the surface preparation of the part to be tested, magnetization techniques, requirements and application of the detection media, and the recording and interpretation of results. Acceptance criteria are not defined.

   Document does not apply to the residual magnetization method.

The research leading to these results has received funding from Horizon 2020, the European Union's Framework Programme for Research and Innovation (H2020) under grant agreement n° 101111888.

3. **EN ISO 9934-2:2015 - Non-destructive testing -- Magnetic particle testing -- Part 2: Detection media**
   Scope of the Standard:
   This part of the ISO 9934 specifies the significant properties of magnetic particle testing products (including magnetic ink, powder, carrier liquid, contrast aid paints) and methods for checking their properties.

4. **EN ISO 9934-3:2015 - Non-destructive testing -- Magnetic particle testing -- Part 3: Equipment**
   Scope of the Standard:
   This part of ISO 9934 describes three types of equipment for magnetic particle testing:
   — portable or transportable equipment;
   — fixed installations;
   — specialized testing systems for testing components on a continuous basis, comprising a series of processing stations placed in sequence to form a process line.
   Equipment for magnetizing, demagnetizing, illumination, measurement, and monitoring are also described.
   This part of ISO 9934 specifies the properties to be provided by the equipment supplier, minimum requirements for application and the method of measuring certain parameters. Where appropriate, measuring and calibration requirements and in-service checks are also specified.

5. **EN ISO 23278:2015 - Non-destructive testing of welds -- Magnetic particle testing -- Acceptance levels**
   Scope of the Standard:
   This International Standard specifies acceptance levels for indications from imperfections in ferromagnetic steel welds detected by magnetic particle testing.
   The acceptance levels are primarily intended for use during manufacture examination. They can also be used for in-service inspection.
   The acceptance levels in this International Standard are based on detection capabilities that can be expected when using techniques specified in ISO 17638 and parameters recommended in Annex A. The acceptance levels can be related to welding standards, application standards, specifications or codes. Such a relationship is shown in ISO 17635 for ISO 5817.
   However, acceptance levels for grouped indications are not covered by this International Standard.

6. **EN 10228-1:2016 - Non-destructive testing of steel forgings -- Part 1: Magnetic particle inspection**
   Scope of the Standard:
   This European Standard describes techniques and acceptance criteria to be used for the magnetic particle testing of forgings manufactured from ferromagnetic materials. The method described is used for the detection of surface discontinuities. It can also detect discontinuities just below the surface but the sensitivity to such discontinuities decreases rapidly with depth.
   NOTE A steel forging is considered to be ferromagnetic if the magnetic flux density is greater than 1T for a tangential magnetic field strength of 2,4 kA/m.

All of the referenced standards were developed for general application and for materials traditionally used in the construction of gas pipelines. Although they are not specifically designed for hydrogen service, they provide an appropriate basis for evaluating the existing infrastructure for potential hydrogen integration.

The research leading to these results has received funding from Horizon 2020, the European Union's Framework Programme for Research and Innovation (H2020) under grant agreement n° 101111888.

3 Survey on Inspection Techniques and Non-Piggable Gas Pipelines

In the course of the realisation of the Task 3.2, the survey on the matter of unpiggables was performed. The survey was distributed among the TSOs and DSOs involved in the project. It consisted of 8 group of questions as listed in the Table 2.

The reason for conducting the survey was to inquire about the gas operators' attitude and experience with the unpiggable pipelines. Another important point was to check the application's history of several listed NDT inspection methods. The idea behind conducting the survey was to check whether there are similarities in these fields across different operators in Europe as well as to compare the attitude towards the unpiggable pipelines.

Table 2: Questions in the survey on Inspection Techniques and non-piggable gas pipelines

No.	Question
1.	Are newly built pipelines (in all cases - even short, small diameter wires) are in piggable design? If not, are there any stricter acceptance requirements during construction? In this case, for what lifetime will expected (will a complete reconstruction done at the end of the planned lifetime).
2.	How often the condition of non-piggable pipelines is being checked? What regulations require the inspection to be performed? [legislation, standard, internal regulation] What regulations contain the scope of the technical content to be performed?
3.	What inspections are performed as the part of the pipeline integrity? Are individual inspections on the case of crossings (e.g. leak measurement on the sniffers).
4.	Do you have experience or are you doing any of the following inspections? • Large Standoff Magnetometry Technology • Current Magnetometry Technology • Pulsed Eddy Current Technology • Guided Waves Technology • Long Range Ultrasonic Testing If other methods are used, please list them.
5.	If any of the type of inspection has been used as described in answer to question 6, is its result considered reliable or has any form of damage been revealed that the test method should have shown?
6.	In the case of non-piggable pipelines, on what basis are decisions made to make repairs (pipeline or coating) or to replace the pipeline?
7.	On what basis are the sites and the number of excavations determined? If an excavation is performed, how many pieces are performed per pipeline?
8.	Are excavation sites selected at random? If not, what are the criteria for designating the excavations? For the non- piggable pipelines, is a temporary pig trap used - if the pipeline could otherwise be piggable?

The research leading to these results has received funding from Horizon 2020, the European Union's Framework Programme for Research and Innovation (H2020) under grant agreement n° 101111888.

Sum-up of the results

The summary of the question 1:

The answer to the question number one shows the significant difference in the obligation of building new pipelines in the piggable design. The first group of answers pointed out that the generally the piggable is the obligation, however, usually with exceptions possible. The conditions or exceptions could be grouped as:

- Specific requirements to be met (MAOP>=24 bar, D>=8 in, L>=15km)
- The exception for the short pipelines (e.g. directly to the end-users) or pipelines with small diameters

The second group highlighted that there is no strict requirement for the piggable design of the pipelines, therefore not all of the newly built pipelines are of piggable design.

The last answer pointed out the specific situation, in which all newly built pipelines are not piggable. This is a direct outcome of the conditions for which these pipelines are built: mainly biomethane transport to existing pipelines. These pipelines are usually of relatively small diameters with insufficient flow for ILI testing.

When considering the designed lifetime for the pipeline the most usual answer was 40 years with one exception citing even longer period of time of 60 years.

The summary of the question 2:

The various condition for checking the unpiggables were listed:

- Condition checked with ACVG inspections every 5 years. Leakage gas detection and cathodic protection revision, just the same as for the piggables pipelines.
- Checks at least every 3 years. The requirements for checkings come from national regulations and related mandatory technical standards.
- No mandatory legislation for either ILIs or inspections of unpiggables. However, the actual exploitation follows the recommendations established in ASME B31.8 and NACE SP0502 Standard Practice – Pipeline External Corrosion Direct Assessment Methodology.
- The frequency of the condition checks is based on the legislation and standards including internal regulation about the exploitation of the transmission system. According to this internal regulation, check of the condition of the pipeline may be done with several methods: pedestrian inspection, air inspection, cathodic protection measurement, UT measurements.

Another answer pointed out the specific situation where the regulatory authority carries out regulatory and supervisory activities for, among others, natural gas. It includes the inspection activities.

One answer may be summarised as “not applicable”.

The summary of the question 3:

One answer to the question on the performed inspections was made as: “not applicable”. The answers from the rest of the operators varied, with listing a significant number of different inspection’s methods. Most frequent answers were:

- Verification of the effectiveness of the cathodic protections (x4)
- LDAR, including all the sniffers, leak detection (x3)
- External inspection, quarterly surveillance of the pipeline (x2)
- ACVG inspections (x2)
- DCVG inspections
- ILI
- Periodic tightness’ checks of pipe connections – through: air inspections as well as specific inspections with soil gas sampling probes
- ECDAs based on the results of the inspection methods described

The summary of the question 4:

The research leading to these results has received funding from Horizon 2020, the European Union's Framework Programme for Research and Innovation (H2020) under grant agreement n° 101111888.

The answer to the question number 4 was consistent among the questioned operators, as there was no experience with the listed technologies. The other methods used that were listed by one of the operators were DCVG and MMM.

The summary of the question 5:

The usual answer to the question number 5 was, taking into account the most frequent answer to the previous question – not applicable. The one answer stated that the results from the DCVG may be seemed as reliable, however, the MMM results are not yest considered in the same way.

The summary of the question 6:

The answers to the question number 6 varied with different operators. The cited reasons for the repairs or pipeline's replacement were:

- After the ACVG inspection, there is performed an excavation sampling
- In case of a leakage or a failure
- Regulatory obligations, infrastructure development and upgrading plans, failure rate analysis
- Based on NACE SP0502 and ASME B31.8 criteria: %IR, defect type, remaining thickness, calculated pipe's life
- Based on the pipeline's condition assessment, which takes into account the results of the cathodic protection, including DCVG, together with the excavations and additional UT testing.

There were also answers that may be summarised as "not applicable".

The summary of the question 7:

The answers listed a series of possible criteria for the determination of the sites for the excavations:

- Indications from cathodic protection and ILI
- Depending on the pipeline's age, presence of stray currents, soil aggressiveness, existence of AC, size of the defect, high humidity, area with a high number of affections
- Depending on the criticality of the defect and the estimated pipeline's life based on the MAOP, pipeline's remaining thickness, defect propagation velocity, orientation and location of the defect in the pipeline.

As for the information about the excavations the answers differred:

- it is decided depending on the previous experiences
- or the pipeline is excavated either in the direct location of the defect or on the longer section if the pipelines lies in the unfavourable/challenging conditions, e.g. in the wetlands, crossings with the rivers,
- or the excavations are always performed with a length that reaches two welds before and after the situation of the defect (or corrosion) detected. In the second situation, in case the defect is located in the weld, 6 meters are opened on each side of the weld.

There were also answers that may be summarised as "not applicable".

The summary of the question 8:

Generally, the answers were negative to both questions. Excavations are based on observations from cathodic protection surveys or ILI or on the % of IR or expected lifetime remained. The common point is that the places are not chosen at random, rather they are selected depending on the criteria (pipeline age, size of the defect etc.). Moreover, generally no temporary traps are used, however, one answer confirming that the pig traps are used for inspection of the pipelines with the pigs.

There were also answers that may be summarised as "not applicable".

Conclusions from the survey – similarities and differences around the Europe; what the results tell us with the matter of the project

The survey among the operators from the SHIMMER project gives an interesting insight into the unpiggable pipelines and NDT methods usage across Europe. The most important thing to start with is that not all of the

The research leading to these results has received funding from Horizon 2020, the European Union's Framework Programme for Research and Innovation (H2020) under grant agreement n° 101111888.

operators have the obligation to make new pipelines piggable. In some cases there are the exact conditions from which the piggable design is an obligation, however, other answers pointed out that there is no strict requirement for the piggable design. In specific cases it was mentioned that newly built pipelines were not of piggable design. As the most important reason for such situation the conditions of the pipeline and flow were mentioned – mainly short sections of pipelines and insufficient flow for ILI testing. The important conclusion from this part of the survey is that the unpiggable pipelines will not disappear and will be a part of the system in the upcoming years, and the proper way to handle their management is of great importance.

Summary of Information on NDT

If unpiggable pipeline exists in the system, then the way to handle its safe exploitation in most cases share much similarities among operators. DCVG/ACVG methods are commonly used, together with the cathodic protection's effectiveness verification. Air or pedestrian inspections and leak detection campaigns are made as well, however, this could find only already damages pipelines, thus occurrence of the leakage. From the other mentioned NDT inspection techniques only Metal Magnetic Memory was selected as being used by one of the operators. From this it occurs that, currently, the pipeline's integrity is being verified by methods that base rather on the information about the insulation condition and verification of leakage's occurrence. The methods that may give insight into the pipe's condition by checking its stress and/or stress concentration zones are currently not widely used.

Summary of Information on Excavations

When considering the excavations, one common conclusion might be that in general, the sites for the excavations are not selected in random. As obvious as it may seem, it is worth noting that the differences occur in the matter of the criteria for the sites' selections. Possible criteria are: results from the cathodic protection, ILI surveys, %of the IR factor among others. There is also no one common standard for performing the excavations. Different answers show that operators' standards in making an excavation differ, each making it according to its best practice, knowledge and experience.

The research leading to these results has received funding from Horizon 2020, the European Union's Framework Programme for Research and Innovation (H2020) under grant agreement n° 101111888.

4 Description of technologies tested within the project

4.1 Magnetic Flux Leakage (MFL)

4.1.1 MFL methodology

Magnetic Flux Leakage (MFL) is a non-destructive testing (NDT) method used to detect corrosion, pitting and other defects in steel structures like pipelines. The basic principle involves magnetizing the steel pipe and then detecting the leakage field that occurs at areas where there are either metal loss or defects. A powerful magnet is used to magnetize the steel and a magnetic detector is placed between the poles of the magnet to detect the leakage flux. MFL tools move inside the pipeline to perform inspections. These tools can operate in both gas and liquid pipelines and are equipped with high-resolution sensors to detect defects. The data collected by MFL tools is analysed to localize, identify and assess the severity of defects and estimate the depth and size of the metal loss. Engineers can use this information to determine the integrity of the pipeline and prioritize repairs [1].

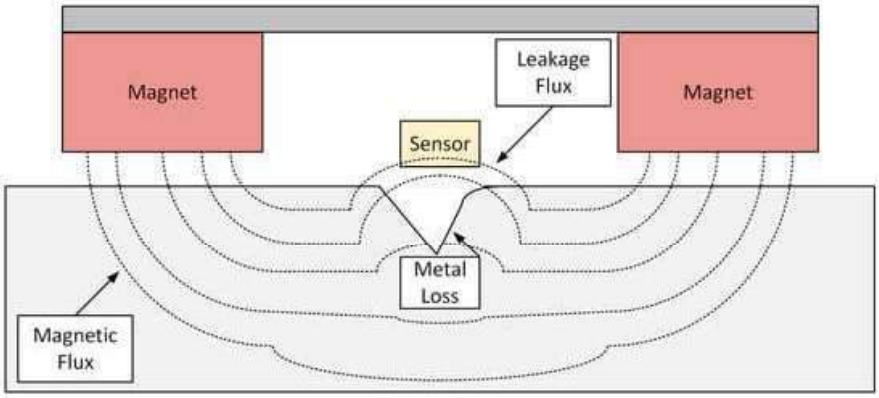

Figure 4-1: The working principle of an MFL sensor [1]

Types of defects that can be discovered

MFL tools can detect a range of defects, including:

- Both internal and external **corrosion**.
- Small, localized areas of metal loss – **pitting.**
- Axial and circumferential **cracks**.
- **Defects in the welds** of the pipeline.
- Dents, wrinkles, and buckles **- geometric anomalies**.

The research leading to these results has received funding from Horizon 2020, the European Union's Framework Programme for Research and Innovation (H2020) under grant agreement n° 101111888.

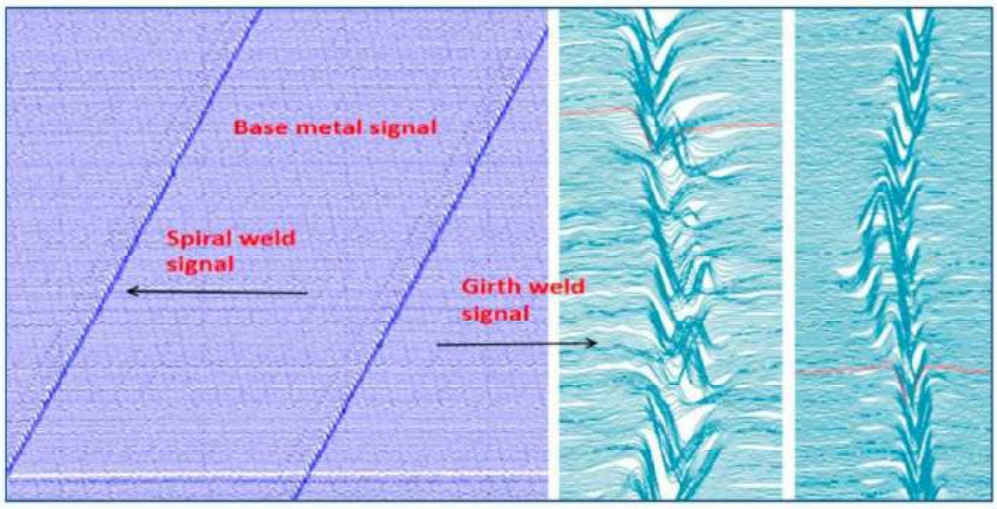

Figure 4-2: A schematic diagram of the defects detected via internal MFL detection [1]

Figure 4-3: Example of external corrosion defects detected via MFL [2]

The research leading to these results has received funding from Horizon 2020, the European Union's Framework Programme for Research and Innovation (H2020) under grant agreement n° 101111888.

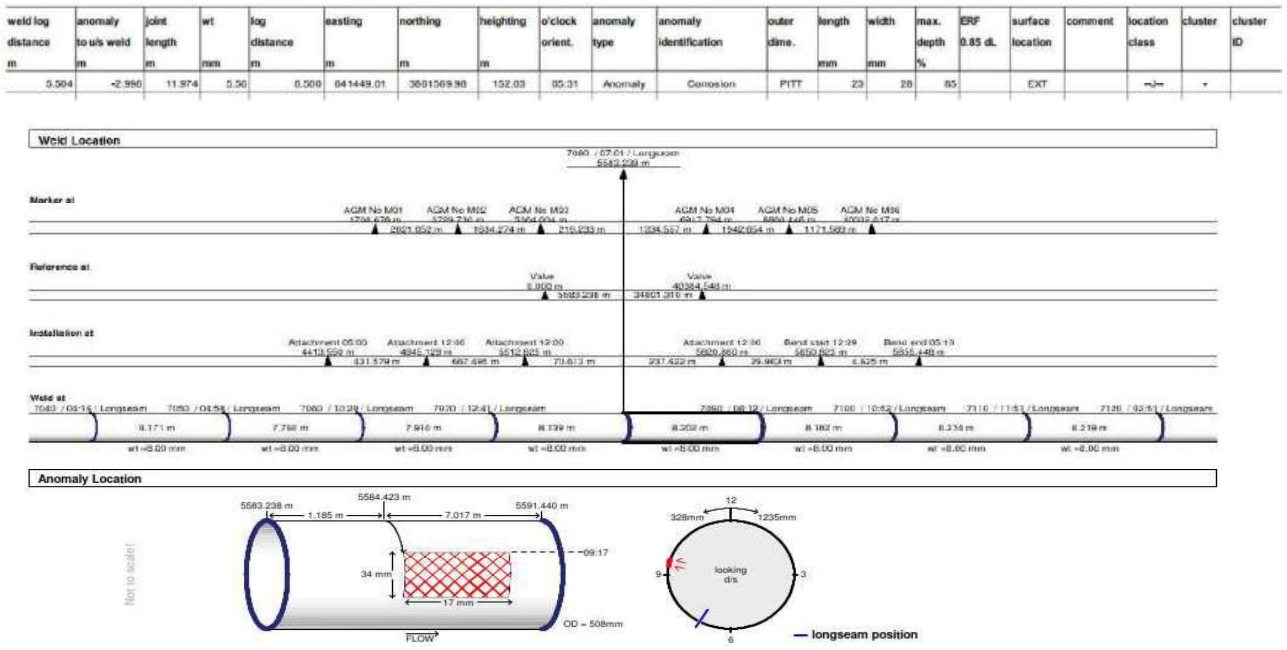

Figure 4-4: The example of the detailed reports from MFL survey [3]

4.1.2 Advantages and disadvantages

Benefits

1. MFL tools provide precise detection and sizing of metal loss, making them highly reliable for identifying defects.
2. Inspections can be performed while the pipeline is in operation, reducing the need for shutdowns and minimizing disruption to service.
3. MFL tools can inspect pipelines at high speed without compromising data accuracy, allowing for quick and comprehensive assessments.
4. Available advanced software which provides short-time analysis of inspection data, enabling prompt decision-making for maintenance and repairs.

Threats

1. Due to the orientation of the magnetic field, some defects could not be detected. Traditional MFL tools are less effective at detecting axially aligned cracks. These cracks run parallel to the pipeline's axis and do not significantly disrupt the magnetic field, which makes them harder to be detected.
2. Inspections of small-diameter pipelines can also be difficult due to less space and pipeline’s geometry.
3. The effectiveness of MFL is influenced by the magnetic properties of the pipeline material. Variations in material properties can affect the accuracy of the defect’s detection.
4. MFL is generally more sensitive to surface and near-surface defects. Detecting deeper cracks can be challenging, as the magnetic flux leakage signal diminishes with depth.
5. Analysing MFL data requires highly skilled and experienced personnel, as the interpretation of magnetic flux leakage signals can be complex and may lead to misinterpretation.
6. After MFL inspection pipelines are highly magnetized, which can be a problem for welding if any repairs are needed. This also affects results of other NDT methods based on metal magnetization i.e. MMM, SCT.

The research leading to these results has received funding from Horizon 2020, the European Union's Framework Programme for Research and Innovation (H2020) under grant agreement n° 101111888.

4.1.3 Hydrogen

While MFL has its limitations, it remains a valuable tool for pipeline inspection, especially when used in conjunction with other inspection technisssques to ensure comprehensive pipeline structural integrity assessments, ensuring it can withstand the specific challenges posed by hydrogen transport.

The minimum crack size that can be detected by Magnetic Flux Leakage (MFL) tools varies depending on several factors, including the tool's design, the pipeline material and the orientation of the crack. Generally, MFL tools can detect cracks with a minimum depth of around 1-2 mm and a length of approximately 20-30 mm. MFL may struggle to detect very small or fine cracks. These minor flaws might go unnoticed, potentially allowing them to develop into more significant issues over time especially under Hydrogen penetration. The values described above are based on information provided by ILI technology providers, who maintain their own technical catalogues, technical specifications, and accuracy data related to their tools. These specifications are typically provided to gas network operators under NDAs, so we provide generalized values in this report without citing the source.

Recent advancements have also improved the ability of MFL tools to detect cracks:

- Circumferential MFL: This method orients the magnetic field around the pipe, enhancing the detection of axial defects, including cracks.
- Combined Methods: Using a combination of axial and circumferential MFL methods, along with high- and low-magnetization technology, can enhance the detection and sizing accuracy of cracks.

With the widespread adoption of new tools, pigging diagnostics will increasingly meet the demand for pipeline condition analyses in the context of hydrogen transport, so pipeline operators can effectively prepare and maintain pipelines for the safe and efficient transport of hydrogen, addressing both existing and potential issues.

Figure 4-5: Circumferential MFL (MFL-C) from ROSEN [4]

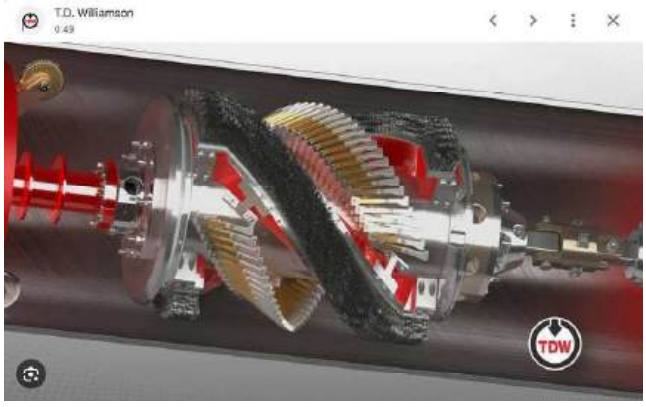

Figure 4-6: Circumferential MFL (SpirALL®) from T.D. Williamson [5]

The research leading to these results has received funding from Horizon 2020, the European Union's Framework Programme for Research and Innovation (H2020) under grant agreement n° 101111888.

Norms and Standards

Several standards govern the use of MFL tools for pipeline inspection:

- **API 1163**: This standard covers the use of inline inspection (ILI) systems for onshore and offshore gas and hazardous liquid pipelines.
- **ASTM E570-09**: Standard Practice for Flux Leakage Examination of Ferromagnetic Steel Tubular Products.
- **BS EN 10246-4**: Non-destructive Testing of Steel Tubes—Automatic Full Peripheral Magnetic Transducer/Flux Leakage Testing of Seamless Ferromagnetic Steel Tubes.
- **POF 100**: Specifications and requirements for in-line inspection of pipelines, provided by the Pipeline Operators Forum.
- **National standards and requirements**.

4.2 The Acoustic Emission Method (AE)

The Acoustic Emission Method (AE) is currently a recognized examination technique used in the diagnostics of civil and industrial engineering structures. Every year, numerous publications on its application are produced by research centers worldwide. The term “acoustic emission” (AE) is used to describe the phenomenon of generating elastic waves in solids and liquids. The sources of these waves include processes such as the formation of microcracks, the creation and disappearance of dislocations, as well as the mutual movement of fragments of the tested element combined with friction. In principle, all materials, including steel, emit elastic (resonant) waves under applied load. There are many phenomena that, by generating elastic waves, can be studied using the acoustic emission method. Among them are plastic deformation (e.g., dislocation slip or twinning), crack initiation and growth, material degradation processes, and phase transformations within the material structure (e.g., rapid martensitic transformations). One of the main sources of acoustic emission in metals is dislocation movement, particularly when accompanied by significant accelerations or decelerations. Under very high external loads, the maximum dislocation velocity approaches the speed of sound. Under moderate loads, it is much lower, reaching even half the speed of sound. Due to the dependence of acoustic emission on the degree of plastic deformation, its rate of increase, and the volume of metal in which the deformation occurs, even during uniaxial tension, several typical variants of AE characteristics as a function of RMS can be observed, as described later in the text. While metal deformation itself produces relatively weak acoustic emission, crack initiation and propagation generate strong AE signals. These signals are proportionally more intense in brittle materials, those with lower ductility and higher durability. The figure below (Fig. 7) presents a schematic representation of acoustic emission.

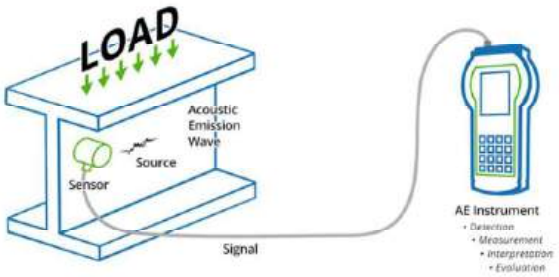

Figure 4-7: Representation of acoustic emission occurrence and detection [6]

The Acoustic Emission Method in the inspection of structures and equipment made of steel materials is classified as a non-destructive testing (NDT) technique. Unlike the most commonly used NDT methods; such as visual, penetrant, magnetic particle, ultrasonic, and radiographic testing; which rely on interactions of

The research leading to these results has received funding from Horizon 2020, the European Union's Framework Programme for Research and Innovation (H2020) under grant agreement n° 101111888.

various physical phenomena with material discontinuities and defects, the acoustic emission method involves passive signal recording. The devices used for acoustic emission monitoring do not emit any signals; instead, they record physical phenomena occurring within the tested object. During acoustic emission testing of structures or equipment, "active" discontinuities are detected; such discontinuities that, under specific operating conditions, exhibit a tendency to alter the stress distribution within the internal structure of the material from which the structure or equipment is made. This is a significant and distinguishing factor that sets acoustic emission testing apart from other NDT methods.

5.1.2.1. AE types of signals.

During acoustic emission measurements, the following types of recorded signals are distinguished. The signals are described below and shown in Figure 8.

1. Hit, an acoustic emission signal that exceeds the preset detection threshold and triggers data acquisition by the system.
2. Amplitude, the highest measured voltage in the waveform, directly related to AE energy. Amplitude is often expressed in decibels (dB) or millivolts (mV).
3. Duration Time, the time interval between the first and last threshold crossing by the AE signal. Duration is typically expressed in microseconds (μs).
4. Rise Time, the time between the AE signal trigger and its peak amplitude. Like duration, rise time is usually expressed in microseconds (μs).
5. Counts, the number of threshold crossings by the AE signal, used to quantify hit strength and acoustic emission activity.
6. Counts to Peak, the number of counts between the initial threshold crossing and the peak amplitude.
7. RMS, a statistical measure defined as the square root of the mean of the squared AE hit amplitudes. The RMS value of AE hit amplitude is commonly used because it is unambiguous and physically meaningful. RMS is typically measured on a linear scale and expressed in volts, similar to amplitude units.
8. ASL, a statistical measure defined as the average amplitude of the AE signal. Since ASL considers amplitude on a logarithmic scale, it must be expressed in decibels (dB).
9. Energy, the measured area under the rectified signal envelope (MARSE), with units typically based on the AE data acquisition method. Energy is generally proportional to the voltage and duration of the AE signal (energy count) and is widely used in acoustic emission measurements due to its sensitivity to both signal amplitude and duration.

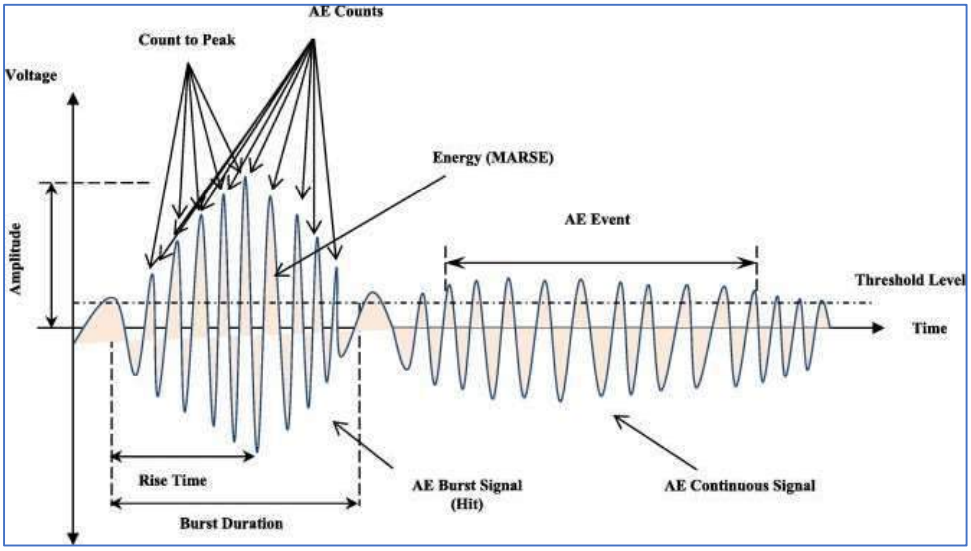

Figure 4-8: The AE signal parameters [7]

The formal procedure for testing steel structures and equipment is described in the European standard EN 13554. This standard outlines the general principles governing the application of acoustic emission for testing

The research leading to these results has received funding from Horizon 2020, the European Union's Framework Programme for Research and Innovation (H2020) under grant agreement n° 101111888.

industrial structures, equipment components, and various other materials subjected to load or environmental conditions that induce internal stresses, with the aim of determining their operational parameters. The standard provides guidelines for preparing application documents related to the requirements for using acoustic emission methods. In the case of acoustic emission testing of typical, regular structures such as pressure equipment or pressure vessel shells, the AE acoustic wave propagates from a source located directly within the material (steel) and is converted into an AE signal by sensors placed on the surface of the tested equipment wall. This signal is then recorded and processed by the measurement system of the acoustic emission testing setup. As shown in the figure (Fig. 9) below:

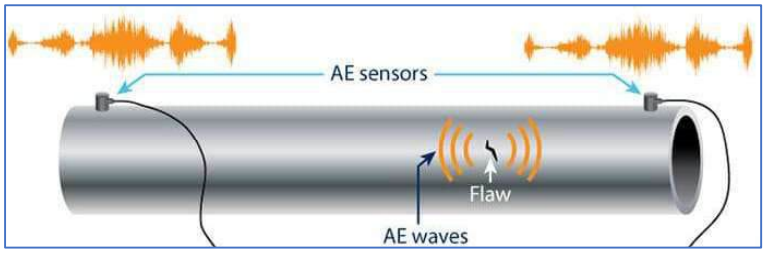

Figure 4-9: Acoustic Emission Testing [8]

In this case, acoustic emission in the form of elastic waves is generated by surface and internal discontinuities present in the material of the pipe or vessel wall, in welded joints, and other components of the tested equipment, subjected to a stimulus in the form of a load (e.g., pressure) established during the test, which results from the release of energy within the material. The situation is different when testing the bottoms of pressure vessels using the acoustic emission method (Fig. 10). In this case, the acoustic wave propagates from a source located at the bottom, through the stored medium (usually liquid), to the vessel wall, where sensors are arranged on its outer surface around the entire circumference according to an appropriate scheme. The acoustic signal is then recorded and processed by the measurement system. For such case, acoustic emission in the form of elastic waves is generated primarily by corrosion processes in the vessel's bottom material (steel) and/or leaks in the bottom, and additionally by surface and internal discontinuities present in the material of the tested bottom or by cracks resulting from material corrosion. The applied stimuli are the maximum load of the tested vessel caused by the pressure of the stored medium (liquid or gas) and any aggressive corrosive environment. These tests therefore differ from each other in measurement methodology, scope, and purpose. Testing a pressure device or the shell of a storage vessel aims to detect and simultaneously locate sources generating acoustic emission signals caused by surface and internal discontinuities in the base material and welded joints of the tested equipment walls. In contrast, testing the bottom of a storage vessel aims to detect and locate sources of AE signals caused by active corrosion processes and/or leaks.

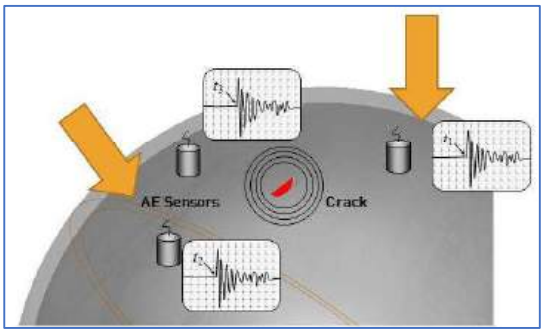

(a)

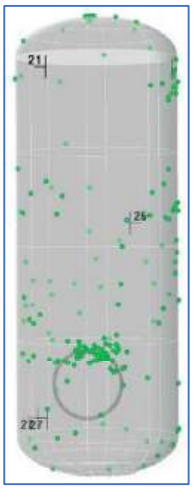

(b)

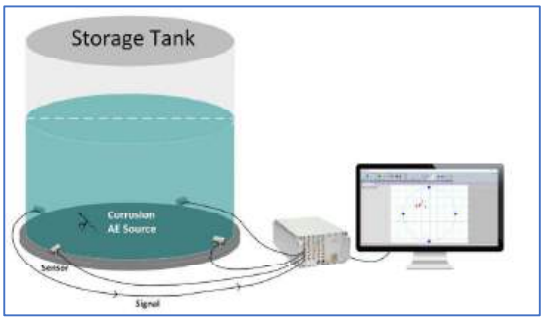

(c)

The research leading to these results has received funding from Horizon 2020, the European Union's Framework Programme for Research and Innovation (H2020) under grant agreement n° 101111888.

Figure 4-10: AE testing: (a) tank bottom plate corrosion detection and location [9], (b) sensor response [6], (c) visualization of material's defects distribution

metallic pressure equipment during proof testing – Planar location of AE sources", it is possible to classify acoustic emission sources in tests of tanks and pressure equipment that represent potential defects occurring in walls, welded joints, and components of the tested equipment shell subjected to load during the test. The standards generally indicate three groups of acoustic emission sources:

a) Class I sources – of minor importance; no further action is required, only monitoring and verification of their development during subsequent tests.

b) Active sources – recommended for verification using other non-destructive testing methods, selected depending on the relationship between the source location and characteristic elements of the tested tank or pressure equipment (e.g., welds, nozzles, supports, etc.).

c) Highly active sources – which determine whether the tested objects can be returned to initial or continued operation; these must undergo additional evaluation using other appropriate non-destructive testing methods, depending on the relationship between the source location and characteristic elements of the tested tank or pressure equipment.

For tests aimed at detecting possible leaks or corrosion processes in tank bottoms, the guidelines of EN 13554 are also applied in conjunction with EN 15856 "Non-destructive testing – Acoustic emission – General principles of AE testing for corrosion detection in a liquid-filled metallic environment", as well as EN ISO 18081 "Non-destructive testing – Acoustic emission – Leak detection using acoustic emission" and EN ISO 8044 "Corrosion of metals and alloys – Basic terms and definitions". Based on the guidelines of these standards, in addition to detecting leaks, it is possible to identify and locate in tank bottoms and in the near-wall zone leaks or elements directly in contact with the stored material that act as sources of acoustic emission, as well as AE sources caused by corrosion processes.

The analysis assumes the use of the acoustic emission method to assess the technical condition of natural gas pipelines during their operation. For this purpose, it is necessary to consider the applicability of acoustic emission for identifying and locating defects characteristic of steel pipeline structures, including the possibility of detecting defects typical of hydrogen-induced corrosion that manifest as cracks.

As demonstrated by Baensch F. in his work [9,10] four-point bending tests were carried out to analyze the acoustic characteristics of damage evolution in steel pipe segments of grade S355J2H, with a length of 2.5 m, an outer diameter of 168 mm, and a wall thickness of 16 mm. To induce stable crack growth, the pipe segments were pre-damaged by introducing a 90-degree circumferential notch at the midpoint of the pipe length. As a result of static bending loads applied to the pipes, microscopic damage and plastic deformations accumulated, forming a macroscopic crack that propagated through the pipe wall until a pressurized medium leak occurred. Four broadband VS 900 M sensors were installed near the notch to monitor acoustic emission. The possibility of describing phenomena such as initial cracking and damage accumulation was investigated, among others, using the acoustic emission technique. Based on the tests performed, it was confirmed that the acoustic emission method is sensitive to detecting the crack initiation stage. The formation of mesoscale and macroscale cracks, as well as their closure and the resulting friction, generate weighted peak frequencies of acoustic emission below 400 kHz, while microscopic cracks generate AE with broadband spectra identified by weighted peak frequencies above 400 kHz. Critical states, such as maximum load level and leak opening, were associated with peak amplitudes exceeding 85 dBAE. The conducted research indicates the possibility of developing a database that could be used to design advanced detection and alarm strategies based on acoustic monitoring of steel structures, including steel pipelines.

In the analysis performed, only AE events detected by all four sensors used (localized events, LEV) were evaluated. AE events were located on the pipe surface in a 2D arrangement (Figures 11 and 12). The localization algorithm was based on the determined AE wave propagation velocity in the defined plane, which was 4695 m/s, with other additional parameters of acoustic emission signal recording established.

The research leading to these results has received funding from Horizon 2020, the European Union's Framework Programme for Research and Innovation (H2020) under grant agreement n° 101111888.

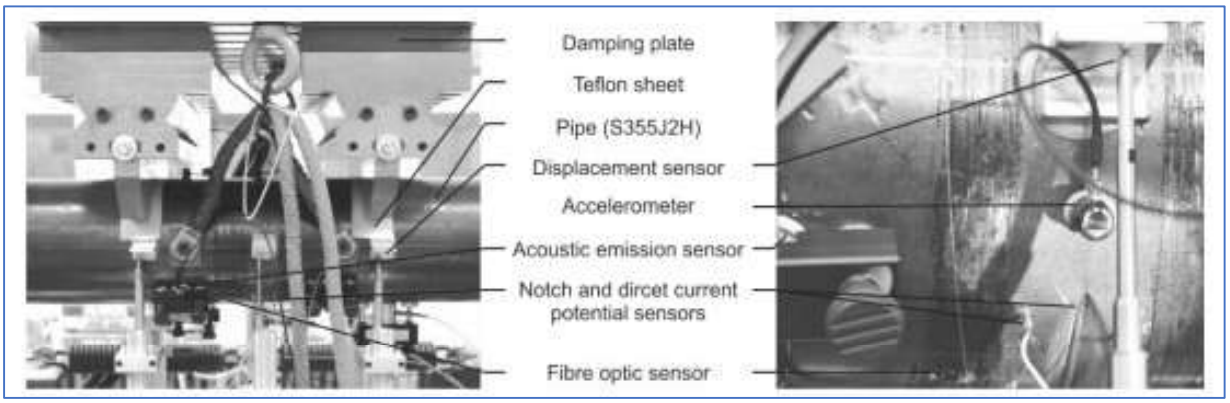

Figure 4-11: Stress experiments performed on a pipe in the work of Baensch F. [10,11]

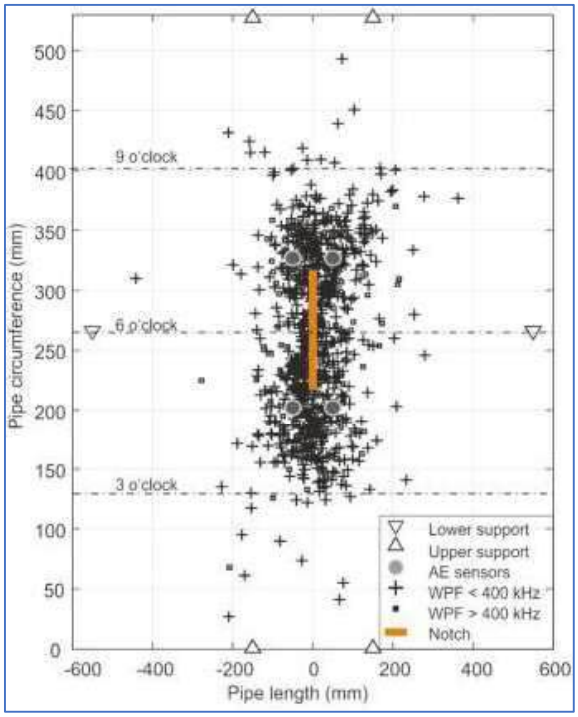

Figure 4-12: Results of experimental investigations, Baensch F. [10,11]

The use of AE for quantitative characterization of microscopic damage behavior in the form of cracks revealed structural changes occurring in the pipeline segment under stress. Crack initiation was recorded at stresses induced by a force of 527 kN (79% Fmax). The recorded signals are shown in Figure 14. The studies demonstrated that the sensitivity of detecting small cracks using the acoustic emission method was also dependent on far-field attenuation between the AE event location and the AE sensor. Comparison with another research [11] showed that increasing the distance between the sensor and the notch negatively affects the sensitivity of detecting small, initial cracks. The chart below (Fig. 13) shows the relationship between the applied load (kN) over time on the pipe and the amplitude height of AE.

The research leading to these results has received funding from Horizon 2020, the European Union's Framework Programme for Research and Innovation (H2020) under grant agreement n° 101111888.

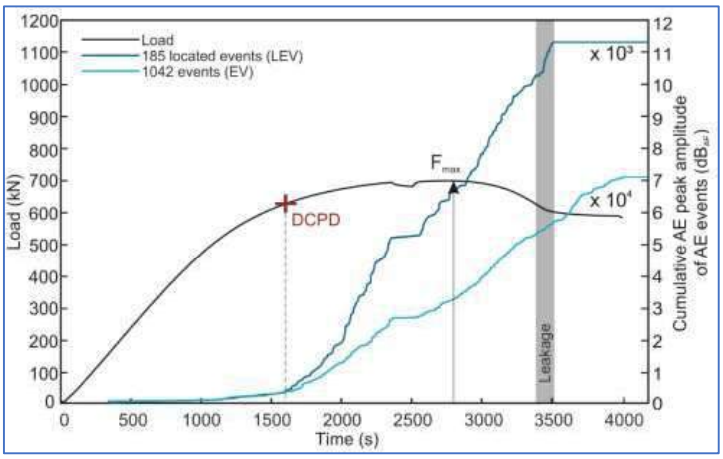

Figure 4-13: Relationship between applied load over time and acoustic emission amplitude during pipe testing. [12]

Based on the research conducted by Reed et al. in the article *Passive Wall Thickness Monitoring Using Acoustic Emission Excitation* [13], it was concluded that, the feasibility of using passive acoustic emission transducers for measuring the wall thickness of a steel pipeline was investigated, utilizing the fact that active pulse-echo measurements can be approximated through autocorrelation of scattered acoustic waves generated by the flow of the transported medium. Experimental measurements were presented using acoustic emission originating from compressed air flow as the excitation source. The results showed very good agreement with active measurements performed using ultrasonic methods for inspecting thick-walled components, i.e., where the element thickness exceeds the ultrasonic wavelength, as well as with resonant ultrasonic spectroscopy for thinner wall thicknesses. Figure 14 shows a comparison between active measurement and the autocorrelation function of passive measurement obtained using a custom-built amplifier and a piezoelectric disk attached to the tested aluminum block. (a) represents the raw RF signal from the passive measurement. (b) is a fragment of (a). (c) shows the comparison of the autocorrelation function of the passive measurement with the active measurement. (d) is a fragment of (c). Active and passive measurements were amplitude-normalized to the peak of the first arrival.

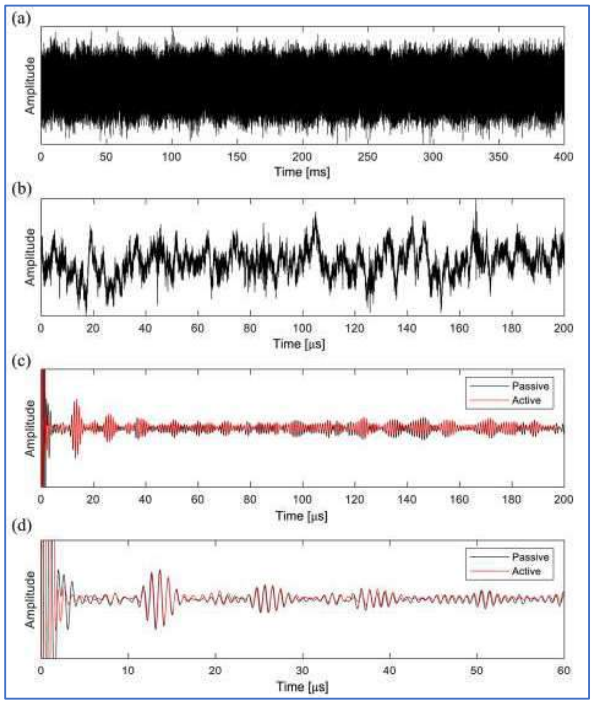

Figure 4-14: Comparison of active measurement with the autocorrelation of passive measurement using a custom amplifier and piezoelectric disk [13]

The research leading to these results has received funding from Horizon 2020, the European Union's Framework Programme for Research and Innovation (H2020) under grant agreement n° 101111888.

As demonstrated in the study *Fatigue crack extension and acoustic emission response law of 316L austenitic stainless steel by hydrogen charging* by He S. et al. [12]: Fatigue tests were conducted on samples of 316L austenitic stainless steel at three different stress levels, both on untreated samples and samples electrochemically charged with hydrogen. Acoustic emission signals were monitored during tests. The results confirm that both the hydrogen environment and stress are the main factors reducing the fatigue life of 316L austenitic stainless steel, and their synergistic interaction accelerates material damage. Hydrogen charging alters the fatigue crack propagation mechanism in 316L stainless steel, increasing the randomness of the crack growth path due to the rising number of secondary cracks in hydrogen-charged samples. During fatigue cracking, the energy release rate of AE signals showed a linear positive correlation with the fatigue crack growth rate. Under lower stress conditions, hydrogen-charged samples exhibited higher fatigue crack propagation rates, with hydrogen remaining as the dominant factor influencing crack initiation. Based on the recorded signals, a quantitative model of AE parameter characteristics was developed, suitable for hydrogen embrittlement environments but insensitive to mean fatigue stress, enabling calculation of fatigue crack growth rates. This study revealed the behavior of fatigue cracks and damage mechanisms in hydrogen-charged 316L stainless steel and confirmed the ability to record AE signals originating from fatigue crack formation progressing with increasing fatigue cycles of the tested material samples.

Figure 15 shows the characteristics of fatigue crack growth induced by applied stress. The logarithmic scale graph presents the relationship between the stress intensity factor and the fatigue crack growth rate for the original sample and the hydrogen-charged sample at a given mean stress. The relationship between the stress intensity factor range (K) and fatigue crack growth (da/dn) follows the three-stage Paris model of fatigue crack propagation. Due to hydrogen embrittlement effects, hydrogen-charged samples in stages II and III exhibit a reduced range of stress intensity factor variation compared to original samples, resulting in shorter fatigue life. Figure 16 shows examples of changes in AE signal amplitude during three different phases of fatigue crack propagation. Figure 17 illustrates the linear proportional relationship between the propagation rate of fatigue cracks and the cumulative energy growth rate of AE signals. Furthermore, according to the graph, hydrogen-charged samples exhibit a significantly higher number of instantaneous energy peaks that can be recorded. This confirms the feasibility of predicting fatigue crack length growth in steel materials in real time, up to complete sample failure, based on AE signals.

In summary, this study indicates that the energy release rate of AE signals and the fatigue crack growth rate are always linearly positively correlated under different mean fatigue stresses. At a mean stress of 167 MPa, hydrogen-charged samples showed a higher fatigue crack growth rate than original samples at the same AE energy release rate. After reaching the intersection point, the crack growth rate of original samples exceeded that of hydrogen-charged samples at the same AE energy release rate. When using AE energy release rate to quantitatively predict fatigue life, applying a single critical warning threshold was insufficient for 316L austenitic stainless steel in both hydrogen and non-hydrogen environments. The observed differences in AE signal registration between samples developing hydrogen-induced cracks and original samples confirm the effectiveness of acoustic emission in such studies.

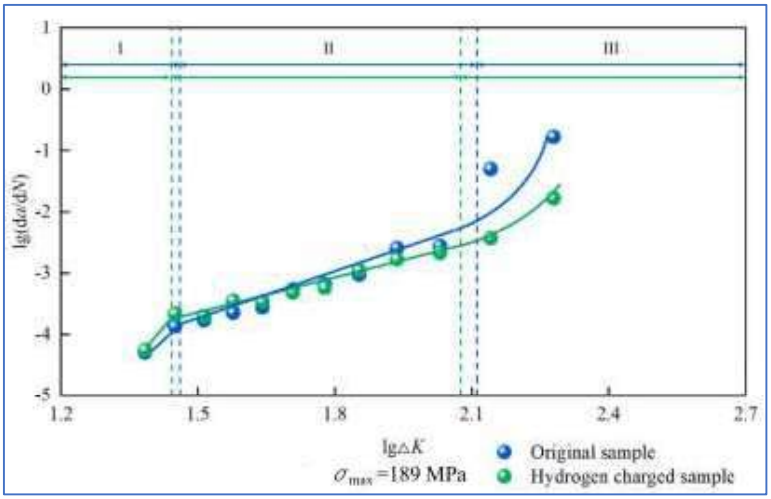

Figure 4-15: Characteristics of fatigue crack growth induced by applied stress. [12]

The research leading to these results has received funding from Horizon 2020, the European Union's Framework Programme for Research and Innovation (H2020) under grant agreement n° 101111888.

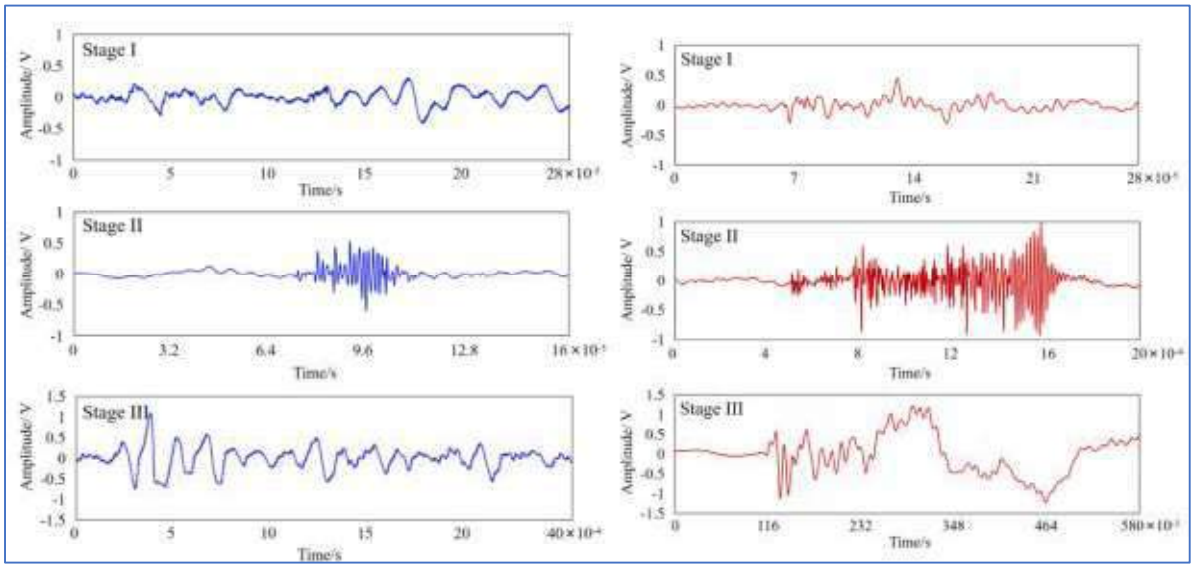

Figure 4-16: Variations in acoustic emission signal amplitude across three distinct phases of fatigue crack propagation [12]

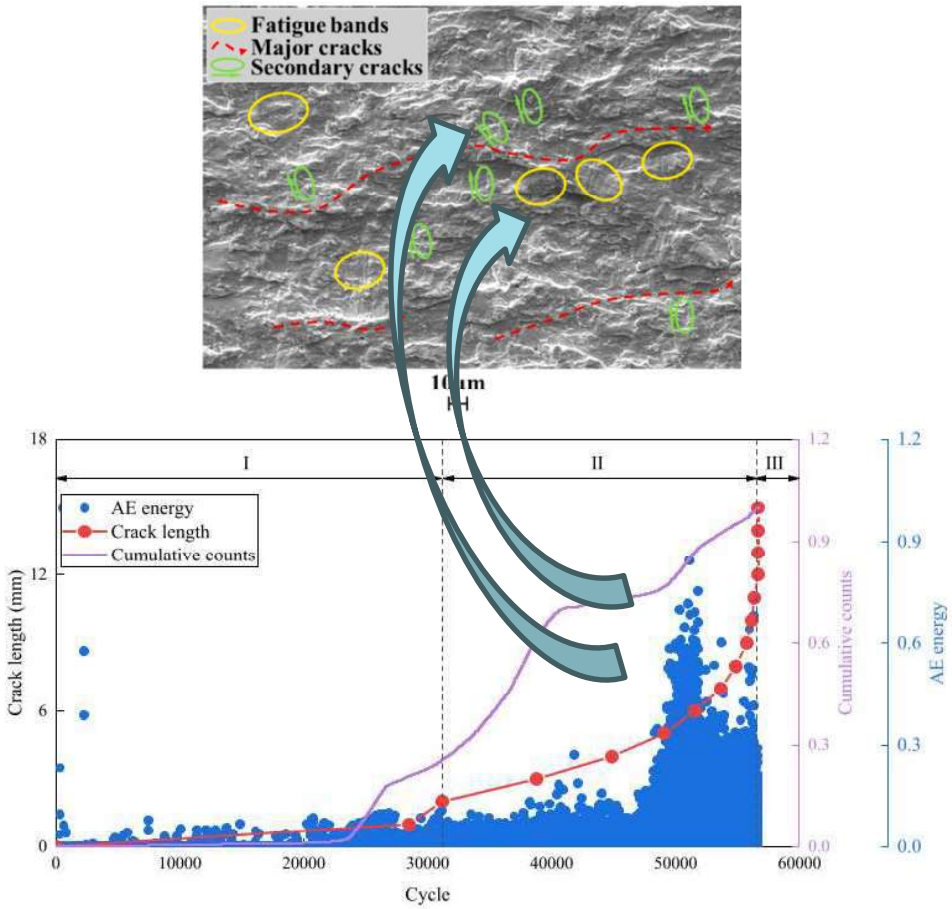

Figure 4-17: Relationship between the propagation rate of fatigue cracks and the cumulative growth rate of acoustic emission signal energy [12]

The research leading to these results has received funding from Horizon 2020, the European Union's Framework Programme for Research and Innovation (H2020) under grant agreement n° 101111888.

The study by He et al. [12] focused on austenitic stainless steel, whereas similar tests for X65 steel, manufactured according to API-5L specifications and used for natural gas pipelines, were conducted by Rahimi et al. [14] In this research, the susceptibility of API X65 pipeline steel to hydrogen embrittlement (HE) was assessed by simultaneously applying slow strain rate tests (SSRT) and acoustic emission monitoring on unnotched samples. As expected, the hydrogen resistance of conventional alloy steel grade X65 was lower than that of stainless steel. Exposure of samples to hydrogen reduced the percentage elongation to fracture while significantly increasing the embrittlement index at higher pressure (10 MPa). SEM images of fracture surfaces revealed that the fracture mechanism changed from ductile to ductile brittle already at 1 MPa, and then to predominantly brittle with quasi-cleavage characteristics during testing under hydrogen pressure of 10 MPa. AE event classification based on waveform analysis showed predominantly shear-mode cracking for the nitrogen sample at 10 MPa, whereas hydrogen-charged samples exhibited a dominant tensile fracture mode. Accordingly, the sample subjected to nitrogen pressure of 10 MPa displayed typical ductile fracture with small dimples, while the sample exposed to hydrogen pressure of 1 MPa initially exhibited mixed ductile and brittle fracture with quasi-cleavage morphology, and then, as hydrogen pressure increased to 10 MPa, nearly pure brittle fractures were observed on the sample surface, with dominant quasi-cleavage features and several small elliptical cracks of approximately 20 μm in diameter, characteristic of hydrogen-induced corrosion. Differences observed in AE signals recorded during SSR testing are shown in Figure 18. Fracture modes can lead to different AE behaviors at various RAAE and AF values. To distinguish the type of fracture damage, AE events were sorted into three clusters:

- Cluster 1 (dots) represents low RAAE values (<200 μs/V) and AF values up to 600 kHz, indicating tensile modes attributable to cleavage or quasi-cleavage fracture mechanisms.
- Cluster 2 (triangles) indicates mixed fracture mode.
- Cluster 3 (squares) exhibits low AF values (<50 kHz) and a wide range of RAAE values (from 100 to 12,000 μs/V), suggesting shear-mode fracture associated with plastic deformation mechanisms such as void nucleation and inclusion decohesion.

Specifically, Cluster 3 identifies the nitrogen sample at 10 MPa with events occurring after yielding and near the necking point, while Cluster 1 characterizes hydrogen samples at 1 MPa and 10 MPa, as shown in the figure below (Fig. 18):

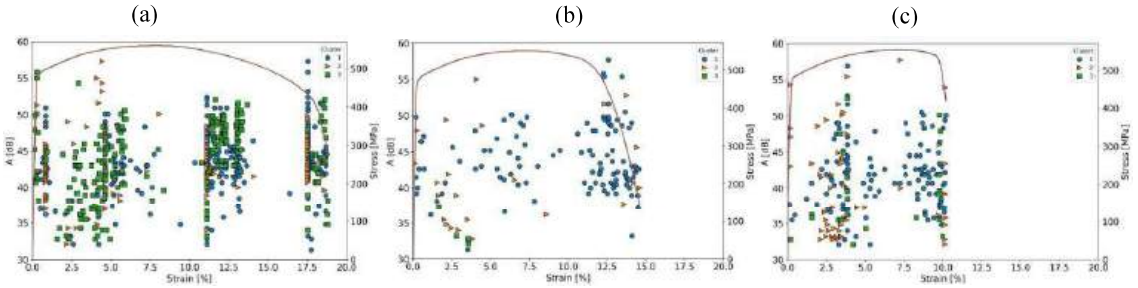

Figure 4-18: AE amplitude events and stress–strain plot during SRRTs: a) 10 MPa nitrogen, b) 1 MPa hydrogen, and c) 10 MPa hydrogen [14]

In the article *Experimental-numerical analysis of the fracture process in smooth and notched V specimens* by Świt et al. [15], tensile tests under uniaxial loading were performed on steel material samples taken from a natural gas transmission pipeline. Both smooth specimens and specimens with a V-shaped notch were tested. Introducing a V-shaped notch caused changes in the stress and strain component fields near the plane of maximum necking, which consequently led to failure through different mechanisms. The testing process included numerical modeling and simulation of specimen loading. After numerical calculations, maps of stress and strain component fields were generated. It was determined that for the smooth specimen, damage initiation was mainly caused by the normal stress component in the central part of the plane with the greatest necking. In contrast, for the V-notched specimen, damage initiation occurred due to the shear stress component, and failure progressed through a shear mechanism. The results of these tests are intended to be used for monitoring the operational safety of gas pipeline networks based on the analysis of acoustic emission signals.

The research leading to these results has received funding from Horizon 2020, the European Union's Framework Programme for Research and Innovation (H2020) under grant agreement n° 101111888.

Numerical calculations allowed determination of the stress and strain fields occurring in the material of the analyzed specimens. Maps of the distribution of stress components and resulting strains were prepared for the loading phase during which advanced necking developed. According to the maps of the stress tensor component in the tensile direction, a higher stress level was identified for the smooth specimen compared to the V-notched specimen. At the moment of fracture, the maximum values reached 1400 MPa and 1000 MPa, respectively. In the smooth specimen, the maximum stress values occurred in the center of the plane of maximum contraction, while in the V-notched specimen, they occurred in the plane of maximum contraction at the notch tip, as shown on the figure (Fig. 19) below:

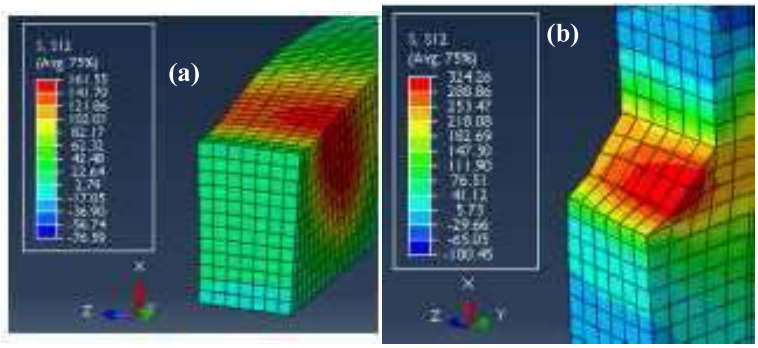

Figure 4-19: Simulation of (a) smooth specimen and (b) V-notched specimen. [15]

The developed stress component maps also showed that the maximum values were located at a certain distance from the plane of maximum necking and in the center of the specimen. At the same time, stress values for V-notched specimens reached significantly higher levels than for smooth specimens. In the V-notched specimen, stress values ranged from 220 to 345 MPa immediately after and during plastic deformation, whereas in the smooth specimen, stress values did not exceed 192 MPa during plastic deformation until failure. Only just before failure did stress values reach 340 MPa. The distribution of stress and strain components in the analyzed specimens influenced the fracture process. In smooth specimens, fracture occurred classically as a result of the interaction of the normal component of the stress-strain tensor. In the V-notched specimen, the normal stress component was below the critical level, so failure did not occur due to this component. However, during deformation, a high shear stress component was present, significantly exceeding the reference level according to the adopted criterion. Based on this, a high development of plastic deformation was indicated, resulting in shear failure in V-notched specimens. The conducted tests utilized the recording and analysis of acoustic emission signals, and the results were then used to establish relationships between characteristic types of AE signals and the failure processes of steel pipes used in gas pipelines.

In the article *Innovative acoustic emission method for monitoring the quality and integrity of ferritic steel gas pipelines* by Świt et al. [16], the results of tests conducted to identify the damage process in steel material samples taken from a natural gas pipeline were presented. For comparison, material from two pipes was examined: S1 – a pipe after long-term operation (40 years) and S4 – a new, unused pipe. The pipes were manufactured at different times in different steel mills and had different strength properties. Both pipes exhibited a ferrite-pearlite microstructure with a grain size of 7–12 μm; however, in the case of S4, thinner and more densely arranged lamellae were observed in the pearlite regions, likely due to faster thermal cooling of the pipe. In another study with similar results, the author examined steel samples of grade S235 taken from a natural gas pipeline with an outer diameter of 168.3 mm and a wall thickness of 4.0–4.5 mm (from *Identification of the Fracture Process in Gas Pipeline Steel Based on the Analysis of AE Signals*, Świt et al. [17]).

Due to the wall thickness of approximately 4 mm, the collected samples were flat and oriented along the pipe axis. The samples were subjected to uniaxial loading, and the tests were carried out in accordance with EN ISO 6892-1 and ASTM E8 standards. The tests were performed at a temperature of +20 ±2°C using a UTS/Zwick 100 testing machine equipped with automatic control and data recording systems. The samples were loaded until failure. During the tests, signals of the applied tensile force and elongation of the measured part of the sample were recorded. Elongation was measured using an extensometer with a gauge length of 25 mm and a resolution of 0.001 mm. Consistent with other studies by this author (Świt et al.), uniaxial tensile tests were also performed on samples with a sharp notch. The V-shaped notch caused changes in the

The research leading to these results has received funding from Horizon 2020, the European Union's Framework Programme for Research and Innovation (H2020) under grant agreement n° 101111888.

mechanical fields in the cross-section and led to sample failure through shear. A detailed analysis of the mechanical fields in smooth and notched samples was presented in a previous work (Świt et al.). The aim of these tests was to induce sample failure according to the dominant shear mechanism and record AE signals during loading, then compare them with AE signals obtained from smooth samples.

To fully understand the process, metallographic examinations of samples subjected to uniaxial tension were also carried out to determine characteristic failure mechanisms occurring in the microstructure at different loading stages. The tests were performed on cross-sections of smooth and V-notched samples taken from pipes S1 and S4. During material strengthening in the uniform deformation range up to F_{max}, no clear symptoms of microstructural failure were observed. Only slight deformation of ferrite grains, cracking of extracted MnS particles, and their detachment from the matrix could be observed (Figures 20a, 20b).

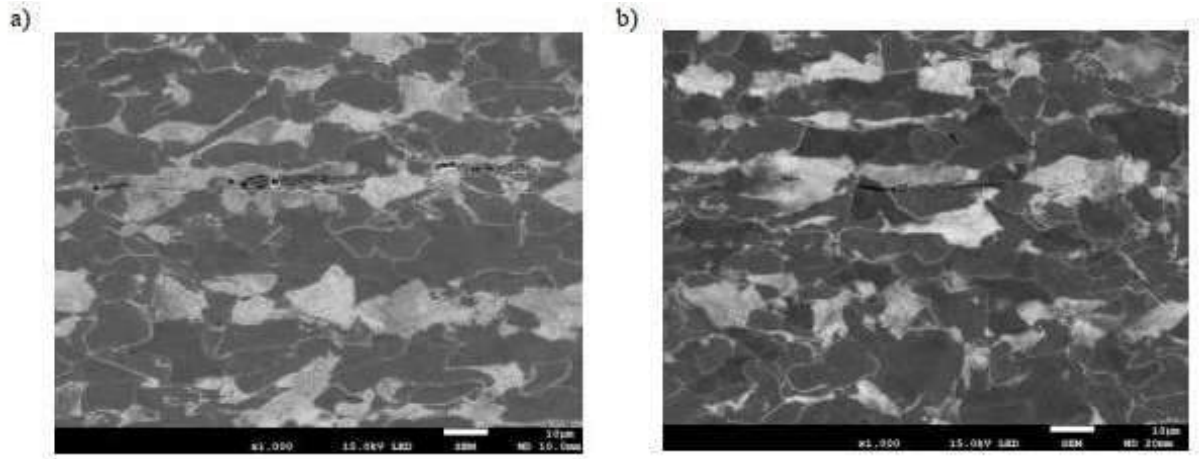

Figure 4-20: Microstructure of samples in the range of uniform deformation just before neck formation: (a) smooth, (b) V-notched [16,17]

Next, during the necking stage in the material microstructure, clear deformation of ferrite grains was observed, as well as cracking and detachment of inclusion particles from the matrix. In the necking region of smooth specimens, these processes were more advanced (Figures 21a, 21b). Just before the failure of the smooth specimen material, significant deformation of ferrite grains (over 200%) and advanced material damage between ferrite and pearlite grains were observed, both in the direction parallel to the load and in the transverse direction (Figure 22a). In the notched specimen, signs of material failure were less visible; however, the deformation of ferrite grains was oriented at an angle of approximately 30° (Figure 22b). Thus, advanced deformation close to rupture occurred.

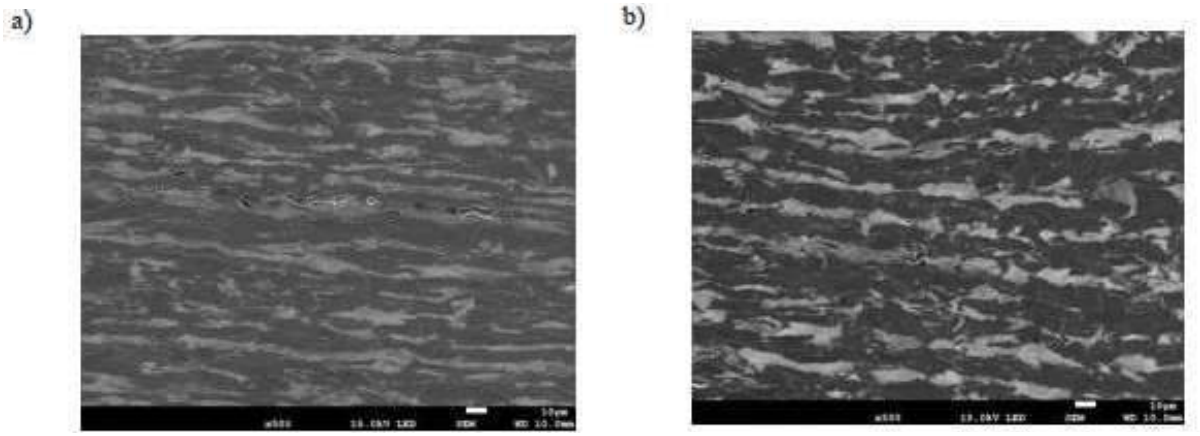

Figure 4-21: Microstructure of samples in the range of neck formation: (a) smooth, (b) V-notched [16,17]

The research leading to these results has received funding from Horizon 2020, the European Union's Framework Programme for Research and Innovation (H2020) under grant agreement n° 101111888.

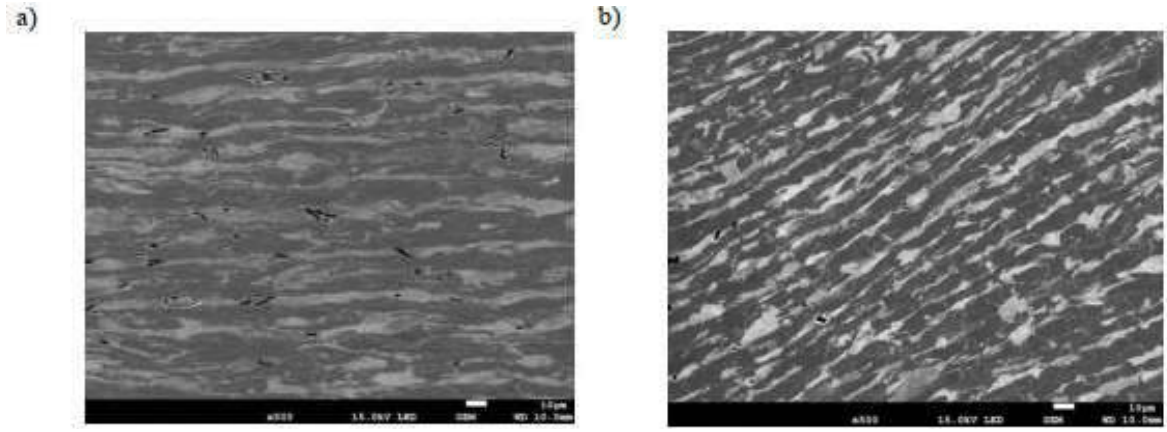

Figure 4-22: Microstructure of samples immediately before destruction: (a) smooth, (b) V-notched [16,17]

The formation of plastic deformation at an angle is caused by the high level of shear stresses in specimens with sharp notches and leads to specimen failure according to the shear mechanism across the entire cross-section of the specimen (Figure 23b). Subsequently, in the central part of the fracture of the smooth specimen, there is an area where the crack developed under the influence of the normal stress component to the cross-section, while only on the lateral surfaces; under the influence of shear (Figure 23a).

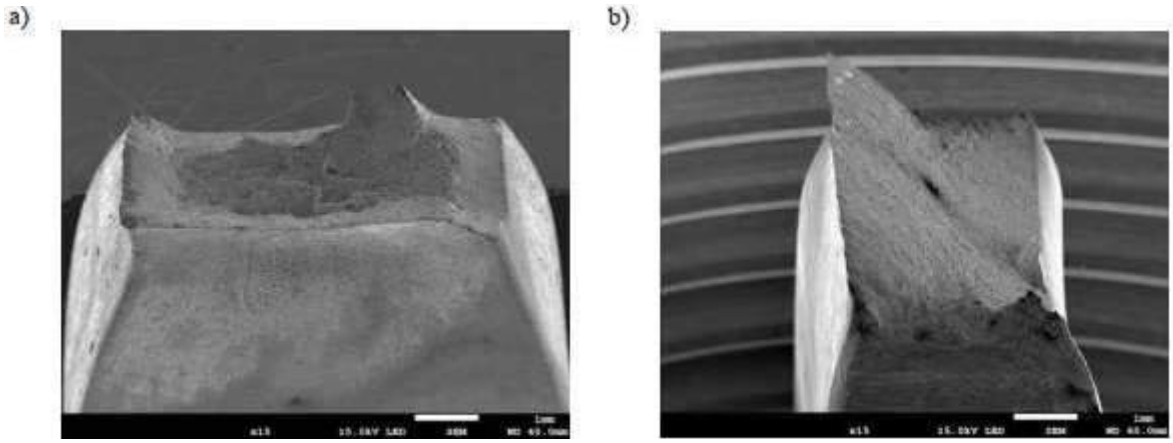

Figure 4-23: The breakthroughs of the test specimens: (a) smooth, (b) V-notched [16,17]

4.2.1 Analysis of AE signals.

After completing the tests, the analysis of acoustic emission signals was carried out. Microstructural studies revealed various signs of material failure during specimen loading; plastic deformation of grains, cracking of non-metallic inclusion particles, delamination between particles and the matrix, as well as between pearlite and ferrite phases, and cracking of ferrite grains. These fundamental failure processes generated acoustic emission signals with specific characteristic features. To determine these features in AE signals recorded at different stages of material failure during specimen tension, a detailed analysis was performed. The study found that these signals respond sensitively to the type of failure through parameters characterizing energy (e.g., energy, signal strength), frequency (e.g., average frequency, reverberation frequency), and waveform shape (e.g., ASL, RMS). Since the load-bearing capacity of the tested specimens varied, time was also presented in normalized form: $t_{norm} = t/t_{max}$. Based on previous experience (Świt et al.), the analysis included AE signals recorded in different ranges of specimen deformation with amplitude levels >40 dB and high energy characteristics (energy or signal strength). AE signals were grouped according to a non-hierarchical approach (k-means algorithm) developed by the author (Świt et al.).

The research leading to these results has received funding from Horizon 2020, the European Union's Framework Programme for Research and Innovation (H2020) under grant agreement n° 101111888.

Against the background of stress-time plots in normalized values, the course of corresponding AE signal characteristics for specimens made from pipe material S1 and S4 was presented. Figure 24 shows changes in average frequency values during specimen loading. Despite significant data scatter, it can be observed that the minimum average frequency values occur at the moment of complete specimen failure. For smooth and notched specimens made from pipe S4, compared to S1, lower values were observed in terms of uniform elongation and higher values at the moment of failure. The ASL level reached its highest values when the specimens failed. In S4 steel specimens, the ASL level, initially lower than S1 in terms of uniform elongation, exceeded the values of S1 specimens at the moment of complete failure (Figure 24).

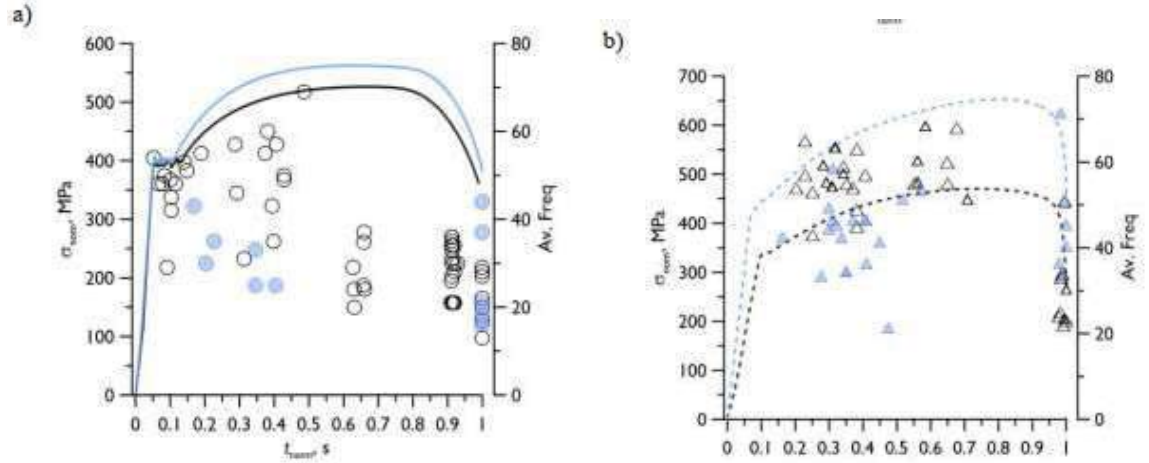

Figure 4-24: Distribution of the Average Frequency parameter over time: (a) for smooth samples S1 and S4, (b) for notched samples S1 and S4 (S1- empty symbols, S4 – filled symbols) [15]

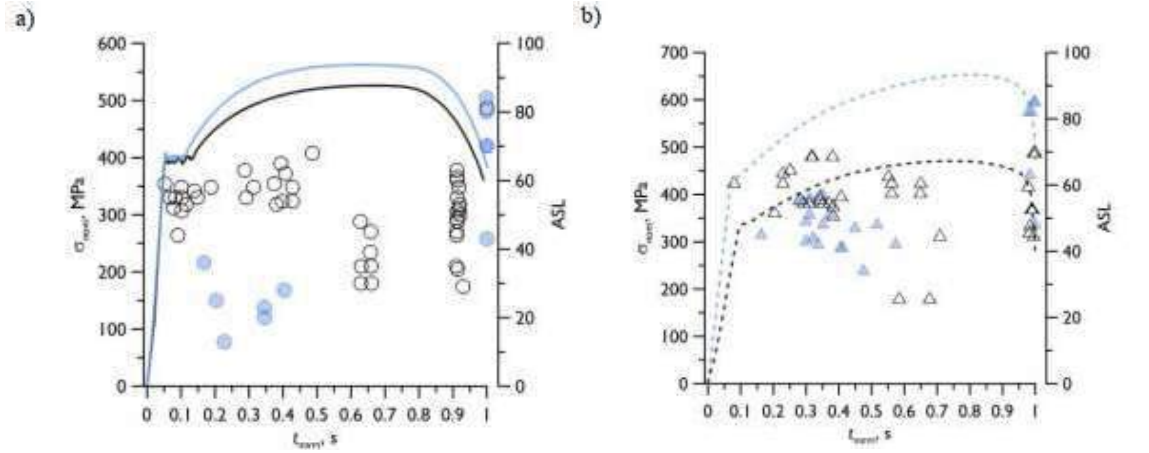

Figure 4-25: Distribution of the ASL parameter over time: (a) for smooth samples S1 and S4, (b) for notched samples S1 and S4 (S1- empty symbols, S4 – filled symbols) [15]

Figures 26 show the distributions of signal strength characteristics during loading of smooth specimens and notched specimens. The figures present signals divided into classes according to the assumptions described in the studies conducted by the author (Świt et al.). AE signals with very high signal strength values (>4.3E07 pV·s) and dark blue color (class 1) usually occur at the moment of complete specimen failure. Occasionally, high levels of signal strength were also observed in other time intervals; during uniform specimen deformation or just before necking formation (Figure 26). Based on observations of microstructure cross-sections, it was found that in the uniform deformation section, these signals were emitted as a result of cracking of non-metallic inclusion particles. Therefore, class 1 signals occurred during the fracture of microstructural elements; non-metallic inclusion particles, pearlite lamellae, and ferrite grains. These signals are characterized by relatively

The research leading to these results has received funding from Horizon 2020, the European Union's Framework Programme for Research and Innovation (H2020) under grant agreement n° 101111888.

low frequency values; average frequency in the range of 15–35 kHz; and relatively high ASL parameter values 70–85. As expected, the maximum signal strength values were recorded at the moment of complete specimen failure. Signals recorded during loading of specimens taken from pipe S4 are higher compared to specimens from pipe S1.

The next group of signals, marked as class 3 (blue), occurred throughout the entire range of plastic deformation. Signal strength values for these signals ranged from $7.5 \cdot 10^6$ to $8.5 \cdot 10^7$ pV·s, average frequency range 17–60 kHz, and ASL 20–65. In specimens from pipe S4, frequency and ASL values were generally lower than in specimens from S1. Based on metallographic studies, it was found that these signals were generated during plastic deformation of the material and during the process of separation of ferrite and non-metallic inclusion particles, as well as pearlite and ferrite phase particles.

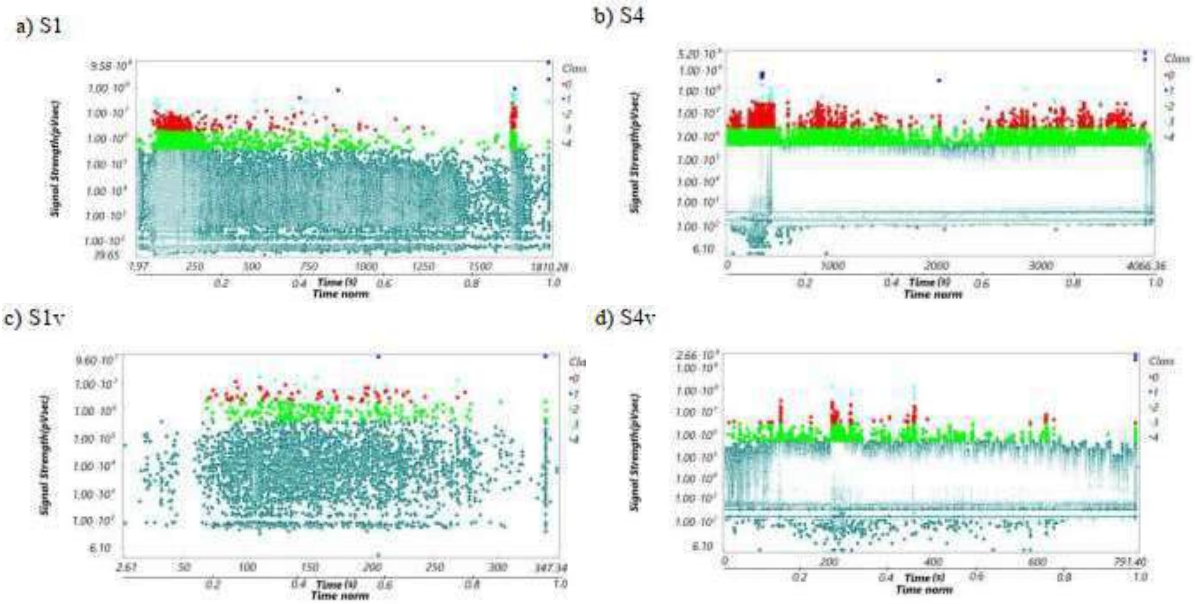

Figure 4-26: Distribution of the Signal Strength parameter over time for samples from pipes S1 and S4: (a and b) for smooth, (c and d) for V-notched samples [15]

It has been shown that signals from classes 0 (red) and 2 (light green) occur within the range of plastic deformation of the material. These signals had similar frequency ranges but differed in signal strength and were generated by plastic deformation of varying intensity. The largest group of signals (class 4), with a low signal strength level ($<4.4 \cdot 10^5$ pV·s), was emitted by various other factors during the loading process; therefore, it was determined that they could be treated as "technological noise".

The presented research results confirmed the possibility of using the acoustic emission method to assess the technical condition of steel natural gas pipelines. The studies confirm the ability to detect changes in the stress state within the material structure, including the presence of defects, material flaws, or cracks. By applying this technique, it is possible to determine processes occurring in the material and correlate acoustic signals with the mechanical parameters of steel.

As indicated by Roberts T.M. in his article *Acoustic emission monitoring of fatigue crack propagation* [18], tests were conducted on steel and welded steel specimens under tensile loading as well as on T-beams. For all steel test specimens and welded steel beams, the results show an approximately linear relationship between log(da/dn) and log K, which can be represented by the Paris equation. Results for welded steel compressed tensile specimens remained entirely or partially within the crack initiation region and were therefore not included in the statistical analysis. In the conducted studies, software was used to support filtering of data obtained from acoustic emission measurements for the recorded narrow band containing fatigue cracks. In this way, only emissions from the vicinity of the crack were recorded. AE events were isolated for small percentages of the fatigue load range near the peak load, which increased with the number of cycles. Experimental confirmation of the relationship between acoustic emission rate and crack propagation rate was

The research leading to these results has received funding from Horizon 2020, the European Union's Framework Programme for Research and Innovation (H2020) under grant agreement n° 101111888.

achieved, suggesting the possibility of predicting the remaining fatigue life of a structure based on short-term acoustic emission monitoring.

As indicated by Han Z. in his article *Acoustic emission during fatigue crack propagation in a micro-alloyed steel and welds* [19], tests were conducted to monitor fatigue crack propagation in materials using acoustic emission signals. AE signals generated during fatigue crack propagation in Q345 steel and its welds were compared. The Q345 steel grade, designated according to Chinese standards, is similar in mechanical properties to ASTM A572 Grade 50 and, in the context of transmission pipes, to API 5L X50 steel, which corresponds to grade L360 (or L360NB/L360NE depending on PSL specification level) according to EN-ISO 3183. The study confirmed faster fatigue crack growth in the welded joint area than in the base metal due to oxide inclusions and coarse ferrite grains present in the weld metal. Higher AE signal counts were obtained during fatigue crack propagation in the weld and in the base metal zone. Decoherence of oxide inclusions and the matrix, increased plastic activity, and ligament shearing with increasing crack propagation rate were also reflected in the recorded AE signals. During fatigue crack propagation in the base metal and welds, three distinct stages of AE signal emission occurred. The mechanism of the first stage was crack initiation, the second stage involved plastic activity in the plastic zone ahead of the crack tip, and the third stage primarily consisted of ligament shearing between micro voids and microcracks. As shown in the graphic (Fig. 27) below:

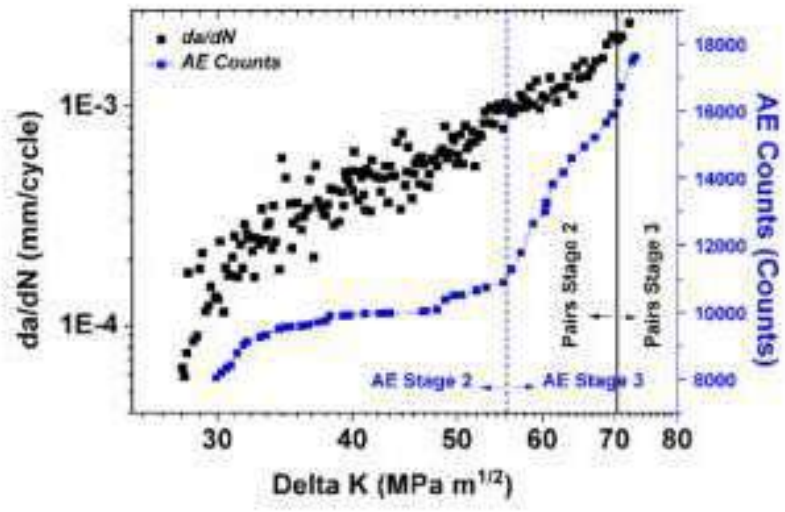

Figure 4-27: Comparison of assumptions derived from LEFM (Linear Elastic Fracture Mechanics) with the recorded changes in acoustic emission signals [19]

Mazal P., in his article *Use of acoustic emission method for identification of fatigue micro-cracks creation* [20], applied acoustic emission signal monitoring to describe the process of micro-crack formation in steel specimens made of low-alloy ferritic Cr–Ni–Mo–V steel, a grade intended for high-temperature applications under high stresses or in corrosive environments. It was clearly observed that changes in AE signals closely corresponded to changes in loading frequency, thus the recorded signals identified structural changes occurring during damage accumulation in the tested specimens under load. The increase in AE signal activity was distinctly marked in the initial phase of cyclic hardening and later during the propagation stage of the main fatigue crack. The authors point out that individual materials differ significantly in acoustic activity and its characteristics. The ability to compare results largely depends on the sensors used, their mounting method on the specimen, the contact points between the material surface and the sensor, and other factors. The shape of the specimens and the distance between the sensor and the monitored defect in the material also play an important role in measurements. These are potential limitations in the application of the acoustic emission method. The AE method can be used to identify processes occurring in materials, particularly those that occur suddenly or slowly under loads during long periods of infrastructure operation, when the resulting stresses and material defects are difficult to identify using other common non-destructive testing techniques. However, it is necessary to develop procedures defining the principles for setting parameters of AE signal analyzers, sensor

The research leading to these results has received funding from Horizon 2020, the European Union's Framework Programme for Research and Innovation (H2020) under grant agreement n° 101111888.

placement, and criteria for evaluating recorded signals. This requires extensive experimental work to identify appropriate parameters of acoustic emission phenomena and adapt them to established infrastructure assessment programs. In this regard, the authors recommend further processes enabling the identification of material processes and the possibility of mapping them through recorded acoustic emission signals.

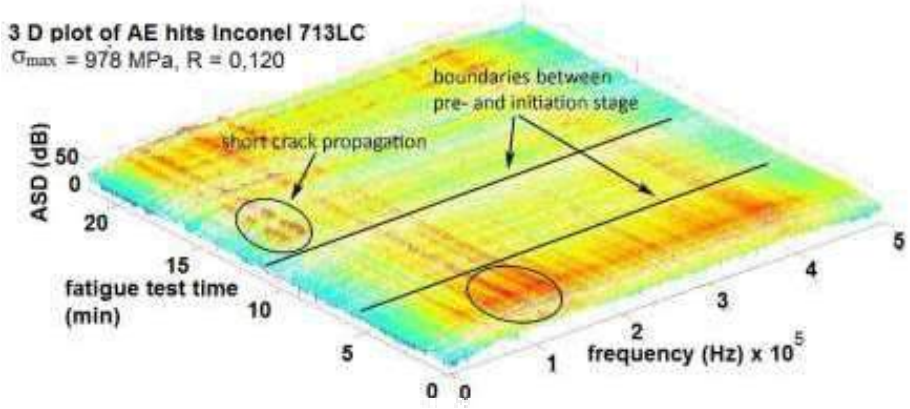

Figure 4-28: 3D mapping of frequency changes in recorded acoustic emission signals during fatigue tests [20]

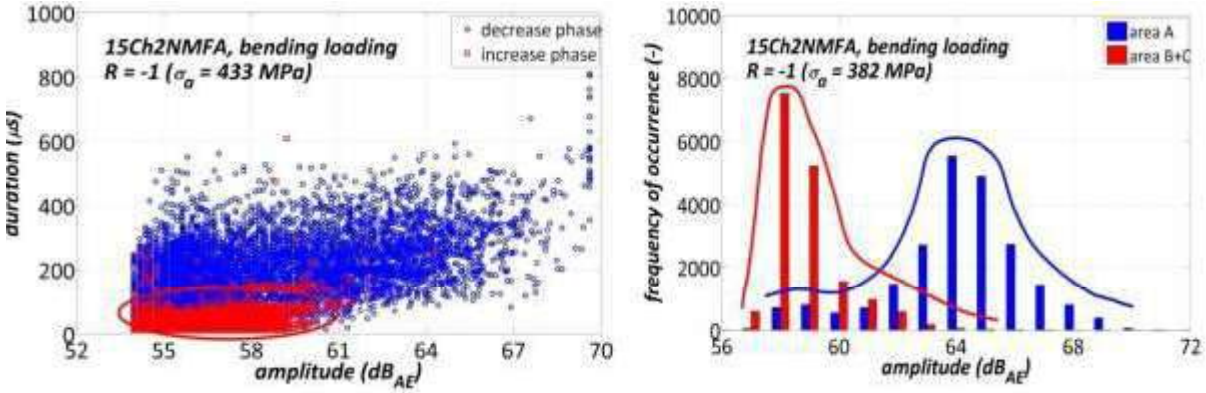

Figure 4-29: Changes in the amplitude of acoustic emission signals at different stages of induced fatigue damage [20]

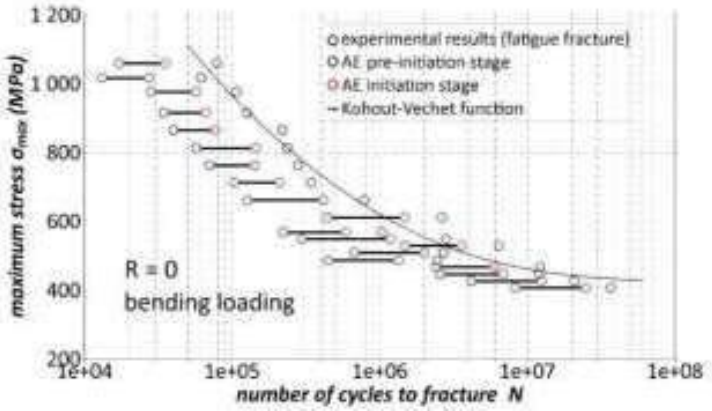

Figure 4-30: Example of results obtained for identifying the stages of pre-initiation and initial propagation of fatigue cracks in the tested steel using the acoustic emission method. [20]

The research leading to these results has received funding from Horizon 2020, the European Union's Framework Programme for Research and Innovation (H2020) under grant agreement n° 101111888.

Chuluunbat T., in his article *Investigation of X70 line pipe steel fracture during single edge-notched tensile testing using acoustic emission monitoring* [21], presents research on the behavior of API 5L X70 steel, a widely used grade for constructing high-pressure natural gas transmission pipelines. The authors confirm the applicability of acoustic emission signal monitoring for detecting plastic deformation, crack initiation, and crack growth. At the same time, they point out that quantitative relationships between AE parameters; such as signal amplitude and frequency and fracture parameters of X70 pipeline steel, including initiation and propagation of ductile and brittle cracks, have not been thoroughly investigated and therefore remain not fully understood during result analysis. The study demonstrates the influence of loading conditions on the fracture behavior of X70 pipeline steel using AE monitoring. Variability in AE parameters was recorded depending on loading conditions, showing that strain rate, temperature, and the properties of the notch introduced to simulate cracking affect the fracture mode and the relative magnitude of AE signatures associated with that mode.

AE monitoring during tensile testing of X70 pipeline steel notably confirmed that AE signal activity begins before reaching stresses within the plasticity range. Subsequently, the number of signals increases sharply due to stress concentration at the crack tip and before reaching maximum load due to crack initiation. At the end of the test, after fracture completion, the density of AE signal bursts increased. The number of AE signals also rises with increasing strain rate and decreasing test temperature. At the beginning of the tests, at lower strain rates, AE signals with amplitudes of 30–40 dB were recorded. As stress increased, impulse signals with amplitudes of 50–70 dB were observed. The crack initiation point can be detected by a sudden change in AE activity in the tested steel, resulting in AE amplitudes of 65–75 dB and an average frequency of 300–350 kHz just before the peak of the load–displacement curve. The crack growth rate can also be predicted by analyzing the effect of stress increase on the count frequency of recorded AE signals. As crack growth progressed, the AE signal count frequency increased. Conversely, a transition to more ductile material behavior; when the number of small voids decreases and the number of large voids increases with decreasing strain rate, resulted in a drop in the average frequency of recorded AE signals.

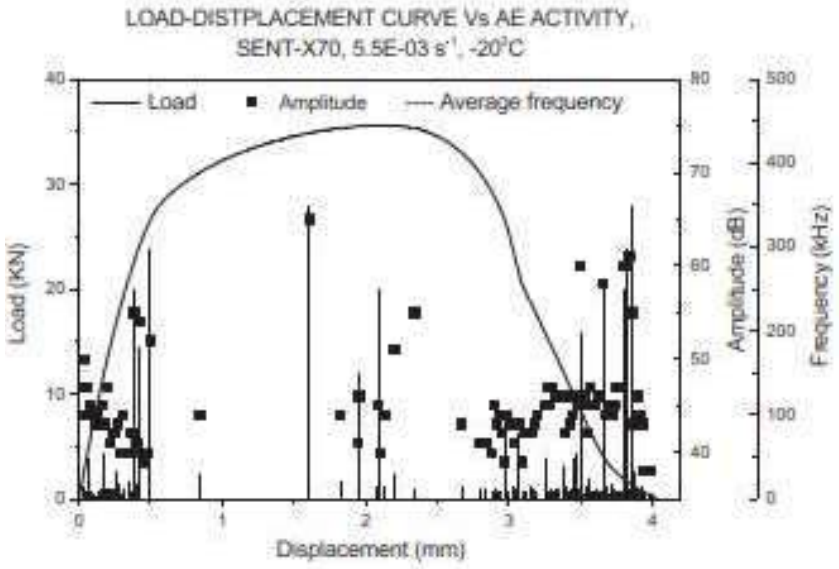

Figure 4-31: Recorded variations in acoustic emission signal parameters correlated with the load–displacement curve plotted for induced deformation in an X70 steel specimen [21]

The research leading to these results has received funding from Horizon 2020, the European Union's Framework Programme for Research and Innovation (H2020) under grant agreement n° 101111888.

Merson E., in the article *Application of Acoustic Emission Method for Investigation of Hydrogen Embrittlement Mechanism in Low-Carbon Steel* [22], examined the phenomenon of hydrogen embrittlement in an electrolytically charged low-carbon steel specimen of grade S235JR, commonly used for natural gas pipeline construction, during a tensile test combined with in situ acoustic emission measurements. The study of this steel grade is considered significant because most research focuses on high-strength or stainless steels. The experiments demonstrated that the reduction in ductility of the tested material correlated with the formation of quasi-cleavage areas induced by hydrogen corrosion, known as "fish eyes", which developed during necking as hydrogen penetrated the material's structure. Acoustic emission proved sensitive to the cracking process caused by hydrogen corrosion and to the associated deformation mechanisms. Plastic deformation generated continuous acoustic noise in the form of low-amplitude AE signals, whereas brittle hydrogen-induced cracking, progressing through a cleavage-like mechanism, produced discrete high-amplitude AE bursts.

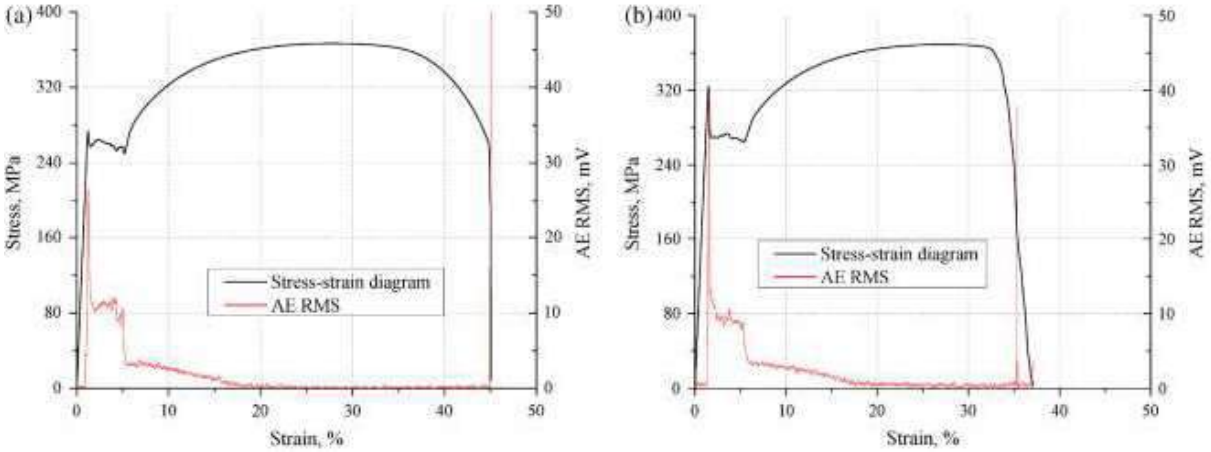

Figure 4-32: Stress–strain curves and root mean square energy of recorded acoustic emission signals for specimens tested without hydrogen charging (a) and after hydrogen charging (b). [22]

Nohal L., in the article *Acoustic Emission Response to Erosion-Corrosion and Creep Damage in Pipeline System* [23], demonstrated that one of the phenomena characterizing changes in mechanical properties under load is creep. Creep refers to the gradual deformation of a material under constant stress. It typically occurs in three stages: the primary stage, marked by a high initial strain rate that decreases over time; the secondary stage, where the strain rate stabilizes at a constant value dependent on temperature and stress; and the tertiary stage, characterized by a rapid increase in strain rate leading to localized damage and eventual material failure. Creep can be classified into several types, including low-temperature, high-temperature, and diffusion creep, depending on loading and temperature conditions. This phenomenon is critical in materials engineering because it affects the durability and reliability of engineering structures, including natural gas pipelines. In the conducted study, the acoustic emission response to creep deformation was found to be very similar to fatigue tests, showing high activity in the first stage, very low activity in the second stage, and strong AE activity again in the final stage. In this regard, AE signal monitoring can be considered a promising diagnostic method, as it offers advantages over conventional local inspection techniques such as ultrasonic or magnetic testing. AE monitoring is suitable for long-term condition assessment of pipelines during operation and enables simultaneous acquisition, remote transmission, and processing of multiple signals, provided that an appropriate AE-based diagnostic system is implemented.

The research leading to these results has received funding from Horizon 2020, the European Union's Framework Programme for Research and Innovation (H2020) under grant agreement n° 101111888.

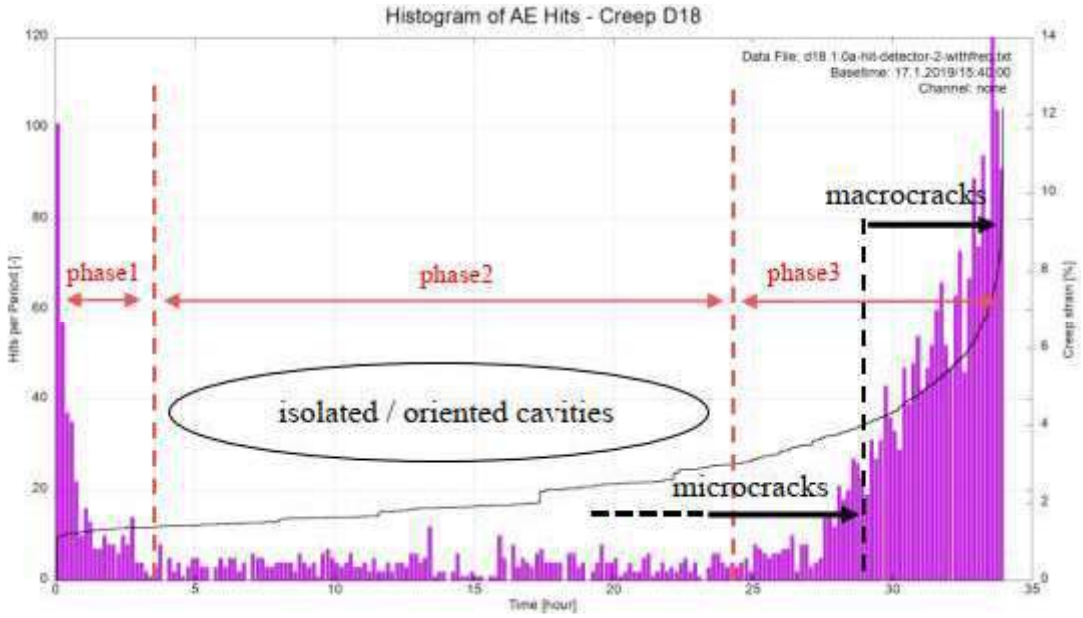

Figure 4-33: Histogram of acoustic emission signal registrations during the creep test [23]

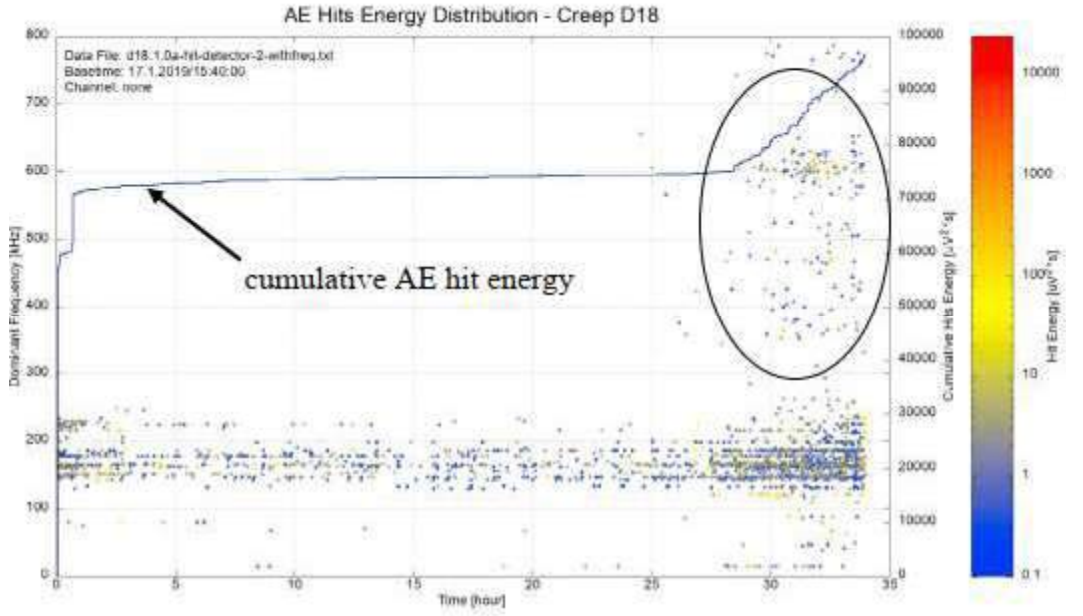

Figure 4-34: Cumulative energy of recorded acoustic emission signals during the creep test [23]

The research leading to these results has received funding from Horizon 2020, the European Union's Framework Programme for Research and Innovation (H2020) under grant agreement n° 101111888.

4.3 Stress Concentration Tomography

4.3.1 The basis of the technology

Figure 4-35: SCT test [24]

Speir Hunter Ltd, in collaboration with the University of Leeds, has used its knowledge of stress magnetization to create a remote pipeline diagnostics tool that can be used on both above and underground pipelines. The technology has been dubbed Stress Concentration Tomography (SCT™).

UNISCAN™ - this is the hardware used to collect raw data for analysis. It consists of:

- an array of sensitive magnetometers that collect data on the pipeline's natural magnetic field from a distance,
- a high-precision GNSS (Global Navigation Satellite System) positioning system for overlaying location data with real-time magnetic data,
- complex programs that control electronic functions and save magnetic localization data to a USB flash drive for analysis in UNISCAN™ Tools software.

UNISCAN™ TOOLS is a software package that analyzes magnetic-location data collected by UNISCAN™ and automatically generates integrity reports and pipeline route maps.

The research leading to these results has received funding from Horizon 2020, the European Union's Framework Programme for Research and Innovation (H2020) under grant agreement n° 101111888.

Figure 4-36: UNISCAN- SCT device [24]

It includes algorithms that:

- detect the presence of defects, their location and stress magnitude,
- report information on 3D mapping of the pipeline route, depth of coverage and lateral position,
- filter out external sources of magnetic interference, such as pipeline cathodic protection currents and overhead power lines.

4.3.2 Short description of how the survey is being prepared and performed

SCT™ directly measures the number of stresses on the pipeline wall by analyzing remotely collected magnetic data. This means that SCT™ can detect any type of damage occurring in a pipeline in any orientation, both inside and outside, and regardless of its clock position on the pipeline.

1. Application

- Inspection of pipelines or parts of pipelines, where it is not possible to use the classic In Line Incpection,
- detection of damage under insulation,
- preliminary identification of damage on a long section of the pipeline, which can then be investigated using more precise methods,
- mapping the route and burial depth of the pipeline - for example, for network inventory purposes,
- spot inspection of previously identified defects to monitor their progress as a complement to classic In-line Inspection,
- verification of weld locations,
- complement to ECDA (direct assessment of external corrosion),
- inspection in geotechnically unstable areas.

2. List of detected defects

- Internal or external corrosion
- Weld defects and defects near the welds or on the welds, such as dents

The research leading to these results has received funding from Horizon 2020, the European Union's Framework Programme for Research and Innovation (H2020) under grant agreement n° 101111888.

- Stress cracks and micro-cracks
- Dents and mechanical damage
- Lateral deformations and buckling caused by earth movements in geologically hazardous regions
- Illegal hot threading of material transported by pipeline
- Linear defects, including cracks, delamination and flaking

3. Results

- Number and location of defects in the pipeline to the nearest meter.
- The level of stress caused by each damage zone on the pipeline wall in relation to the design maximum working circumferential stress and the specified minimum yield strength of the material.
- Identification of circumferential welds and their location with accuracy to one meter.
- Variation of pipeline wall thickness and diameter and their location with accuracy to one meter.
- 3D mapping - the depth of the pipeline cover with an accuracy of 5% of the actual depth and the lateral position with an accuracy of 1 cm.
- Detection and localization of kinks with prediction of stress levels.
- Detection and location of casing pipes with sub-meter accuracy
- Prediction of bending stresses in geologically hazardous regions

4.3.3 Advantages and disadvantages

Advantages:

- Inspections without excavation or disruption of the pipeline;
- Ability to analyze pipeline's condition without stripping insulation
- Ease of operation and low mobilization requirements
- Can be used in difficult geological conditions (via drones)
- Can be used regardless of the sent medium, including H-NG blend or hydrogen
- Could be used for the non-piggable pipelines
- Technology providers claim it may be used for detecting defects typical for hydrogen

Disadvantages:

- Not suitable for use in plastic pipelines
- Less precision compared to traditional methods;
- Test results may be less accurate

4.4 Metal Magnetic Memory Method

4.4.1 The basis of the technology

Metal Magnetic Memory Method (MMM) is a passive non-destructive testing method based on self-registration of the magnetic scattering field of the test piece [25]. The basic MMM methods include:

- the magnetoelastic effect,
- the scattering effect of external magnetic fields on discontinuities,
- healing processes affecting magnetic fields with dislocations and their accumulation.
- The following are of key importance during MMM testing:
- Magnetoelastic effect - The effect of magnetic field dispersion caused by discontinuities or structural inhomogeneities in the material.

The research leading to these results has received funding from Horizon 2020, the European Union's Framework Programme for Research and Innovation (H2020) under grant agreement n° 101111888.

- Villari effect - This involves a change in magnetization under the influence of uniaxial stress and involves the conversion of mechanical strain energy into magnetic energy.

The opposite phenomenon to the Villari effect is magnetostriction. External magnetic fields, mechanical and thermal stresses, changes in material temperature, and material structure degradation processes lead to material magnetization, which enables the recording of diagnostic data. Properly conducted evaluation of recorded MMM measurement data, after excluding false magnetic anomalies, can be correlated with SCZ in categories I, II, and III, as well as inhomogeneities in chemical composition and structure. The MMM method's distinguishing feature compared to other non-destructive testing methods is that, in addition to detecting cracks, it also locates early stages of material fatigue and structural defects, represented by stress concentration zones. The MMM method is used to test ferromagnetic materials and metastable paramagnetic materials. During MMM testing, the following are recorded and analyzed:

- the existing distribution of the material's permanent magnetization component, including among others:
  a) residual magnetization for an unloaded structure,
  b) stress magnetization for a loaded structure,
  c) magnetic traces left after MT (UT) and RT (RT) defectoscopy.
- local magnetic anomalies deviation from the trend, taking into account the shape of the object being examined and its position relative to the Earth's magnetic field.

The gas pipelines are investigated with the MMM method in two stages:

4.4.2 Short description of how the survey is being prepared and performed

STAGE I - Non-Contact Magnetometric Diagnostics (NCMD) consist of a walking inspection of the pipeline. In the NCMD, magnetic parameters worked out in the MMM method on the basis of standard PN-ISO 24497 -1:3 [26] are used. As a result, the localizations of the observed anomalous Stress Concentration Zones (SCZ) are obtained.

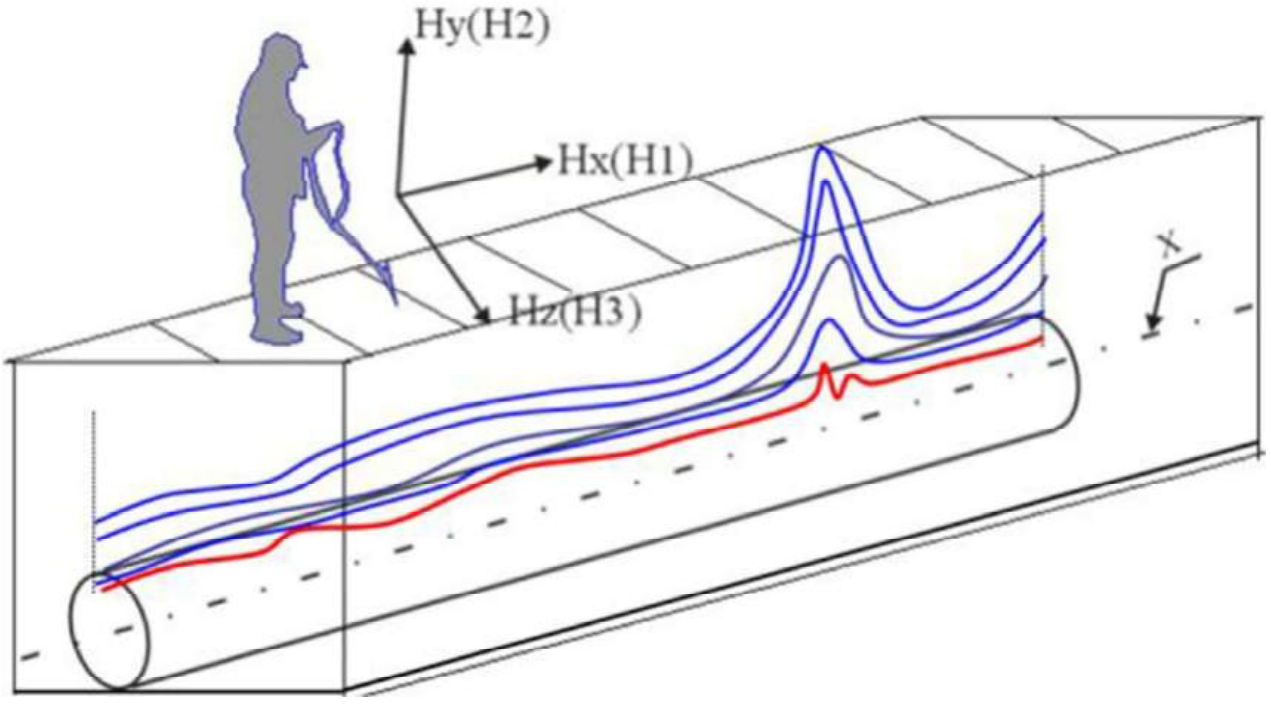

Figure 4-37: Schematic of measurements performed with the NCMD method [27]

The NCMD method makes use of magnetic parameters defined according to standard [26]:

- Vectors of measured magnetic field (Hx, Hy, Hz),
- Derivative of vectors of measured magnetic field dHp/dx.

The research leading to these results has received funding from Horizon 2020, the European Union's Framework Programme for Research and Innovation (H2020) under grant agreement n° 101111888.

The character of change of measured field (Hz frequency, amplitude) depends on the deformation of the pipeline under the influence of technological and mounting stress, working loads, and stresses caused by self-compensation of the pipeline when the temperature changes and when the ground displaces.

Three types of SCZ could be identified in the course of NCMD [28]:

Type I – numerous zones of stress and failure concentrations in the analyzed pipeline section. Zones classified as group I will have to undergo respective obligatory earth works. In the future the earth works on the analyzed pipeline section and SCZ will allow for a direct evaluation of the technical condition, on the basis of which the state of the pipeline mantle can be classified (whether or not a given pipeline section needs to be replaced, or the pipeline refurbished).

Type II – single zones of stress concentration in a given section of the pipeline. Section classified as type II will undergo optional earth works. Periodical monitoring (12 to 60 months from the date of the last inspection) of the pipeline section may be recommended if no earth works were performed.

Type III – zones to be monitored in a period of 60 to 84 months from the date of the last inspection, non-invasive for the further operation of the pipeline. An example of device used for NCMD is a highly specialized sensitive twelve-channel scanning device with integrated three-component flux-gate transducers and analogue-digital converter- Fig. 40. It is designed for non-contact magnetometric diagnostics of gas- and oil- pipelines being buried at the depth of 2-3 m. The scanning device is manufactured in the form of a telescopic bar with a rod for mounting of four three-component sensors. The rod length and the distance between the sensors depend on the diameter of the inspected pipe. The scanning device mounted on the road measuring wheel.

Figure 4-38: Scanning device [29]

The character of change of measured field (Hz frequency, amplitude) depends on the deformation of the pipeline under the influence of technological and mounting stress, working loads, and stresses caused by self-compensation of the pipeline when the temperature changes and when the ground displaces.

STAGE II

At this stage the earth works are performed and SCZ (selected at stage I with the use of MMM method) are investigated and referred to ultrasonic measurements.

The following diagnostic operations are performed:

- Visual assessment of the condition of the pipeline insulation.
- Measurements with the MMM method to reveal the stress concentration zones.
- Visual evaluation of detected stress concentration zones after the insulation was removed.
- Analysis with the MMM method of the pipeline mantle and possibly welds, after the insulation was removed.

The research leading to these results has received funding from Horizon 2020, the European Union's Framework Programme for Research and Innovation (H2020) under grant agreement n° 101111888.

- Ultrasonic tests – Ultrasonic Thickness Testing (UTT) of the pipeline mantle.
- Ultrasonic Tests (UT) – analysis of welded connections.

Figure 4-39: Scanning device Type 1-8M [28]

Figure 4-40: Tester of Stress Concentration TSC-7M-16 [28]

The measurements performed on the opencast are performed with the use of devices presented in Fig. 39. This type of scanning device with eight flux-gate transducers in their two-component installation for simultaneous measuring of the normal (Hpy) and tangential (Hpx) components of the magnetic field is designed for inspection of pipelines, vessels and extended welded joints. It is manufactured in form of a 4-wheel trolley with four flux-gate transducers and a length-counting device. It is possible to inspect the objects on distance of 2-5 m at the use of a specialized extension rode. It is used with TSC - 7M - 16. device (Fig. 40).

"MMM-System" allows simultaneous processing of several hundreds of residual magnetization distribution graphs. Diagram plotting parameters are controlled. Using the residual magnetization distribution graphs (Hp-graphs) the program is able to automatically plot graphs of distribution of the Hp function differentials and gradient (dH/dx, dH/dz, |grad Hp| - graphs), characterizing the level of stress concentration, and using them, according to the inspection technique, to determine the limiting stress concentration zones (damage development zones). The measurement data are analyzed in view of occurrence of the stress concentration zones. In the case of zones of highest stress concentration index the ultrasonic tests (UT) are performed.

Examples of defects identified by the MMM method:

The research leading to these results has received funding from Horizon 2020, the European Union's Framework Programme for Research and Innovation (H2020) under grant agreement n° 101111888.

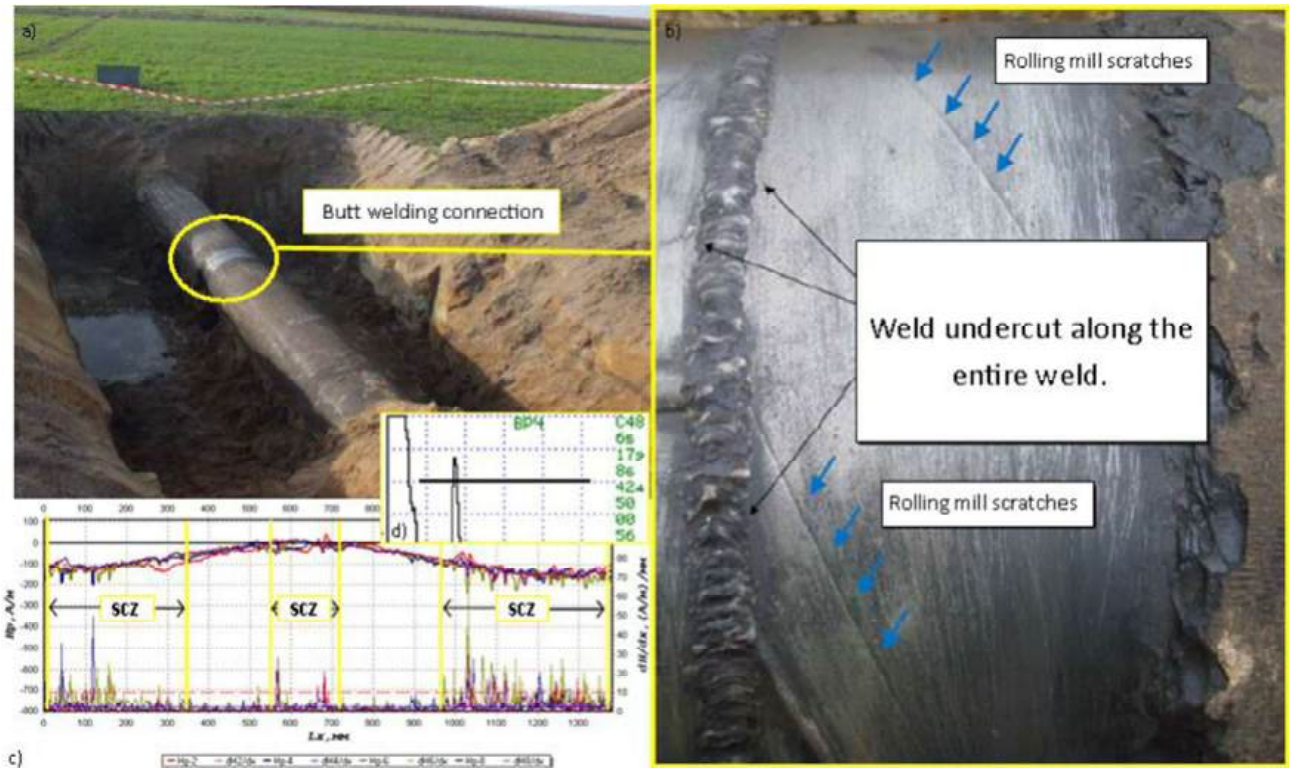

Figure 4-41: a, b) Pic. Uncovered gas pipeline in the anomalous were weld undercut along the entire weld and deformations of material due to pipe forming process; c) Distribution of magnetic field with indicated areas of SCZ (zones of stress concentration) registered on the butt weld. SCZ are about 300 and 800 mm long. Undercuts are visible on the whole length of the butt weld, disqualifying the weld for further exploitation; d) Confirmed presence of discontinuities in the SCZ with ultrasonic testing (UT) – in both instances of SCZ the discontinuity in the weld on the whole length – confirmed lack of undercuts in the weld. Minimum thickness of the mantle measured in areas of removed insulation in the earth works site B2 equaled to 7.9 to 8.0 mm [28]

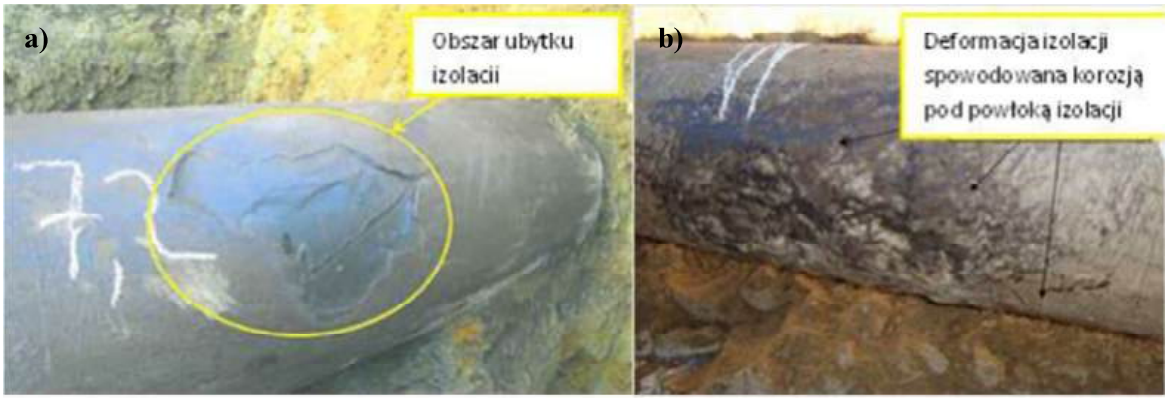

Figure 4-42: a) Uncovered gas pipeline within the anomaly zone. Pittings up to 5 mm of diameter and 0.5 to 2 mm of depth; b) Discontinuity confirmed with ultrasonic testing method – discontinuity in the weld on 300 mm in the SCZ. Minimum thickness of the mantle measured in the zones of removed insulation along the earth works A3 was 7.7 to 7.9 mm [source GAZ-SYSTEM]

The research leading to these results has received funding from Horizon 2020, the European Union's Framework Programme for Research and Innovation (H2020) under grant agreement n° 101111888.

However, sometimes during the earth works the SCZ were also discovered on other objects, e.g. insulator pipes, other pipelines – photo no. A3 or metal objects. An example of the latter is a metal rod undug at ca. 200 mm depth during earth works on SCZ of pipeline DN100 [30].

Figure 4-43: Crossing pipelines [30]

Figure 4-44: Metal bar detected during the tests [30]

4.4.3 Advantages and disadvantages

Advantages:

- Effective method for testing gas pipelines.
- An alternative to probabilistic methods.
- No preparatory work (NCMD).
- Accurate SCZ readings.
- Great development potential - defect book.
- Can be used regardless of the sent medium, including H-NG blend or H_2
- Could be used for the non-piggable pipelines

Disadvantages:

- Appropriate selection of parameters for leak detection.
- Interference caused by other metal objects - inability to test gas pipelines in casing pipes, etc [31].
-

4.5 Direct Current Voltage Gradient (DCVG)

4.5.1 The basis of the technology

The Direct Current Voltage Gradient survey has risen from the concept of assessing the pipeline's coating condition using - typical for pipelines – the Cathodic Protection system. The sources indicate that the DCVG technique was developed as early as in the 1980s, which confirms the DCVG's maturity as a pipeline inspection method [32]. The DCVG technique is currently well-established, renowned technology, frequently used for the coating and corrosion assessment, as part of the ECDA (External Corrosion Direct Assessment) concept [33].

The concept of the DCVG comes from the principle that the voltage gradient is observable whenever the steel surface of the pipeline, with the electric current going through the pipe, is in direct contact with the surrounding

The research leading to these results has received funding from Horizon 2020, the European Union's Framework Programme for Research and Innovation (H2020) under grant agreement n° 101111888.

soil. The main point of interest during the DCVG survey is to measure the voltage gradient on the ground. For the survey to be possible, there is a need for the pipeline to be electrically connected i.e. having the known direct current flow "inside" – it is technically done by the cathodic protection system. The basic principle of the cathodic protection is to connect the pipeline electrically in such a way that the pipeline itself becomes the cathode. As a consequence, the pipeline is not a subject to the oxidation (corrosion) process, as it occurs on the anode. Coming back to the DCVG survey, when there is no failure in the insulation, the electric current does not flow through the soil and during the survey no voltage gradient is observed. However, when there is a defect in the insulation, during the survey some voltage gradient, due to the electric current flowing, may be observed (fig. 45). The observed value of the gradient is dependent on some constraints, such as soil resistivity, pipeline burial depth, and size of the fault in the coating. Even with its limitations, the properly made DCVG survey can help in finding defects on the pipeline coating and subsequently possible corrosion areas.

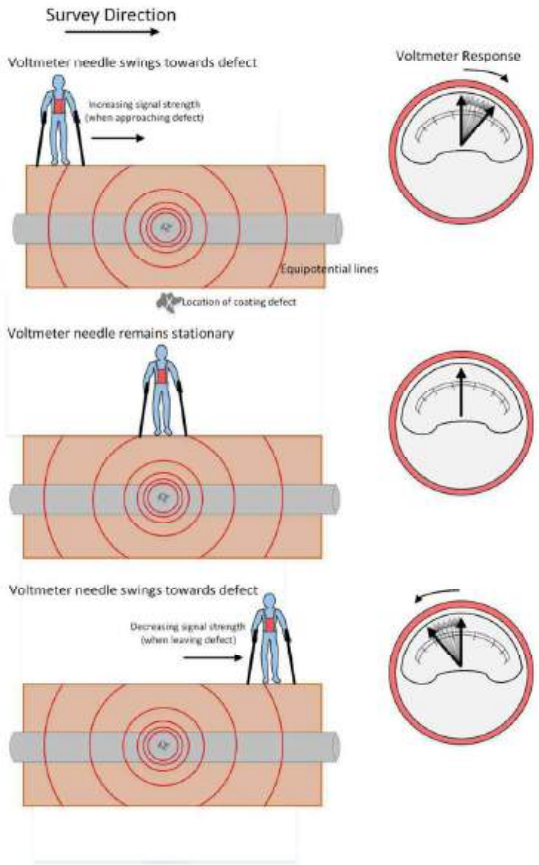

Figure 4-45: The sequence of indications on the meter [34]

4.5.2 Short description of how the survey is being prepared and performed

The first thing to start the DCVG survey is to ensure the Cathodic Protection current flows. For the sake of the survey it is often necessary to increase the current of the cathodic protection. This is a result of the Ohm's law, as with the higher current the voltage gradient associated with the coating's defect would be higher and hence easier to be detected [32].

Once the electric conditions are set the actual survey begins: an operator walks along the pipeline's route with voltmeter needles checking the voltage value. The typical practice is to measure the voltage gradient between the needles placed 1 - 2 m from each other. When approaching the defect, the value of the gradient rises and subsequently, when moving away from it, the value of the gradient gradually fades.

To properly assess the defect severity the %IR factor is usually introduced. It takes into account the electric conditions such as voltage gradients and cathodic protection potentials. In addition to the %IR factor, taking into account the soil's resistivity allows for consideration of the soil's corrosive aggressiveness as well. Then %IR*wzgl* (%IR*rel*) factor may be introduced, which informs about the defect's importance together with the

The research leading to these results has received funding from Horizon 2020, the European Union's Framework Programme for Research and Innovation (H2020) under grant agreement n° 101111888.

information about the corrosion potential of the surrounding environment. Such knowledge helps in assessing which of the found defects should be dealt with beforehand and which are of lesser importance and for which therefore no immediate actions are necessary.

4.5.3 Advantages and disadvantages

Advantages/strengths:

- DCVG uses the existing cathodic protection system of the pipeline – does not need to install additional equipment on the pipeline
- DCVG survey may be used for all types of pipelines, regardless of the transported medium (natural gas, water, chemicals, hydrogen).
- Method's suitability for being used in combinations with other pipelines inspection methods – gives the valuable and reliable information about the coating condition.
- Reliable results of the insulation/coating condition – detection of even small damages to the coating is possible.
- Gives the information about the size of the detected defect – possible identification of the major and minor defects of the pipeline.
- The inspected pipeline does not need to be of piggable design.

Disadvantages/limitations

- Due to the very nature of the technology, the information given by the DCVG survey is about the insulation condition [41]. Therefore, any pipeline's degradations/defect that does not result in the insulation break yet, may be not visible during the DCVG survey.
- The measurement on the parallel pipelines may be interfered with each other. The signal from one pipe may be influenced by the signal from the other one (e.g., its cathodic protection) [42].
- The speed of making the DCVG survey is limited due to the fact that it is done by a person walking on the ground.
- Anomalies in the bottom part of the pipeline may be hard to be detected due to the possible signal attenuation [42].
- DCVG is not possible to use under asphalt roads and railway tracks [40].
- Some parts of the pipelines may be hard to be tested due to the limited overground accessibility (e.g. crops, fences, rivers).

4.6 iDiaGaSys System

The operation of gas pipelines requires continuous monitoring of their integrity and changes in their surrounding environment. Due to the complexity and vastness of the transmission network, the use of advanced measurement and analytical technologies is essential. The *iDiaGaSys* system is designed for periodic detection of methane leaks and identification of potential hazards in the area of gas pipelines. It consists of two main components: a *measurement subsystem*, which includes a helicopter equipped with infrared spectroradiometer and a visible light camera; and *IT subsystem* for processing image data [35].

4.6.1 System Structure

The *iDiaGaSys* system consists of two primary components:

- *Measurement Subsystem* – responsible for data acquisition from the helicopter platform.
- *IT Subsystem* – responsible for processing, analyzing, classifying, and visualizing the measurement data.

Measurement Subsystem

The measurement subsystem is based on an aerial platform, manned helicopter that performs periodic patrol flights along pipeline sections. This subsystem includes the following components [35]:

The research leading to these results has received funding from Horizon 2020, the European Union's Framework Programme for Research and Innovation (H2020) under grant agreement n° 101111888.

- *Imaging Fourier Transform Infrared Spectroradiometer* – a hyperspectral camera that enables the detection of methane emissions in the long-wave infrared range. It analyzes the spectral signatures of gases using atmospheric correction methods and radiative transfer modeling (ART).
- *Visible Light Camera* – captures high resolution images of the terrain, which are used to generate orthophotomaps and analyze land features. It also supports the identification of potential anomalies near pipelines using deep neural networks.
- *GPS System* – ensures precise geolocation of image data, time synchronization, and enables georeferencing of the captured images.

To ensure stable operation of the measurement equipment, a dedicated mounting suspension system was developed and evaluated under real-world conditions. Tests with accelerometer confirmed that the vibration damping level is sufficient, eliminating the need for additional dampers. Data transmission from the hyperspectral camera to the control and measurement system is conducted via fiber optics, ensuring high signal quality and resistance to interference [36].

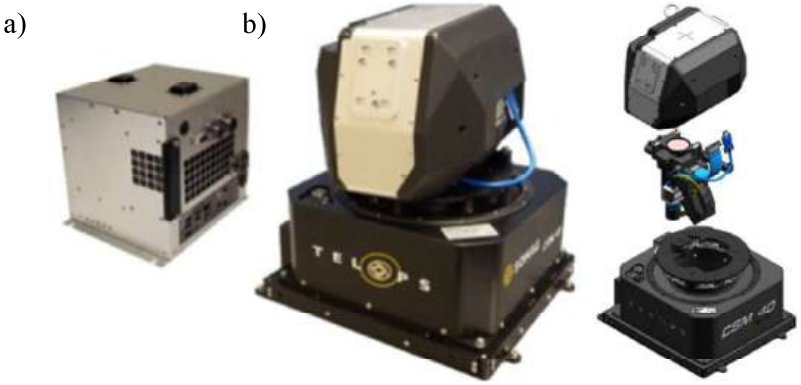

Figure 4-46: TELOPS hyperspectral camera (b) with computing module (a) [35]

The optimal flight altitude has been determined to be 285–300 meters above ground level, which allows for the registration of a terrain line approximately 160 meters wide in the visible light range and about 60 meters in the infrared band, at a speed of approximately 50 kts (92.6 km/h) [35,36]. The measurement system operates in three data acquisition modes:

- *Targeting* – imaging of the area around a designated ground point (for more detailed analysis of a terrain fragment),
- *Mapping* – imaging of a terrain strip along the flight path,
- *CorridorMapping* – imaging along a defined terrain line, e.g. a gas pipeline.

The *Mapping* and *CorridorMapping* modes are intended as the primary modes in the context of system operation by the gas pipeline operator, due to their ability to quickly survey large areas [35].

IT Subsystem

The IT subsystem consists of a computing server with installed software for processing measurement data [36].

The data processing begins with the launch of the *data copying module*, which imports data from the hyperspectral camera's storage medium, creates a directory structure, indexes the data, and extracts auxiliary information (e.g., navigation data, optical parameters). The validity of the data structure is verified in the *parsing module*. Then, the *orthophotomap generation module* is launched, which processes images from the visible light camera, optimizes the optical path parameters, creates a point cloud, and builds a digital terrain model. The *visible light image analysis module* enables the detection and classification of objects interfering

The research leading to these results has received funding from Horizon 2020, the European Union's Framework Programme for Research and Innovation (H2020) under grant agreement n° 101111888.

with gas infrastructure, i.e., those located in its immediate proximity and potentially threatening its safe operation. A separate data processing path is used for infrared band data. The *hyperspectral data analysis module* enables the detection, visualization, and quantification of methane emissions based on advanced statistical algorithms. The process includes preliminary data processing (e.g., atmospheric correction), methane detection using matched filters, and analysis of characteristic spectral pixels to estimate gas concentration. The method is based on the Beer-Lambert law and uses reference spectral databases. In the next two layers, the processing results are converted into a GIS compatible format and exported to the ArcGIS system as map layers [36]. The block diagram of the IT subsystem is shown in Fig. 47:

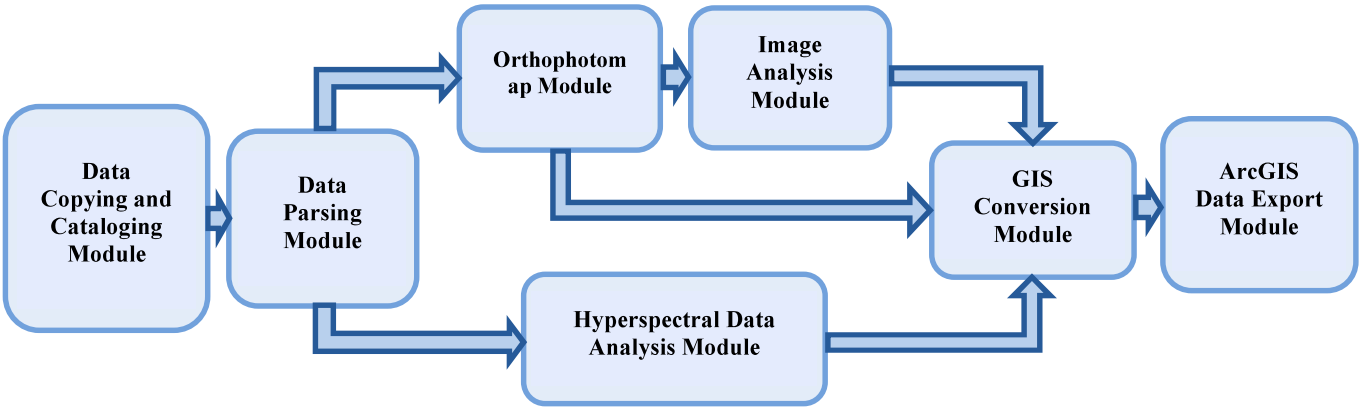

Figure 4-47: Block diagram of the iDiaGaSys IT subsystem [36]

4.6.2 Measurement Method and Data Interpretation

The *iDiaGaSys* system performs advanced environmental and infrastructure measurements along transmission gas pipelines, using two independent yet integrated analytical approaches: Hyperspectral data analysis for methane emission detection, and visible light image analysis for identifying objects that interfere with gas infrastructure.

4.6.2.1 Methane Emission Detection and Analysis (Hyperspectral Module)

Hyperspectral Technology

The hyperspectral camera operating in the long-wave infrared range records the radiation spectrum for each pixel of the image. Unlike most terrain materials, which behave as so-called "gray bodies" (they do not show distinctive spectral features), gases such as methane (CH_4) and water vapor (H_2O) are selective absorbers and emitters of infrared radiation. Their presence can be detected through characteristic absorption bands visible in high spectral resolution data. Thanks to the use of an imaging Fourier transform infrared spectroradiometer, it is possible to obtain the full radiation spectrum for each point of the observed terrain. The camera records data in a format that allows for spectral analysis, atmospheric correction, and identification of gas signatures [37].

The research leading to these results has received funding from Horizon 2020, the European Union's Framework Programme for Research and Innovation (H2020) under grant agreement n° 101111888.

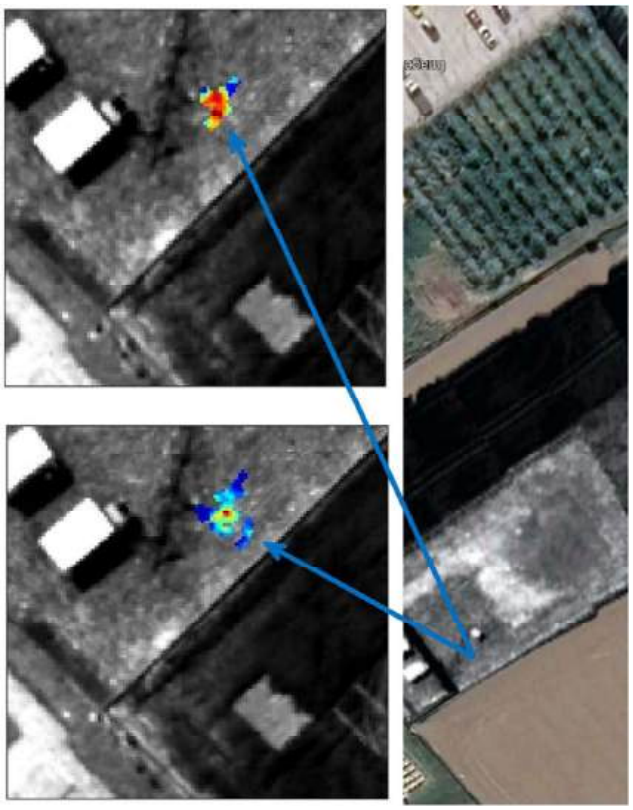

Figure 4-48: Result of hyperspectral data analysis from two flights with visible methane cloud [35]

Methodology of Analysis

The process of hyperspectral data analysis includes [36,37]:

- *Preprocessing*: noise removal, radiometric calibration, atmospheric corrections using the ART (Atmospheric Radiative Transfer) model, data normalization.
- *Methane detection*: algorithms based on the Adaptive Matched Filter (AMF) were applied, supported by CMF (Matched Filter for Clutter) and SAM (Spectral Angle Mapper) methods. The PNNL reference library was used for the spectral characteristics of methane.
- *Emission quantification*: methane concentration is estimated based on the analysis of absorption intensity in characteristic spectral pixels.

Method validation

As part of the research, 520 controlled emission tests were conducted (ranging from 5 to 40 l/min), which allowed for the evaluation of the method's effectiveness. The results showed [37]:

- Sensitivity of the method: 95.7% for emissions of 7 l/min, 100% for emissions ≥10 l/min.
- Lower detection limit: <5 l/min with ≥50% detection probability.
- Specificity: no false alarms under test conditions (potentially 100%, confirmation requires a larger test sample).
- Accuracy: consistent with sensitivity, meeting the ≥70% criterion.

The results confirm the usefulness of the method as a tool for detecting methane emissions in the field. The system also enables visualization of the detected methane cloud and its location relative to gas infrastructure [37].

The research leading to these results has received funding from Horizon 2020, the European Union's Framework Programme for Research and Innovation (H2020) under grant agreement n° 101111888.

4.6.2.2 Image Analysis and Classification of Interfering Objects (Visible Light Module)

RGB Image Processing

The image analysis module in the visible light spectrum uses orthophotomaps generated from images captured by the visible light camera. The goal is to identify physical objects that may interfere with gas infrastructure like: vehicles, buildings, trees, excavations, poles. Artificial intelligence methods based on deep neural networks were used for object classification. A separate network was trained for each object class, which allowed for high recognition accuracy (≥85%) [37].

Data Aggregation and Visualization

Detected objects are aggregated in a dedicated module (see Fig. 47), and data from flights over the same area are archived in a database. This allows to create map layers and time-based change analysis in the GIS system. The system also allows for comparison of classification results with reference data (e.g., masks marked by the operator), which supports the validation process and the improvement of algorithms.

4.6.3 Results of Conducted Inspections

The *iDiaGaSys* system is a tool supporting gas infrastructure inspections using hyperspectral data and visible light images. Tests were conducted using the system over selected sections of gas pipelines owned by GAZ-SYSTEM. The purpose of the inspection flights was to detect potential leaks, terrain anomalies, and methane emissions.

4.6.3.1 Scope of Activities

Inspections were conducted on October 22, 2024, and October 24, 2024, over the following pipeline sections:

- Pipeline 1 – 41 km
- Pipeline 2, DN500 – 17 km
- Pipeline 3 – 1 km

Additionally, two flights were conducted over the Gas Node [38].

4.6.3.2 Inspection Results

Data analysis revealed a substantial number of false methane emission detections, particularly on sections (1) and (2), where all detections were false. In other locations, cases of emissions with high detection probability (PD) were also recorded, although their number was limited. The results for individual flights are summarized in the table below (Table 3):

Table 3: Summary of methane emissions detected during flights [38]

Pipeline Section	Number of Images	Methane Detections	False Detections	High PD	Comments
Section (1)	2038	64	64	0	—
Section (2)	1878	43	43	0	—
Section (3)	793	7	5	2	—
Section (4)	787	26	25	1	—
Section (5)	21	3	1	2	No confirmation
Section (6)	21	4	0	4	No confirmation
Section (7)	57	0	0	0	—

The research leading to these results has received funding from Horizon 2020, the European Union's Framework Programme for Research and Innovation (H2020) under grant agreement n° 101111888.

Based on the hyperspectral analysis data, limitations of the system related to the classification of terrain objects were identified [38].

The quality of classification is influenced by:

- *Season* – autumn and winter data reduce the effectiveness of classifiers, especially in the case of trees.
- *Weather conditions* – partial cloud cover causes variability in image brightness.
- *Camera specifics* – tonal characteristics of the sensor affect classification; it is necessary to adapt the training dataset to the currently used camera.

During the analysis of images acquired from the visible light camera, significant difficulties were observed in the identification of certain object classes. This particularly applies to earthworks, water bodies and forested areas, whose classification is highly dependent on the tonal properties of the sensor and environmental conditions (season, lighting). The current training dataset does not account for the full variability of these features, which results in classification errors. To improve classification effectiveness, it is necessary to expand the dataset, annotate it, and tune the algorithms to the specifics of the target camera. The system shows limitations in the classification of certain terrain objects, although in most cases, identification is correct [38].

This applies especially to:

- *Trees* – tonal variability of data from different cameras affects classification accuracy; it is necessary to enrich the training dataset with data from the camera and from different seasons.

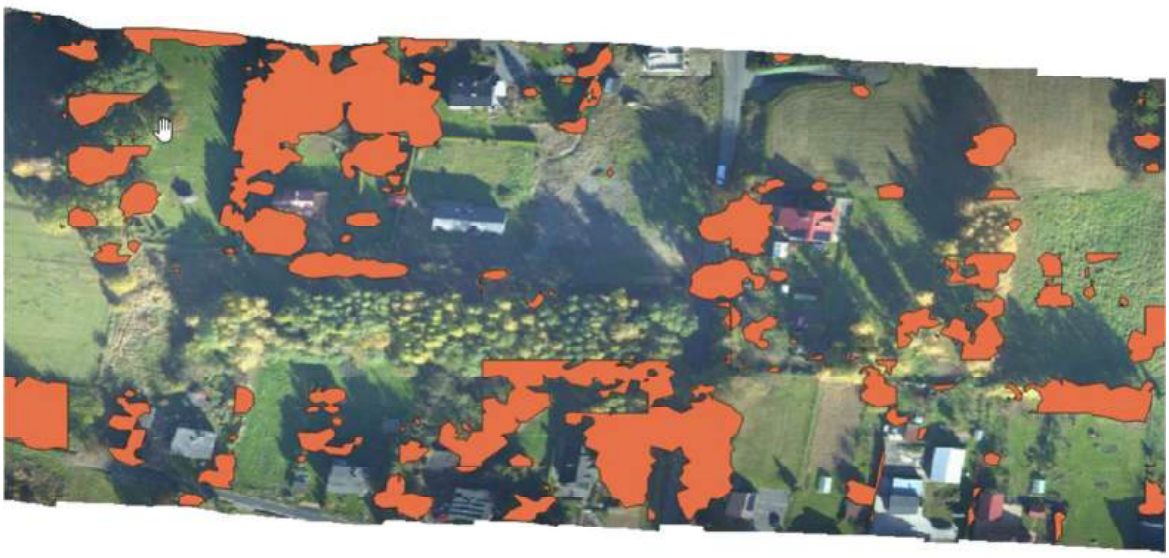

Figure 4-49: Problem with identifying trees in autumn colors [38]

The research leading to these results has received funding from Horizon 2020, the European Union's Framework Programme for Research and Innovation (H2020) under grant agreement n° 101111888.

- *Earth objects (excavations, mounds)* – a high number of false alarms results from an insufficient number of training examples and the classifier's sensitivity to environmental conditions.

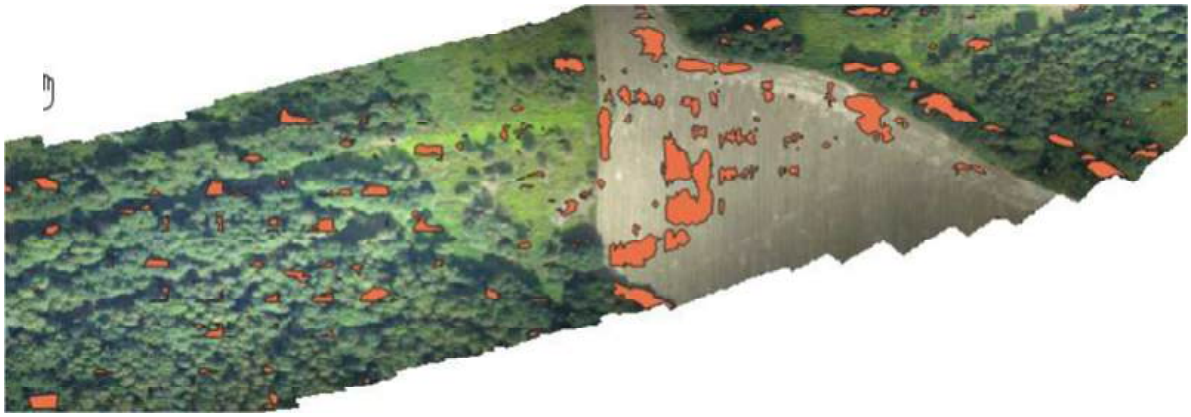

Figure 4-50: Example of shadows identified as excavations [38]

- *Water bodies* – difficulties arise due to the lack of distinct textures and variability in shapes; it is recommended to use additional spectral bands and retrain the classifier.

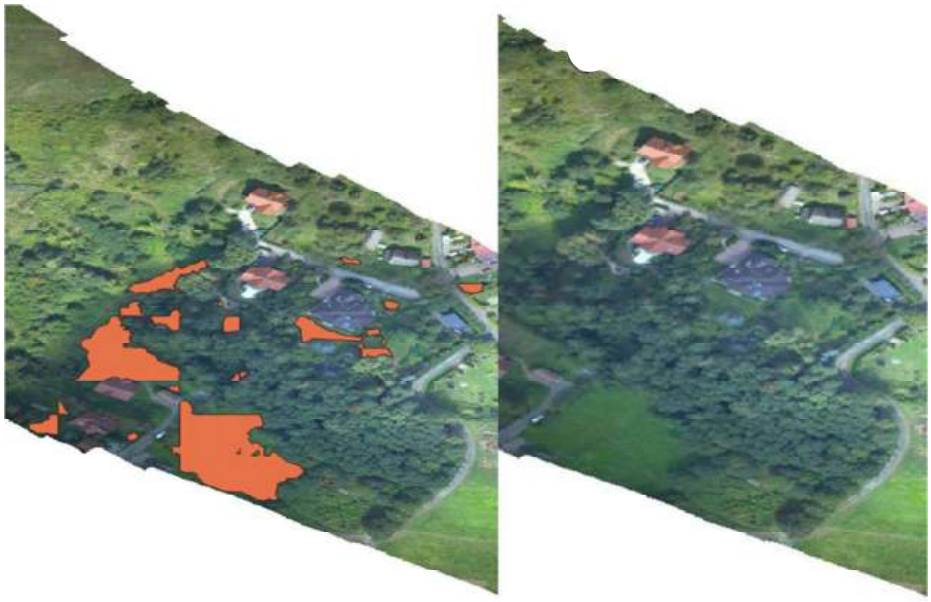

Figure 4-51: Tree shadows classified as water bodies [38]

The research leading to these results has received funding from Horizon 2020, the European Union's Framework Programme for Research and Innovation (H2020) under grant agreement n° 101111888.

- *Storage areas and parking lots* – classification is mostly correct; however, there are misclassifications of objects with similar features (e.g., greenhouse roofs, sports fields).

Figure 4-52: Example of incorrect identification of a storage area [38]

The history change analysis module operates correctly. The most frequently detected anomaly was vehicles, due to their mobility. Other objects, such as trees, excavations, or water bodies, require longer time intervals between flights to observe significant changes [38].

Figure 4-53: Representation of the same area during the second flight (different vehicle location) [38]

4.6.3.3 Conclusions and Recommendations

As part of the inspection, an analysis of the development needs of the *iDiaGaSys* system was also conducted.

The following is recommended:

- Expansion of the training dataset with data from different seasons and weather conditions,
- Annotation of data from the currently used camera,
- Updating and prioritizing object classes in cooperation with GAZ-SYSTEM,
- Development of classifiers for earth, water, and forested objects,
- Further operational testing of the system under various environmental conditions.

The research leading to these results has received funding from Horizon 2020, the European Union's Framework Programme for Research and Innovation (H2020) under grant agreement n° 101111888.

5 Field surveys

Figure 5-1: Selection of a representative section of the gas pipeline for field surveys using non-destructive (NDT) inspection methods [source GAZ-SYSTEM]

Table 4: Pipeline section selected for inspections [source GAZ-SYSTEM]

GAS PIPELINE INSPECTED:	
Pipeline diameter	28” (DN700)
Operational Pressure	5,39 MPa
Total pipeline length	L = 51,41 km (two sections) 2 sections of ~25 km each)
Material / steel grade	18G2A
Pipe type	SAWL, SAWH
Design factor	0,4 (0,50 and 0,55)
Pipeline operator (TSO)	GAZ-SYSTEM
Availability of reference inspection	ILI report’ 2023
Location	south of Poland
Medium transported	natural gas

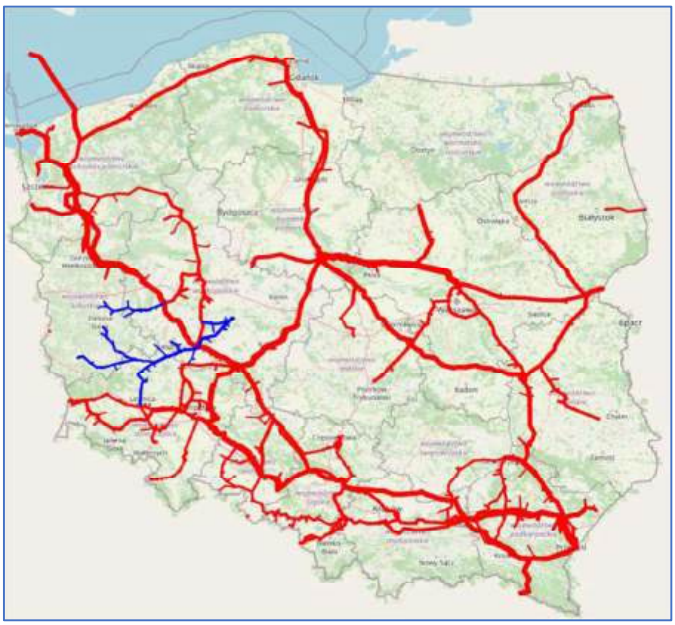

Figure 5-2: Map of the transmission system in Poland [source GAZ-SYSTEM]

The research leading to these results has received funding from Horizon 2020, the European Union's Framework Programme for Research and Innovation (H2020) under grant agreement n° 101111888.

5.1 MFL inspection report - the reference survey.

The tables 5-7 summarises basic information about the MFL survey that was done on the DN 700 pipeline.

Table 5: MFL tool operational data [source GAZ-SYSTEM]

MFL tool operational data:	
Geometry survey tool	DEF.XYZ.28
Magnetic flux leakage measuring tool	GMFL.28.ALL
Pipeline maximum wall thickness	10 ÷ 14.20 mm
Maximum tool velocity	3.048 m/s - 4.878 m/s
Minimum bend radius	1.5D > 3D
Minimum internal diameter	572 mm
Tool Length	2.74 m

Table 6: Reference inspection, basic information [source GAZ-SYSTEM]

MFL inspection basic information:	
Launch Date/Time	19/10/2023 08:24:51
Receive Date/Time	19/10/2023 14:45:48
Run duration	6.35 Hours
Average Velocity	2.25 m/s
Sampling Rate	780 samples per second
Magnetic Field Strength	26000 A/m for 10 mm of wall thickness

Table 7: Pipeline cleaning pig routing prior to inspection [source GAZ-SYSTEM]

Cleaning pig routing:	
1-st foam pig	hardness G3, DN700, length 110 mm
	launched 9/10/2023
1-st. cuff pig with magnet	d711, length 1003 mm (1033 mm with antenna), weight: 180 kg
	launched 11/10/2023
2-nd cuff pig with magnet	d711, length 970 mm (1113 mm with antenna), weight: 200 kg
	launched 13/10/2023

The research leading to these results has received funding from Horizon 2020, the European Union's Framework Programme for Research and Innovation (H2020) under grant agreement n° 101111888.

3-rd cuff pig with magnet	d711, length 970 mm (1113 mm with antenna), weight: 200 kg
	launched 13/10/2023
4-th cuff pig with magnet	d711, length 970 mm (1113 mm with antenna), weight: 200 kg
	launched 14/10/2023
5-th cuff pig with magnet	d712, length 1044 mm (1119 mm with antenna), weight: 250 kg
	launched 14/10/2023
Effect: Gas pipeline considered to be clean for further inspections.	

Figure 5-3: Photographies of cleaning pigs used [source GAZ-SYSTEM]

5.1.1 Results of inspection of the DN 700 pipeline with DEF and MFL measuring pigs on the selected section of the gas pipeline – reference measurements.

The inspection of a 28" (DN 700) natural gas pipeline was carried out on the full section of approximately 25 km using DEF and MFL type measuring pigs. The report prepared from the measuring pig tests was considered an essential reference measurement for verifying the other inspection methods used in the project. The project analyses used the report results collected on a fixed section of 1000 m, which covered defects detected in the DEF and MFL pig tests with an ERF index of ≥ 0.85 according to the classification based on ASME B31G, including a single defect with an ERF index of ≥ 1. Defects below an ERF index of 0.85 were neglected, and their significance in the project was not analyzed. Then, all alternative non-destructive inspection (NDT) methods were tested on the same selected section of the gas pipeline. The exception was the acoustic emission test, which was performed on a shorter section of approximately 150 m, but considering the location of the defect with the highest ERF factor.

The research leading to these results has received funding from Horizon 2020, the European Union's Framework Programme for Research and Innovation (H2020) under grant agreement n° 101111888.

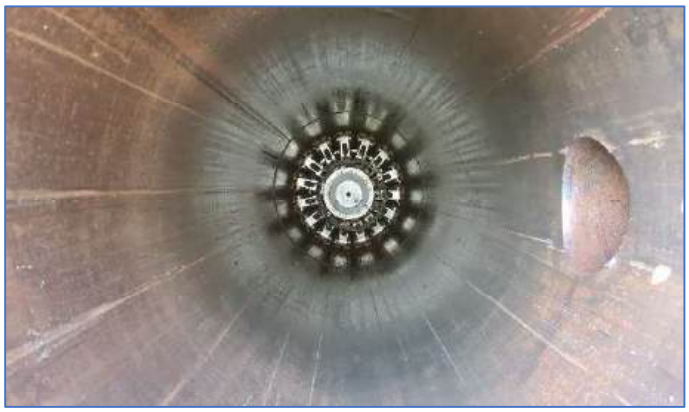

Figure 5-4: Photography of the MFL inspection tool installed inside the pig launcher [source GAZ-SYSTEM]

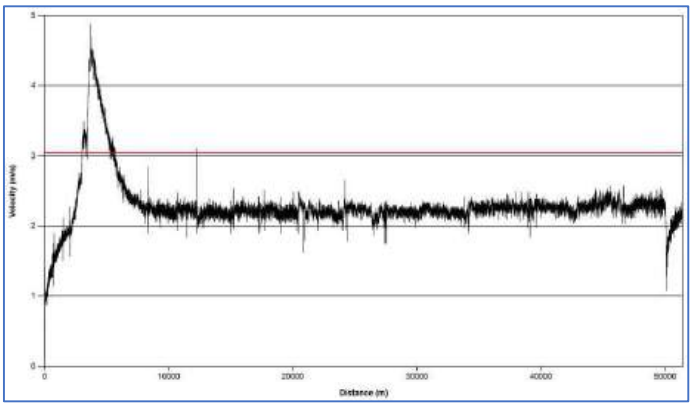

Figure 5-5: Pig velocity during the single pipeline run [source GAZ-SYSTEM]

The figures show the location of the section of the gas pipeline under investigation in the field. An important element of inspection measurements performed on a gas pipeline located in a vast area along the route of such a pipeline is linking the locations of the points specified in the report to specific locations in the field using geographical coordinates. This makes it possible to locate a defect in the field to verify the accuracy of the measurements taken by the measuring instruments used in the tests and to repair any defects identified if needed. The project uses the widely available Google Earth application. The application allows the use of satellite images to which the coordinates of characteristic points can be assigned. It is important to note that coordinates from files supported by this application can be loaded from a local computer, thus eliminating the need to export data outside the organization, which is particularly important for a gas transmission system operator (TSO) protecting data on technical infrastructure in the field.

The research leading to these results has received funding from Horizon 2020, the European Union's Framework Programme for Research and Innovation (H2020) under grant agreement n° 101111888.

Figure 5-6: Gas pipeline section selected for comparison of NDT test results [source GAZ-SYSTEM]

Figure 5-7: Location of welded joints on the analyzed section of the gas pipeline [source GAZ-SYSTEM]

The research leading to these results has received funding from Horizon 2020, the European Union's Framework Programme for Research and Innovation (H2020) under grant agreement n° 101111888.

Figure 5-8: Appearance of feature points obtained from the reference survey in the Google Earth application [source GAZ-SYSTEM]

Figure 5-9: Overlay of all methods on the examined section of the gas pipeline. Data presented in Google Earth [source GAZ-SYSTEM]

The selected section of the gas pipeline crosses flat terrain, which, for the most part, guaranteed access for testing using alternative non-destructive inspection methods. The pipeline was first marked out in the field, including locating the geometric coordinates of the circumferential welded joints connecting the individual pipe sections. Regarding the defect with an ERF of ≥ 1 (1.035), the gas pipeline operator took steps to verify the nature of the defect. After excavating the pipeline, non-destructive radiographic testing was performed to confirm the location and depth of the defects, including those on the inside and outside of the pipeline. The detected defect consisted of a cluster of smaller material defects located on the inside of the pipe, covering an area of approximately 0.05 m² with a maximum depth of 1.3 mm, which corresponded to the information from

The research leading to these results has received funding from Horizon 2020, the European Union's Framework Programme for Research and Innovation (H2020) under grant agreement n° 101111888.

the piston indicating a defect area of 0.41 m² and a maximum of 1.4 mm (14% wall thickness loss). The location of the defect on the pipe circumference was also confirmed, indicating 04:10 according to the pig measurement, versus the indication of 04:00 on the pipe circumference according to direct inspection after excavation in the field. The cause of the pipe material loss was determined to be material defects from the pipe production stage. In this case, the MFL test confirmed its effectiveness and high measurement accuracy.

Figure 5-10: Localization of the ERF ≥ 1 defect in the field [source GAZ-SYSTEM]

5.2 Acoustic emission (AE) measurements.

The table 8 summarises basic information about the field survey done with the acoustic emission method.

Table 8: AE Operational Data [source GAZ-SYSTEM]

AE operational data:		
Measurement interpretation method	Method/database created by the Contractor.	
Anomaly classification / description	Classes and codes of AE signals describing anomalies.	
	5 anomaly classes	3 levels of risk
Tests date	08/08/2024	
Tested pipeline distance	150 m	
Duration of measurement in the test	3600 sec. (1 hour)	
Type of sensors used	VS-75 SCI (20 ÷ 100 kHz)	
Number of sensors used	4 separate sensors	
Additional sensor features	built-in preamplifiers	
Signals recording unit	32-channel EA processor with measurement channels and AE software win for Express -8	

The research leading to these results has received funding from Horizon 2020, the European Union's Framework Programme for Research and Innovation (H2020) under grant agreement n° 101111888.

Figure 5-11: Installation and geodetic coordinates measurements of the location of AE sensors on the pipeline wall, connection of sensors to the signal recording computer [source GAZ-SYSTEM]

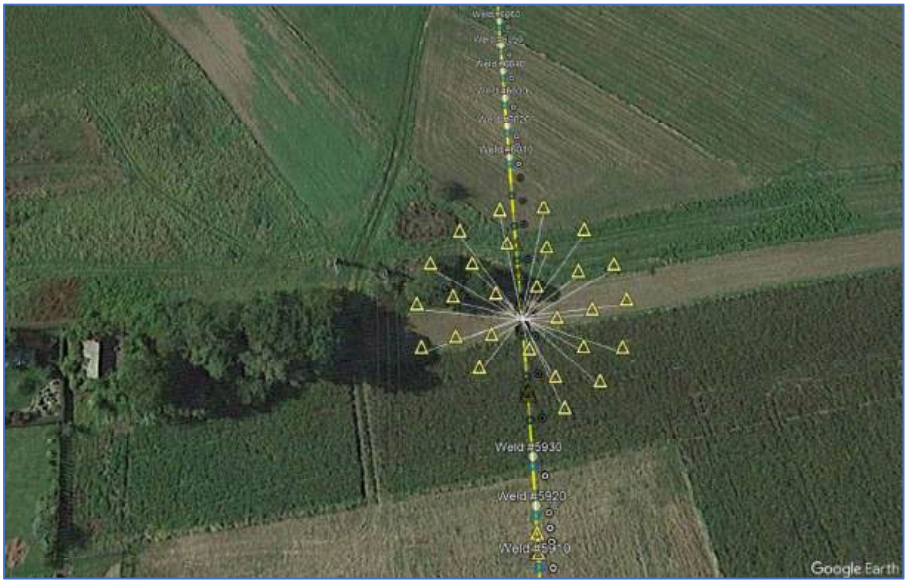

Figure 5-12: The appearance of signals accumulated into a single point presented in Google Earth application [source GAZ-SYSTEM]

5.2.1 Obtained AE inspection results.

During the measurements, anomalies were detected in the recorded signals, with two main parameters: signal strength and ASL amplitude. The recorded signals were then filtered using the Contractor's reference signal database, which allowed for the isolation and identification of anomalies. Three main areas generating anomalies were observed in the measurements:

Area 1, covering a 30-meter section (from 0 to 30 m), showed increased generation of anomalies in classes 3 and 4 in two locations. The signals detected can be interpreted as potential corrosion processes resulting in a thinner wall thickness, up to 5% at locations 20 m and 25 m. Area 2, covering a 12-meter section (from 75 m to 87 m), showed increased generation of anomalies in classes 3 and 4. The signals detected can be interpreted

The research leading to these results has received funding from Horizon 2020, the European Union's Framework Programme for Research and Innovation (H2020) under grant agreement n° 101111888.

as potential corrosion processes resulting in a thinner wall thickness, up to 30% at location 87 m. Area 3, covering a 23-meter section (from 116 m to 139 m), showed increased generation of anomalies in classes 3 and 4 in two locations. The signals detected can be interpreted as potential corrosion processes. resulting in a thinner wall thickness, up to 5% at the 120 m and 139 m locations.

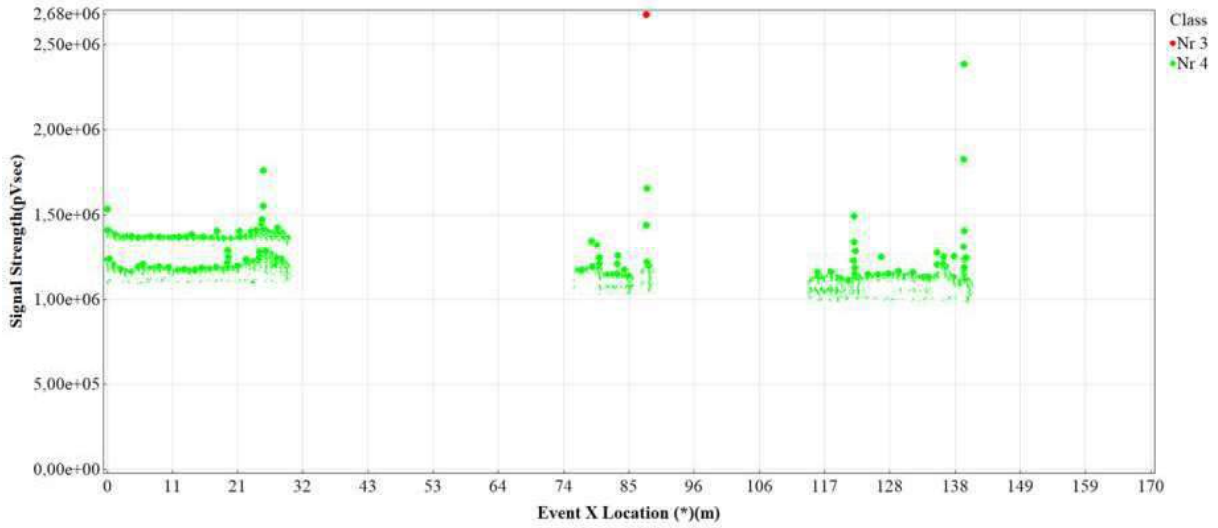

Figure 5-13: Location of anomalies along the length of the tested section as a function of the signal strength parameter (pV·s) [source GAZ-SYSTEM]

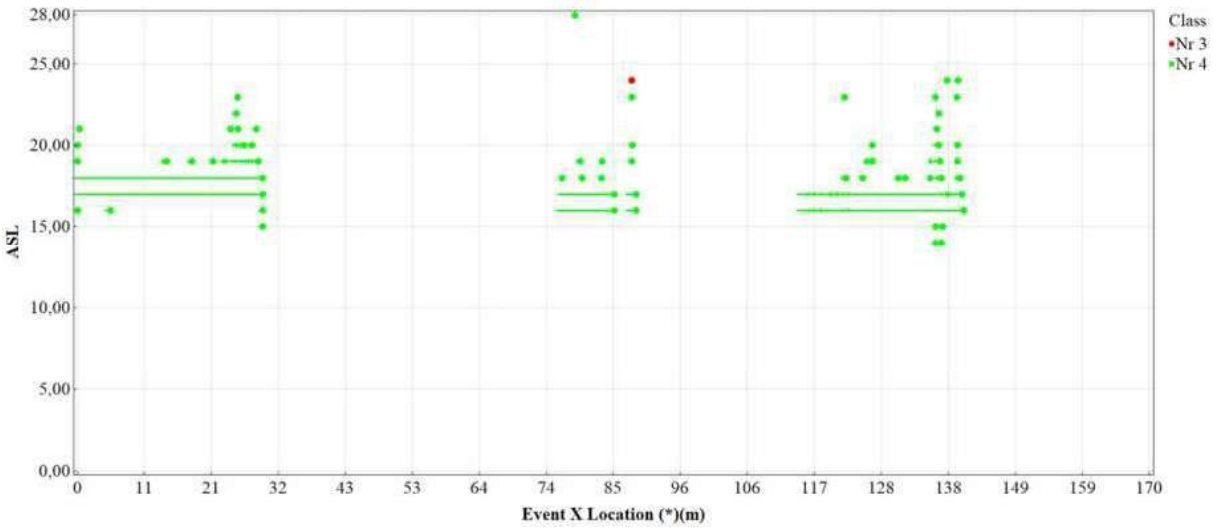

Figure 5-14: Location of anomalies along the length of the tested section as a function of the average amplitude value parameter (ASL) [source GAZ-SYSTEM]

No defects in the form of dents, ovalization, longitudinal or transverse cracks, including cleavage cracks, were found on the tested section of the gas pipeline, which are assumed to generate acoustic emission signals. These defects were also not confirmed by the reference test using DEF and MFL pigs. The internal pressure during the acoustic emission test was 4.23 MPa, representing 78% of the MOP, a value relatively close to the maximum operating pressure permitted by the design documentation for this gas pipeline. However, this value is significantly lower than the yield stress or strength limit of the steel pipeline, where acoustic emission signals are strong and intense. Therefore, during the recording of acoustic emission (AE) signals, calibration of the instrument sensitivity and setting low acoustic emission (AE) signal discrimination thresholds were necessary.

The research leading to these results has received funding from Horizon 2020, the European Union's Framework Programme for Research and Innovation (H2020) under grant agreement n° 101111888.

5.2.2 Additional comments.

During the measurements, it was found impossible to identify welded joints in the gas pipeline pipe sections using the acoustic emission method. This was considered an important element in verifying the use of the acoustic emission method for detecting material defects in steel pipelines, as the ILI method refers defect location to distance relative to circumferential welded joints. The entity performing acoustic emission (AE) measurements on the gas pipeline indicates that the ability to locate welded joints will only be possible if weld defects occur – structural defects or cracks caused by overloading. This issue is important in relation to the magnetic field leakage (MFL) measurements, because in this test, the welded joint causes significant distortion of the magnetic field distribution lines, making detection of welded joint defects impossible. Based on the measurements, it can be concluded that the lack of recording of acoustic emission (AE) signals in the elastic range (class 5) from circumferential welded joints existing in the tested pipeline section indicates the absence of weld defects. More accurate description of the technical condition of welded joints using the acoustic emission method requires adapting the system to the technology used to make these joints. Then the entity carrying out the researches, declares the possibility of using acoustic emission signals according to classes 1 ÷ 4.

5.3 Stress Concentration Tomography (SCT)

The table 9 summarises basic information about the field survey done with the Stress Concentration Tomography method.

Table 9: SCT operational data [source GAZ-SYSTEM]

SCT operational data:		
Measurement interpretation method	Contracor's internal competency assessment program.	
Anomaly classification / description	Stress concentration zones (SCZs)	
	Each SCZ is given a localised hoop stress reading in absolute terms (MPa) and as a percentage of the pipeline material SMYS.	
	Estimated Stress Level [MPa]	Estimated Stress [% of SMYS]
Tests date	2024/10/2	
Tested pipeline distance	1014,27 m	
Duration of measurement in the test	~ 3 hours	
Survey ID	24-FW-POL-GAZ-01-FR	
Type of device used	UNISCAN	

5.3.1 The influence of gas pipeline residual magnetism on the measurements performed.

During the measurements, residual magnetism from the MFL inspection was detected, which could have affected the SCT results, particularly in some sections. This was taken into account in the assessment. Residual magnetism was strong enough to saturate SCT sensors in specific areas, potentially leading to elevated stress values. However, the relative differences between SCZs remain valid and reliable for evaluation. Finite element analysis has been applied to refine these stress values where residual magnetism may have caused inaccuracies. Additionally, any errors introduced by residual magnetism are expected to diminish over time, particularly as the interval from the MFL inspection exceeds 12 months, allowing for increasingly accurate SCT assessments.

The research leading to these results has received funding from Horizon 2020, the European Union's Framework Programme for Research and Innovation (H2020) under grant agreement n° 101111888.

The search algorithms applied may detect magnetic anomalies generated by the MFL tool, rather than by increased localized stress (i.e., the Self Magnetic Flux Leakage that SCT is designed to detect). The magnetic signatures reported by the SCT algorithms are assumed to correspond to defects and are likely influenced by the residual magnetization similarly, when the girth weld detection algorithm was deployed, a spool length of 12 m was assumed. It is important to note that while residual MFL magnetic fields may affect SCZ detection, they are not expected to impact the accuracy of the 3D mapping algorithm or subsequent bending strain calculations.

5.3.2 Obtained SCT inspection results.

During the measurements, no significant clustering of SCZs was observed throughout the inspected section of the gas pipeline, indicating that the SCZs are generally isolated rather than the result of systemic external loading or localized pipeline damage. Additionally, no significant bending strain was observed during the surveys conducted.

The SCT survey on the pipeline identified 185 stress concentration zones (SCZs). Key observations from the data are as follows – SCZ summary in table 10.

Table 10: SCZ Summary [source GAZ-SYSTEM]

SCZ summary								
Pipeline diameter	Number of SCZs	Assumed nominal operating hoop stress		Minimum Identified Localised Stress		Maximum Identified Localised Stress		Design Max Hoop Stress
28" / DN700	185	[MPa]	% of SMYS	[MPa]	% of SMYS	[MPa]	% of SMYS	[MPa]
		168	47	49	14	266	75	192

SCZs above nominal hoop stress.

- 112 SCZs were detected with hoop stress exceeding the nominal value of 192 MPa (47% of SMYS). These anomalies may represent defects that could develop over time, so periodic monitoring is recommended to map their development.
- Among these, one SCZ (SCZ ID 29426) has a significantly elevated stress value compared to the others. This anomaly should receive closer attention and further analysis to assess the potential risk.

Bending strain and depth of cover calculations.

Bending stress classification is based on 3D mapping data included in the report. Lateral and vertical bending strain coefficients are calculated. SCT predicts cover depth and lateral displacement. Using these results, along with accurate GNSS data, SCT recreates the pipeline geometry, including up/down and/or left/right movements. Bending strain, including horizontal and vertical, is calculated based on geometry. Stresses are not included in the calculations, as the methodology does not utilize local stress data occurring in the SCZs.

Magnetic flux leakage (MFL) influences.

An MFL inspection was performed in October 2023, and then an SCT test was performed in October 2024. Although there is a guideline for a 12-month period and this was met, it was determined during measurements that residual magnetism after the MFL inspection may still be present. This could have affected the SCT test results, particularly in some sections, and this was taken into account in the assessment. However, the assessment of the entity performing the SCT recommends further monitoring of the pipeline to evaluate potential long-term changes in SCZ stress values. It is possible that this effect will be particularly noticeable in the vicinity of girth welds, making it difficult to draw definitive conclusions about the SCZ detected in these areas of girth welds.

The research leading to these results has received funding from Horizon 2020, the European Union's Framework Programme for Research and Innovation (H2020) under grant agreement n° 101111888.

Distribution of SCZs.

SCZs appear evenly distributed along the pipeline, with no major clustering, suggesting they are not due to localized external loading or damage but are instead dispersed throughout the pipeline.

Girth weld proximity.

The 9 SCZ zones determined to be above the maximum allowable circumferential stress (DMAOHS), 5 are located within or 1 meter of the girth weld. This proximity may indicate welding defects such as misalignment, inclusions, or linear defects, as well as possible corrosion or metal loss. However, the influence of residual MFL magnetization around the circumferential welds may have affected the accuracy of the absolute stress magnitude reported by SCT, and therefore it was considered that further monitoring of these areas is needed to determine whether the magnitude remains as predicted in this report. If so, or if the stress value increases, the defect having a significant impact on the pipeline wall stress will be confirmed as greater than the design allowable, and a decision can be made regarding its impact and future action.

The four SCZs exceeding the DMAOHS are located more than 1 meter away from any girth weld. Two of these SCZs are among the highest stress estimates in the study and may indicate the need for further inspection of these locations.

3D Mapping and Bending Strain.

According to the SCT measurements performed, no significant changes in depth of cover or significant bending strain are present in the segment inspected.

Gaps in surveys on the measured section of the gas pipeline.

During the survey, there were interruptions caused by the presence of inaccessible areas, metal fencing, and ditch. The survey was conducted using a device carried by the person performing the measurements. Such gaps can be prevented by using a drone for measurement from the air. The interruptions were recorded in the appropriate places and were not considered in the survey evaluation.

Evaluation of the SCT measurement method for DN 700 gas pipeline technical condition assessment.

The SCT method used to assess the pipeline condition successfully identified stress concentration zones (SCZs) along the pipeline. These zones represent areas that may require further investigation for potential metal loss or deformation. The presence of residual magnetism from previous MFL inspections could have saturated the SCT sensors in some sections, potentially leading to elevated stress values. However, the SCT methodology still provides valuable information on the overall stress distribution, and the relative differences between SCZs remain reliable. SCZ locations are mapped and can be periodically monitored to track any changes in stress levels. SCT is suitable for identifying areas of high stress concentration, but it does not characterize the defect causing the local stress increase. While SCT cannot directly identify SCCs, it will report the location of abnormally high, local stress increases which might be attributable to SCCs even at the early stages of microcrack development.

The research leading to these results has received funding from Horizon 2020, the European Union's Framework Programme for Research and Innovation (H2020) under grant agreement n° 101111888.

Figure 5-15: Characteristic points collected during measurements using the SCT method presented in Google Earth application [source GAZ-SYSTEM]

Figure 5-16: Aerial view of the pipeline route [source GAZ-SYSTEM]

The research leading to these results has received funding from Horizon 2020, the European Union's Framework Programme for Research and Innovation (H2020) under grant agreement n° 101111888.

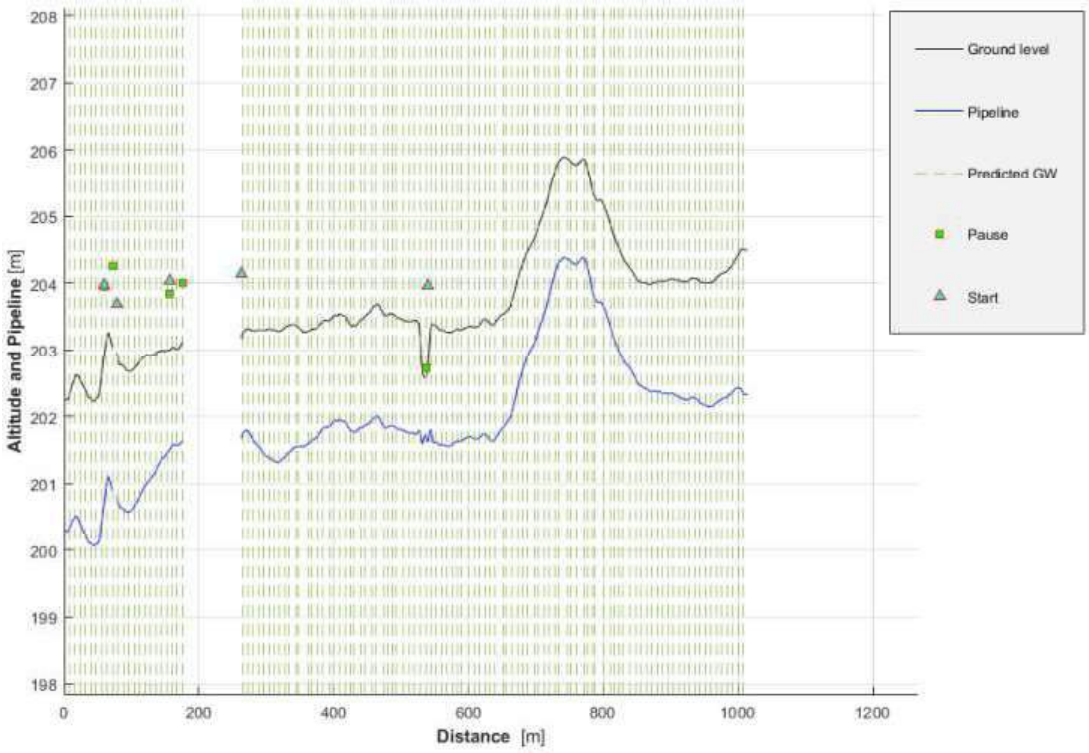

Figure 5-17: Pipeline depth of cover from start to end point [source GAZ-SYSTEM]

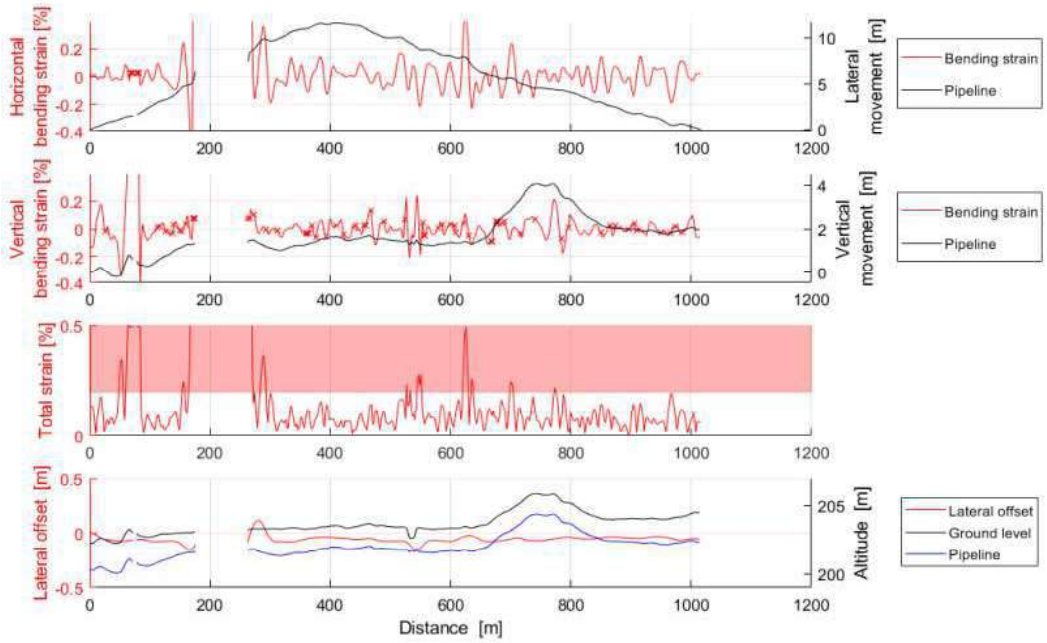

Figure 5-18: Bending strain and depth of cover from start to end point [source GAZ-SYSTEM]

5.4 Metal Magnetic Memory Method

As part of the analyses carried out, two cases were reviewed in which the results of MMMtests were compared with the results of MFL pigging.

The research leading to these results has received funding from Horizon 2020, the European Union's Framework Programme for Research and Innovation (H2020) under grant agreement n° 101111888.

5.4.1 Determining the correlation of indications from gas pipeline pigging using MFL inspection pigs with the indications from tests performed using the MMM-NCMD method, based on the example of a DN300 transmission pipeline.

a) Operational data

The DN300 pipeline with MOP 6.3 MPa, for which MMM-NCMD, MFL, and GEO tests were performed, was built before 1983. Its total length from the sending trap to the receiving trap is 38.8 km.

The maximum operating pressure (MOP) for the DN300 pipeline is 6.3 MPa. The pipeline was constructed from spiral-welded or seamless pipes with an external diameter Dz = 323.9 mm and a wall thickness WT = 5.6 mm. The steel used for the pipeline, grade G355, has the following mechanical properties:

- Yield strength Re = 355 MPa,
- Tensile strength Rm = 450–620 MPa.

b) Area of testing and technical analysis

For the DN300 pipeline, which was subjected to MFL testing along its entire length (starting point: DN300 ball valve installed at the exit from the sending trap), the analysis covers a subsection of the DN300 pipeline bounded by points Pt10.3.1 (MFL distance 6881.626 m) and Pt10.56.10 (MFL distance 15027.154 m).

a) Obtained MFL results

For the designated DN300 pipeline subsection bounded by points Pt10.3.1 (MFL distance 6881.626 m) and Pt10.56.10 (MFL distance 15027.154 m), the following were detected:

- 811 circumferential welds;
- 37 bends – including 5 to the right, 8 to the left, 16 downward, and 8 upward;
- 5 AGM reference points (markers);
- 37 changes in pipeline wall (change in wall thickness or pipe type);
- 1 triple connector;
- 4 STOPPLE-type fittings;
- 9 other nozzles (including one on the underside of the pipe);
- 1 casing pipe;
- 1 monoblock (the image from data recorded by the magnetic MFL inspection pig looks almost identical for monoblocks and flange connections);
- 15 metallic objects within the pipeline area (close/in contact);
- 29 geometric anomalies of dent type with depths in the range of 1.0 ÷ 3.3%;
- 1 geometric anomaly of weld leak type;
- 231 metal losses with depths in the range of 5 ÷ 59% and estimated repair factors (ERF) in the range of 0.830 ÷ 0.886;
- 52 metal losses of MFG type (manufacturing defects) with depths in the range of 8 ÷ 40%.

After the MFL inspection pig run was completed, the inspection service provider delivered a summary of the most severe anomalies detected by the inspection tool. Based on mutual agreements, a decision was made to verify an external metal loss with a depth of **59%**.

The research leading to these results has received funding from Horizon 2020, the European Union's Framework Programme for Research and Innovation (H2020) under grant agreement n° 101111888.

Figure 5-19: Metal loss anomaly of manufacturing origin classified as "Slivers", detected based on the results of magnetic inspection pigging of the DN300 pipeline [39]

As a result of field verification:

• The verified metal loss anomaly originated during the pipe manufacturing process. In the pipeline anomaly atlas "Macaw's Pipeline Defects," the most similar shape corresponds to the anomaly described as "slivers." According to the definition in the PN-EN10163-1 standard, this type of anomaly should be classified as "**slivers**" [39].

The location where the anomaly was verified had previously been subjected to MMM NCMD measurements. **No SCZ occurrence was reported for this location** [39].

- **Obtained MMM-NCMD results**

For the designated DN300 pipeline subsection bounded by points Pt10.3.1 (MFL distance 6881.626 m) and Pt10.56.10 (MFL distance 15027.154 m), the following were detected:

• 2 magnetic anomalies in the form of Stress Concentration States in category II with individual numbers SCZ 48 and SCZ 50,

• 5 magnetic anomalies in the form of Stress Concentration States in category III with individual numbers SCZ 45, SCZ 46, SCZ 47, SCZ 49, and SCZ 51.

The length of the area where stress concentration states occurred ranges from 1 to 2 m (SCZ 48 to SCZ 51) and 20 m for SCZ 45.

- **Comparison of results**

When directly comparing the results presented in this report, it should be noted that for all seven areas of SCZ occurrence, it is possible to associate them with three (**3**) metal losses, six (**6**) manufacturing-origin metal losses, and two (**2**) geometric anomalies of the dent type. Considering the total number of anomalies reported from inspection tools, this gives effectiveness for individual defect types at the following levels:

i. For metal losses: three (**3**) metal losses are associated with SCZ, which, given the total number of 231 recorded by inspection tools, gives an effectiveness of **1.3%.**
ii. For manufacturing-origin metal losses: six (**6**) manufacturing anomalies are associated with SCZ, which, given the total number of fifty-two (**52**) recorded by inspection tools, gives an effectiveness of **11.5%.**
iii. For geometric anomalies of the dent type: two (**2**) geometric anomalies are associated with SCZ, which, given the total number of twenty-nine (**29**) recorded by inspection tools, gives an effectiveness of **6.9%.**

The research leading to these results has received funding from Horizon 2020, the European Union's Framework Programme for Research and Innovation (H2020) under grant agreement n° 101111888.

• As a result of analyzing the causes of stress concentration states based on data recorded by inspection tools, it should be stated that:

a) In five (**5**) locations, SCZ may occur due to the presence of bends made on-site from spiral pipes with a small angle and large bending radius, used to adapt the pipeline to terrain conditions;
b) In two (**2**) locations, SCZ may occur due to the presence of manufacturing-origin metal loss anomalies;
c) In two (**2**) locations, SCZ may occur due to the presence of metal loss anomalies;
d) In one (**1**) location, SCZ may occur due to the presence of a geometric anomaly of weld leak type;
e) In two (**2**) locations, SCZ may occur due to the presence of geometric anomalies of the dent type;
f) The above-mentioned causes are mostly interconnected in various configurations.

5.4.2. Comparative analysis of diagnostic methods for DN500 pipeline

The input data for the analysis from the MFL tool are the information obtained during the run carried out in November 2014. At that time, a DN500 pipeline with a length of 38.92 km was inspected. The comparison was made using Google Earth, where data from the tool inspection, the list of SCZ (Stress Concentration Zones) from the NCMD-MMM test, and additional location data related to repair activities on the DN500 pipeline were previously loaded.

Next:

a) Anomalies detected by the tool that were within 5 m of identified SCZ of type 2 or 3 were marked;
b) The length of SCZ was verified;
c) If the tool indication falls within the SCZ length or the difference is up to 2 m, it is considered that the tool and SCZ indicated the same location. Other results were rejected;
d) Then, all available data were compiled in a tabular format to search for analogies in the test results.

Next:

a) Anomalies detected by the tool that were within 5 m of identified SCZ of type 2 or 3 were marked;
b) The length of SCZ was verified;
c) If the tool indication falls within the SCZ length or the difference is up to 2 m, it is considered that the tool and SCZ indicated the same location. Other results were rejected;
d) Then, all available data were compiled in a tabular format to search for analogies in the test results.

Results of the analysis:

The MFL tool inspection over a section of approximately 9500 m, where NCMD-MMM was also performed, revealed 238 anomalies from the CDP tool run and 13 anomalies from the AFD tool. One of these anomalies was included in the “list of the most severe anomalies,” selected based on four principles:

Principle 1: anomalies with a depth greater than or equal to 80% of wall thickness

Principle 2: anomalies with ERF greater than 1.0

Principle 3: anomalies with ERF greater than or equal to 0.95 and less than 1.0

Principle 4: anomalies with a depth greater than or equal to 20% of wall thickness and less than 80%

The anomaly in question was a “circumferential weld anomaly” (selected based on Principle 4) with a depth of 31%, located at 7111.071 m at the 10:30 position on the pipe. This anomaly was not indicated during NCMD-MMM testing. The NCMD-MMM test indicated 29 SCZ type 2 sections and 104 SCZ type 3 sections in the examined area.

After analyzing the data over a section of 9404.818 m, 15 locations were identified that were indicated both by the MFL tool and by the MMM test, where they were classified as SCZ2 or SCZ3. Regarding the tool, all results came from the standard MFL-CDP tool. Below is the list:

The research leading to these results has received funding from Horizon 2020, the European Union's Framework Programme for Research and Innovation (H2020) under grant agreement n° 101111888.

Table 11: Results indicated both by MFL tool and the MMM test [source GAZ-SYSTEM]

Nr SKN	Rodzaj SKN	Km tłok	Wskazanie tłoka	Godz.	depth%	length	width
Y05-III	SKN3	13919.306	Anomaly-Girth weld irregularity	12:21			
Y10-III	SKN3	12715.889	Anomaly-Girth weld anomaly	10:09	15	21	193
Y13-III	SKN3	12589.168	Anomaly-Girth weld irregularity	08:55			
Y27-III	SKN3	10465.691	Repair-Welded sleeve begin				
Y31-III	SKN3	10317.269	Anomaly-Girth weld irregularity	09:40			
Y47-III	SKN3	9828.033	Anomaly-Spiral weld anomaly	09:02	16	33	22
Y53-III	SKN3	9596.449	Anomaly-Girth weld anomaly	09:44	19	15	63
Y60-III	SKN3	8912.031	Anomaly-Girth weld irregularity	10:02			
Y62-III	SKN3	8888.525	Anomaly-Girth weld irregularity	08:53			
Y66-III	SKN3	8696.663	Casing end				
Y67-II	SKN2	8684.622	Casing begin				
Y82-III	SKN3	7730.526	Weld-Bend end				
Y87-II	SKN2	7573.183	Anomaly-Girth weld anomaly	11:33	14	22	80
Y103-III	SKN3	6671.426	Anomaly-Pipe mill anomaly	06:22	15	25	18
Y105-III	SKN3	6651.911	Anomaly-Corrosion	03:30	10	18	25

8 out of the **15** indicated locations concerned circumferential welds, 6 of which were located in the upper half of the pipe, which indicates that the MMM method has greater accuracy for indications located on the upper part of the pipe, which is logical considering the testing method.

On the examined section, the tool detected 179 anomalies related to circumferential welds. The greatest depth of such an anomaly indicated by the ILI tool was 31%, while NCMD-MMM tests showed anomalies up to a depth of 18%. Regarding the length and width of anomalies, the ILI tool also found larger anomalies than the maximum indicated by the NCMD-MMM method.

In the case of the anomaly corresponding to SCZ type 2 Y87-II, an excavation was performed during the verification of MMM tests.

The research leading to these results has received funding from Horizon 2020, the European Union's Framework Programme for Research and Innovation (H2020) under grant agreement n° 101111888.

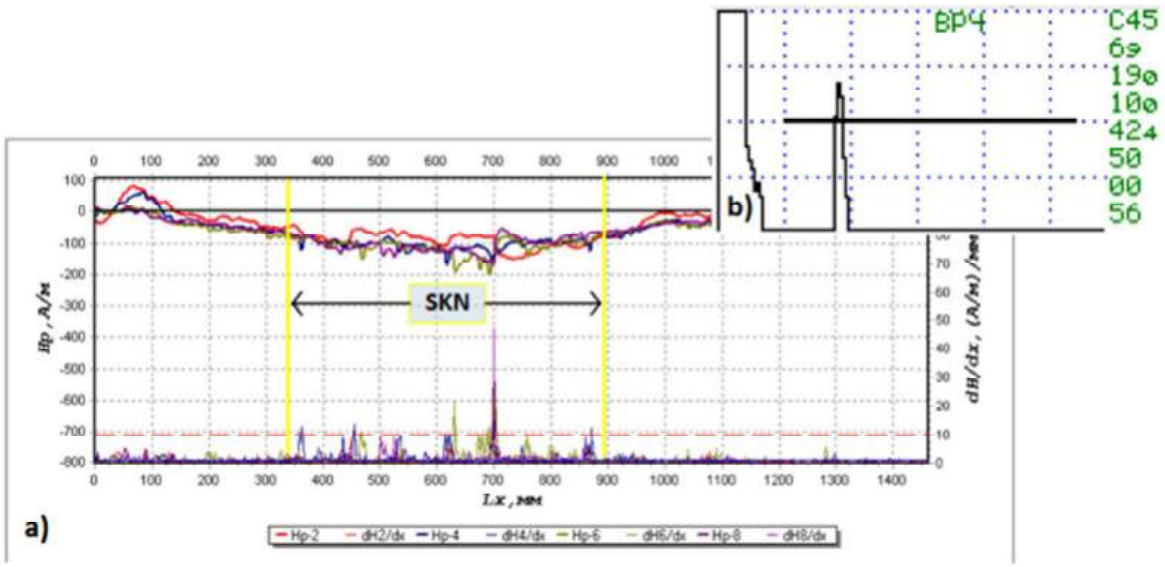

Figure 5-20: Detected anomaly [source GAZ-SYSTEM]

2 out of the 15 results correspond to the beginning and end of a single casing pipe. Essentially, the NCMD-MMM method is not effective for road/railway crossings in casing pipes, and in this case, SCZ indicates the start and end of the casing pipe, with no actual stress concentration zone present. On the examined section, the ILI tool detected 7 casing pipes, which were likely visible during the MMM test as well, but based on visible ventilation columns, they were rejected as SCZ. There are no real anomalies/SCZ in these locations.

1 out of the 15 locations (SCZ У82-III) corresponds to the end of a bend. On the examined section, the inspection ILI tool detected 19 bends.

1 out of the 15 locations (SCZ У27-III) indicates the location (start) of a repair sleeve. During NCMD-MMM testing, such sleeves, sealing elements, and blind connections are often indicated as stress concentration zones. No anomalies occur there; the indication results from interpreting the magnetogram without knowledge of the placement of these elements. On the examined section, the ILI tool detected 5 repair sleeves (10 indications).

1 out of the 15 locations (У47-III) is an indication of a spiral weld anomaly on the pipe at the 9 o'clock position. This anomaly was not included in the list of the most severe anomalies and would not qualify for further action. It was one of two anomalies of this type indicated by the ILI tool. The second anomaly was comparable, located at the 3 o'clock position, thus in a similar location relative to ground level.

1 out of the 15 locations (У103-III) was identified as a pipe processing anomaly (manufacturing defect) located on the underside of the pipe (6 o'clock) with ERF = 0.78. The ILI tool detected 54 anomalies of this type on the examined section (including 43 by the standard MFL), all with ERF values ranging from 0.78 to 0.80. The dimensions and depth of the anomaly do not differ from other anomalies that were not identified as stress concentration zones.

1 out of the 15 locations (У105-III) corresponded to a corrosion anomaly located at the 3:30 position. The CDP tool detected 9 anomalies of this type with ERF values in the range of 0.78–0.80. The dimensions and depth of the anomaly do not differ from other anomalies that were not identified as stress concentration zones.

5.4.3. Summary

The analysis confirm that both diagnostic methods can identify, to some extent, the same locations during testing. However, taking the number of anomalies indicated by the ILI tool (251) as a reference and comparing it to the number of SCZ corresponding to anomalies (after excluding results indicating casing pipe ends, bends, and repair sleeves), stress concentration zones were detected in about 4.4% of anomalies. Based on the analyzed data, it can be concluded that the probability of identifying the same locations with both methods is low.

The research leading to these results has received funding from Horizon 2020, the European Union's Framework Programme for Research and Innovation (H2020) under grant agreement n° 101111888.

The analysis did not show that any specific type of anomaly is particularly classified as SCZ. There is no visible correlation with depth, length, or width of anomalies.

In summary, both the MFL tool run and the MMM-NCMD test serve to assess the technical condition of the pipeline, using magnetic phenomena, but the results are not highly consistent.

For unpiggable pipelines, these tests are a method that can be used to assess the technical condition of the pipeline over a longer linear section:

• Magnetic inspection pig results are based on indirect measurements requiring proper interpretation.

• The process of obtaining GPS coordinates for each feature recorded by the inspection pig consists of a series of independent measurements that are later overlaid. As a result, measurement errors from individual tests accumulate, providing an approximate location of anomalies recorded by the magnetic inspection pig.

• The magnetic inspection pig is not a tool for assessing weld quality; therefore, in these areas, there may be no correlation with data from the MMM-NCMD test.

• The MMM-NCMD test results provide information on stress concentration states based on indirect measurements requiring proper interpretation.

• Limited access to MMM-NCMD test results, restricted to SCZ data only, does not allow for a thorough assessment and verification of whether indications recorded by inspection pigs always correspond to indications from the MMM-NCMD test.

• To confirm the causes of stress concentration states, it is recommended to perform control excavations at indicated locations. Unfortunately, repeated MMM or MMM-NCMD testing may not show SCZ due to magnetization of the pipeline during magnetic pig inspection. Other available non-destructive testing methods should be used to verify SCZ indications.

• Based on the above comparative analyses of MMM-NCMD and ILI tests, it can be concluded that there are common areas where the results of both tests confirm each other. Unfortunately, the non-overlapping areas are significantly larger; therefore, these methods (MMM-NCMD and ILI) should be considered complementary rather than mutually exclusive in assessing the technical condition of the pipeline.

5.5 Direct Current Voltage Gradient (DCVG).

The table 12 summarises basic information about the field survey done with the DCVG method.

Table 12: DCVG operational data [source GAZ-SYSTEM]

DCVG operational data:		
Measurement interpretation method	Direct reading of the potential difference from the measuring device.	
Anomaly classification / description	Location of damage to the coating of a pipeline protected by CP.	
	%IR	$\%IR_{rel.}$
Tests date	2024/11/25	
Tested pipeline distance	1304 m	
Duration of measurement in the test	~ 2 hours	
Survey ID	DCVG survey internal report.	
Type of device used	Sonel MRU-200	

The research leading to these results has received funding from Horizon 2020, the European Union's Framework Programme for Research and Innovation (H2020) under grant agreement n° 101111888.

5.5.1 Obtained DCVG inspection results.

Measurement Method

In cathodic protection, when current flows through resistive soil to exposed steel at the locations of protective coating damage, a voltage gradient is created in the soil. The larger the damage, the greater the current flow, and therefore the voltage gradient. This technique is used to prioritize damage for repair. The voltage gradient is observed using a millivoltmeter to measure the imbalance between two electrodes. When two electrodes are placed approximately 1.5 meters apart on the ground, along the voltage gradient from the coating damage, one electrode assumes a more positive potential than the other, allowing the direction of current flow and the location of the damage to be determined. To simplify the interpretation of the damage location, the applied potential is isolated from all other DC influences, such as telluric current, DC traction, etc., by asymmetrically pulsing the local potential. The pulsating DC current originates from the pipeline's potential system itself.

The measurements were performed on a pipeline with cathodic protection current supplied from an interrupted source - a cathodic protection station. Usually, for correct defect location, it is necessary to obtain a voltage drop of approx. 300 mV in the soil within a radius of 2 m from the center of the damage. For this purpose, the cathodic protection current was periodically increased for the duration of the measurements. During DCVG measurements, the gradient was measured, i.e., the difference in voltage changes on the ground surface resulting from the flow of electric current. The person performing the measurements moved

along the pipeline, placing two electrodes on the ground at a distance of 1 to 2 m from each other and observing the gradient measurement when the current source was switched on. As the defect was approached, the gradient value increased and then gradually decreased as the distance from it increased. In this way, the location of the defect can be identified. DCVG (Direct Current Voltage Gradient) measurements enable the detection of defects in the insulation coating of pipelines using electric current. The measurements taken do not allow for an assessment of the effectiveness of cathodic protection in areas where defects occur, but only for an assessment of the corrosion risk resulting from When assessing a defect, the gradient (measured in relation to the distant ground) is referred to as the difference between the switch-on and switch-off potential measured at the nearest measuring points. Another important parameter used to assess the corrosion risk is the resistivity of the soil; the lower the resistivity of the soil, the greater its corrosive aggressiveness.

Measuring device settings.

An analog DCVG set was used for measurements, which is considered to be much more accurate than digital instruments with GPS localization. After the defect was identified, its location was assigned to specific geographic coordinates. The location of insulation defects was compiled in tabular form, together with the characteristics of the defects and the corrosion risk. The measurements were carried out with the electrodes positioned parallel to the gas pipeline axis and a measurement step of approx. 1.5 m. Soil resistivity measurements were performed using the 4-electrode Wenner method with an electrode spacing of 3 m. At and near the location of the insulation coating defect. A Sonel MRU-200 meter was used for measurements.

Ground / soil corrosion intensity factor.

The intensity of soil corrosion depends, among other things, on its resistivity. Three soil corrosivity levels were used in the study, which were then assessed based on resistivity measurements, as shown in the table below.

The research leading to these results has received funding from Horizon 2020, the European Union's Framework Programme for Research and Innovation (H2020) under grant agreement n° 101111888.

Table 13: Ground / soil corrosion intensity factor in DCVG measurements [source GAZ-SYSTEM]

Ground / soil corrosion intensity factor in DCVG measurements.	
ρ [Ω / m]	Class
ρ > 1000	low resistivity
100 < ρ ≤ 1000	medium resistivity
ρ ≤ 100	high resistivity

DCVG measurement conditions.

The existing cathodic protection station of the tested DN 700 gas pipeline was used for the tests. Existing cathodic protection (CP) station was used to generate a synchronously variable cathodic protection current in a 0.3 s On / 0.7 sec. - Off cycle. The measurements were performed with increased timing parameters of the cathodic protection station.

$$\%IR_{rel.} = \left[\frac{dE_{ON} - dE_{OFF}}{E_{ON} - E_{OFF}}\right] \cdot \frac{100}{\rho}$$

dE_{ON} - turn-on gradient,

dE_{OFF} - turn-off gradient

E_{ON} - turn-on potential,

E_{OFF} - turn-off potential,

ρ - soil / ground resistivity.

The defect classification criterion used was adopted according to the table below.

Table 14: DCVG defect classification criteria [source GAZ-SYSTEM]

DCVG defect classification criteria	
Relative weight $\%IR_{rel.}$	Class
$\%IR_{rel.} \leq$ 16 %	low
16 % < $\%IR_{rel.} \leq$ 34 %	medium
34 % < $\%IR_{rel.} \leq$ 70 %	medium high
1$\%IR_{rel.}$ > 70 %	high

The research leading to these results has received funding from Horizon 2020, the European Union's Framework Programme for Research and Innovation (H2020) under grant agreement n° 101111888.

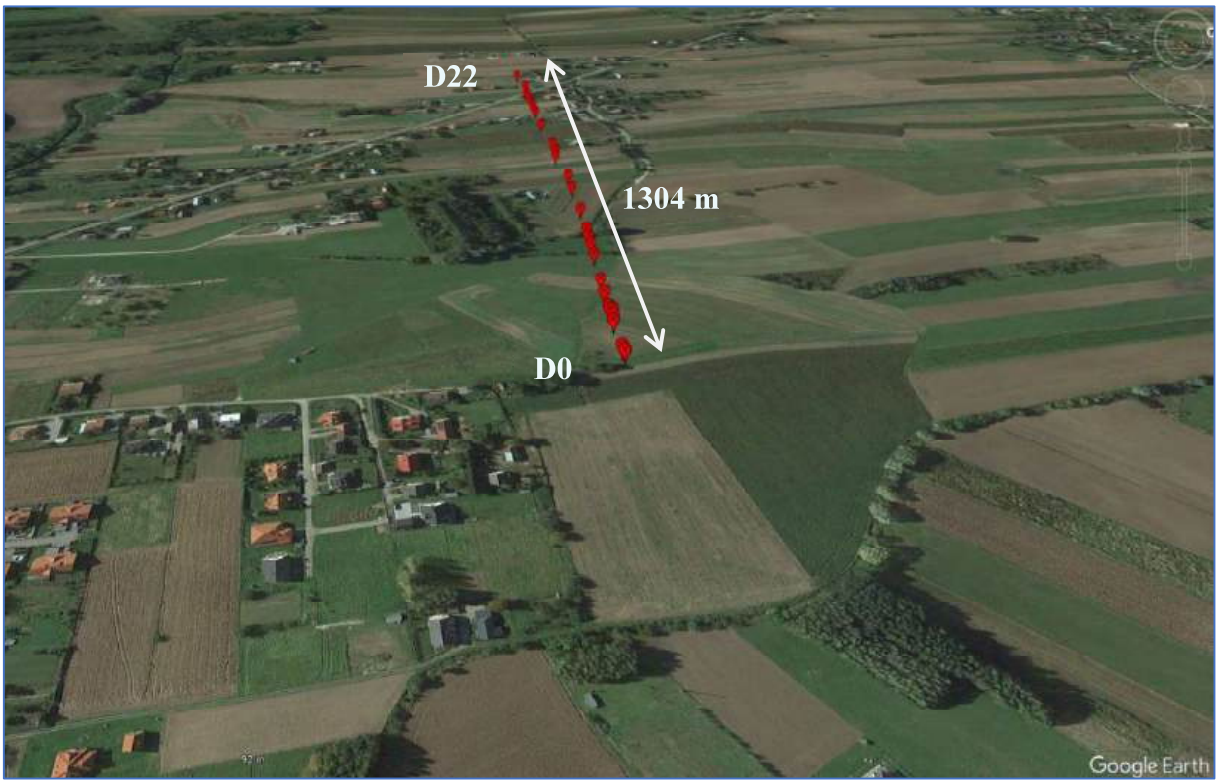

Figure 5-21: Characteristic points collected during measurements using the DCVG method presented in Google Earth application [source GAZ-SYSTEM]

The research leading to these results has received funding from Horizon 2020, the European Union's Framework Programme for Research and Innovation (H2020) under grant agreement n° 101111888.

Table 15: Summary of DCVG test results for a pipeline section [source GAZ-SYSTEM]

Defect	Distance	VG (*)	soil corrosion intensity factor	%IR (*)	$\%IR_{rel.}$ (*)
	[m]	[mV]	[Ω / m]	[-]	[-]
D0	0	-			
D1	18				
D2	57				
D3	67				
D4	79				
D4-1	-	-	181,7		
D5	90				
D6	114				
D7	141				
D8	194	high	53,6	high	high
D9	215				
D10	232				
D11	250				
D12	298				
D13	359				
D13-1	-	-	54,5		
D14	478				
D15	499				
D16	525				
D16-1	-	-	49,0		
D17	991				
D18	1006				
D19	1153				
D19-1	-	-	44,5		
D20	1202				
D21	1248	high		high	high
D22	1304	-			

(*) VG, %IR $\%IR_{rel.}$ - values available in the internal GAZ-SYSTEM report from DCVG measurements of the DN 700 gas pipeline.

In the standard DCVG report the defects are also described with the precise GPS coordinates (latitude, longitude) not shown in the table above.

DCVG survey results.

During the inspection, 21 defects were found in the insulation coating. The DN 700 gas pipeline being inspected is insulated with a bituminous coating, which poses a challenge during the inspection due to the persistent defect "background" along the entire length of the tested section. The defect size is measured by its gradient, and the inspection revealed defects with gradients ranging from 0.4 to 40 mV. Defects D8 and D21 were the dominant defects in the tested section. The corrosion risk of the defect is related to the soil resistivity. The defects are located in soils with medium (D1 to D5) and high (D6 to D21) corrosion risk. However, the relative weight ($\%IR_{rel.}$) of the defects, which is the reference of the gradient value to the soil resistivity, was small for all defects, which allowed the classification of the detected defects in the range of low corrosion risk.

The research leading to these results has received funding from Horizon 2020, the European Union's Framework Programme for Research and Innovation (H2020) under grant agreement n° 101111888.

5.6 iDiaGaSys System.

The table 16 summarises basic information about the field survey don wth the iDiaGaSys system.

Table 16: Operational data [source GAZ-SYSTEM]

iDiaGaSys operational data:	
Measurement interpretation method	Measuring subsystem: Hiperspectral data analysis; IT subsystem: database infrastructure and diagnostic software.
Anomaly classification / description	Detection of methane leaks and forbidden objects located in the gas pipeline zone.
Tests date	10/2024
Tested pipeline distance	~1 km
Number of inspections	single pass
Type of device used	A helicopter equipped with a hyperspectral imaging camera

5.6.1 Obtained airborne inspection results.

The iDiaGaSys system is designed for periodic detection of methane leaks and identification of potential hazards in the area of gas pipelines. It consists of two main components a measurement subsystem which includes a helicopter equipped with infrared spectroradiometer and a visible light camera, the second component is IT subsystem for processing acquired image data.

A complete system was used for detection of methane leaks and identification of potential threats in the area of the monitored DN 700 gas pipeline section. The main components used were a measurement subsystem, which included a helicopter equipped with an infrared spectroradiometer and a visible light camera, and an IT subsystem for image data processing. During the inspection, no methane leaks were located along the gas pipeline route, nor were any objects located within the monitored area of the gas pipeline. However, the system correctly located characteristic objects located near the DN 700 gas pipeline, but outside the monitored area. The lack of interpreted methane leaks was consistent with information from other inspections, which did not indicate defects that could cause methane leaks.

The research leading to these results has received funding from Horizon 2020, the European Union's Framework Programme for Research and Innovation (H2020) under grant agreement n° 101111888.

Figure 5-22: Photographs taken with a camera installed on a drone, taken from a 50 and 120 m suspension, with the approximate location of the gas pipeline in the field marked on the drawings with a dashed line [source GAZ-SYSTEM]

The research leading to these results has received funding from Horizon 2020, the European Union's Framework Programme for Research and Innovation (H2020) under grant agreement n° 101111888.

5.7 Comparison of data from MFL reference measurements and data acquired from measurements performed using selected alternative NDT methods.

5.7.1 Data from the reference measurements using the DEF and MFL tools.

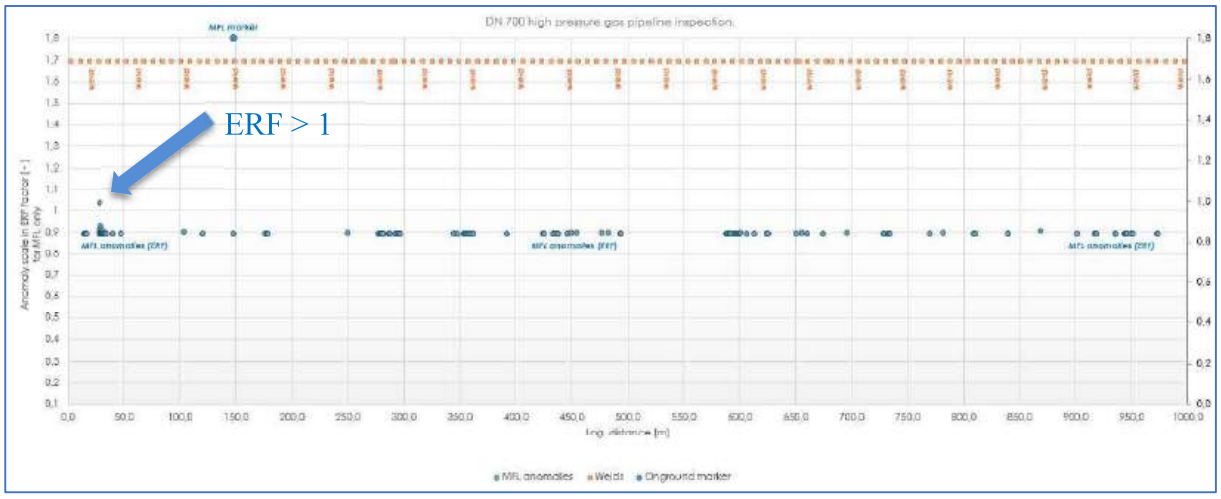

Figure 5-23: reference measurement – DEF and MFL tool inspection [source GAZ-SYSTEM]

The graph shows the results of high-frequency magnetic flux leakage (MFL) measurements detecting material defects in combination with tests using adjustable frequency electromagnetic tools (DEF) to identify shape defects such as ovalization or dents in pipes. The design analysis used the results of the report collected along the entire length of this gas pipeline, including a selected 1,000 m section, which included defects detected in DEF and MFL tests with ERF ≥ 0.85 according to the classification based on ASME B31G, including a single defect identified with coefficient ERF ≥ 1. Defects below ERF 0.85 were omitted and their significance was not analyzed in the project.

5.7.2 Data from acoustic emission (AE) measurements.

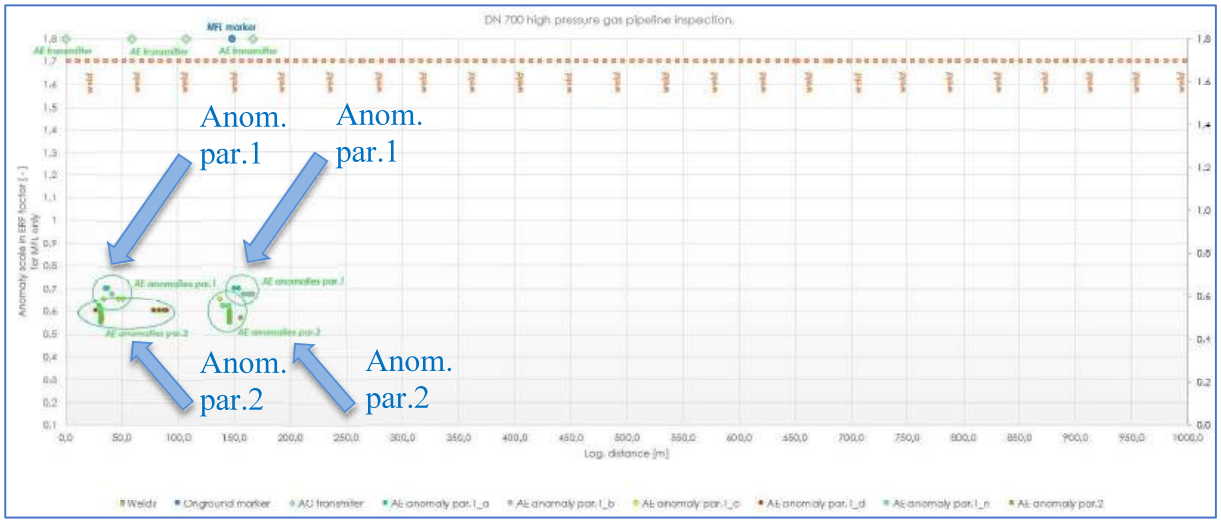

Figure 5-24: Acoustic emission (AE) measurements [source GAZ-SYSTEM]

The graph shows the results of an acoustic emission inspection 150-meter section of a DN 700 pipeline. Signals were recorded from four measuring sensors installed at 50-meter intervals. During the measurements, internal stress anomalies were detected in the recorded signals with two main parameters: signal strength and ASL signals. The recorded signals were then filtered using the Contractor's reference signal database, which

The research leading to these results has received funding from Horizon 2020, the European Union's Framework Programme for Research and Innovation (H2020) under grant agreement n° 101111888.

allowed the anomalies to be isolated and identified. The measurements revealed three main areas generating potential anomalies indicating increased stress inside the pipe wall.

Area 1 covering a 30 m section (from 0 to 30 m) where increased generation of anomalies in classes 3 and 4 was observed in two places.

Area 2 covering a 12 m section (from 75 m to 87 m) where increased generation of class 3 and 4 anomalies was observed.

Area 3 covering a 23 m section (from 116 m to 139 m) where increased generation of anomalies in classes 3 and 4 was observed in two places.

The anomalies were then classified into two groups on a risk scale: parameter 1 – significant, parameter 2 – less significant, requiring additional verification.

5.7.3 Data from stress concentration tomography (SCT) / metal magnetic memory (MMM) measurements.

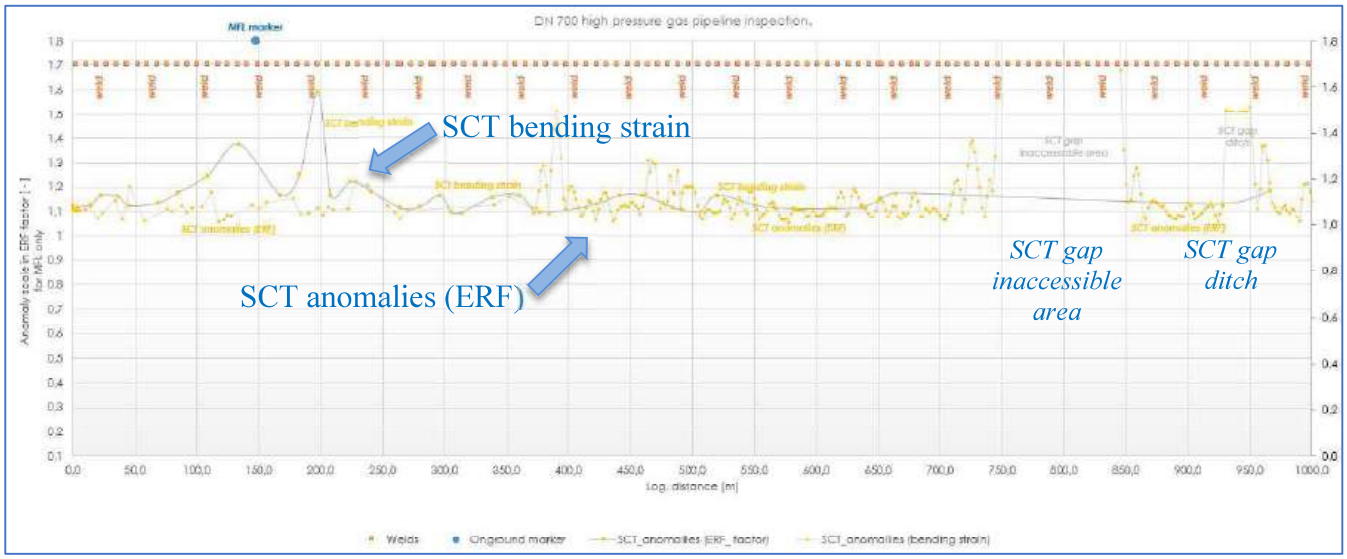

Figure 5-25: Chart showing the results of inspection using the SCT method / magnetic metal memory [source GAZ-SYSTEM]

The graph shows two curves, the SCT anomaly curve (ERF values on this line are on a reference scale other than the MFL test scale) relating to stresses occurring in natural gas pipeline material resulting from various potential phenomena, including possible material defects, and the bending stress curve resulting from possible pipeline displacements in the ground.

5.7.4 Data from DCVG voltage gradient difference measurements.

During the inspection, 21 defects in the insulation coating were detected. It should be noted that the gas pipeline is constructed using bituminous coating insulation technology, which makes inspection difficult due to the constant background interference throughout the entire length of the inspected section. The defect size is measured by its gradient, and the inspection revealed defects with gradients ranging from 0.4 to 40 mV.

The research leading to these results has received funding from Horizon 2020, the European Union's Framework Programme for Research and Innovation (H2020) under grant agreement n° 101111888.

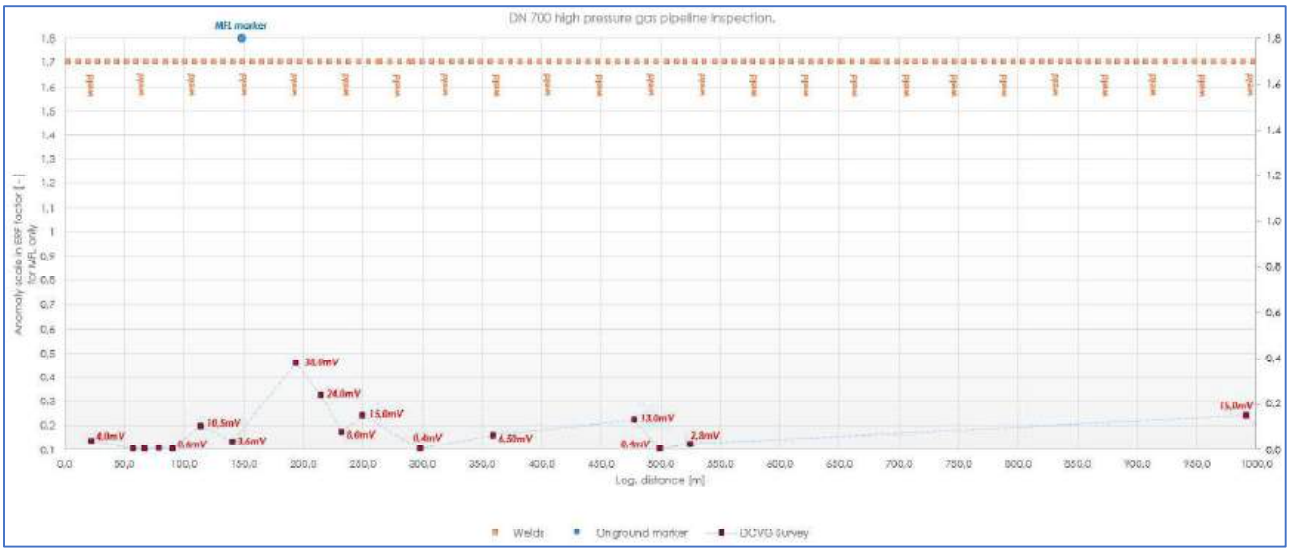

Figure 5-26: Data from DCVG voltage gradient difference measurements [source GAZ-SYSTEM]

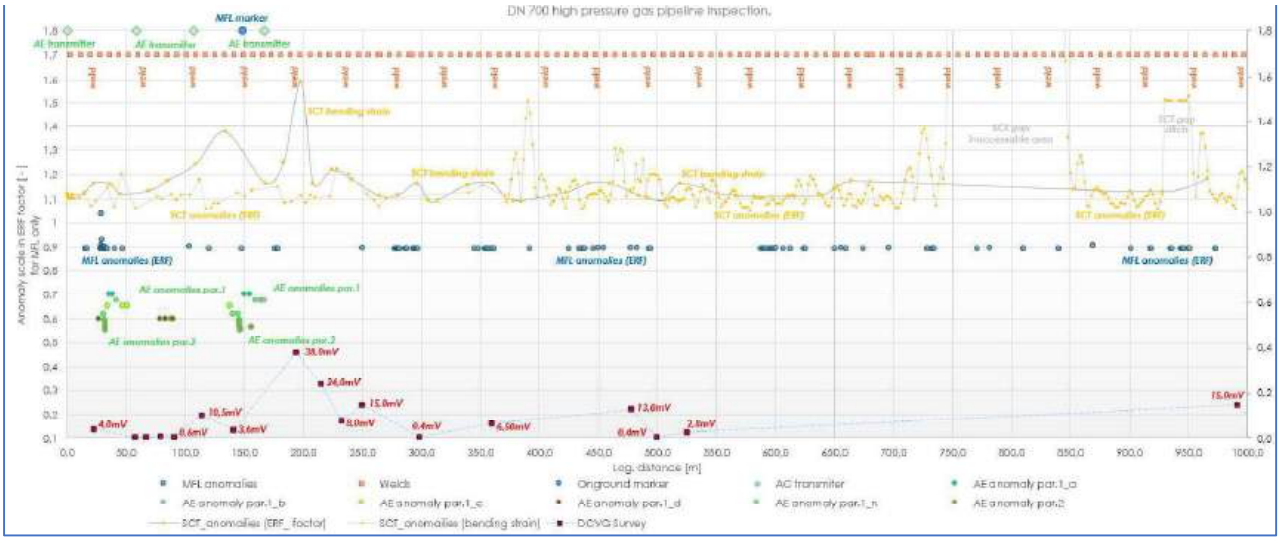

Figure 5-27: Data from measurements performed using three different alternative methods, compared with the reference measurement from the ILI test using MFL-DEF tools [source GAZ-SYSTEM]

Finally, the graphs obtained from all NDT methods used were overlaid onto a single graph containing data from the MFL-DEF reference survey. The top of the graph shows the locations of the four sensors measuring acoustic emission signals. The position of the coordinate control marker used during the gas pipeline pig survey is also marked. Slightly below are the points indicating the location of the circumferential welds connecting the pipes. The two lower grey-orange curves represent measurements taken using stress concentration tomography. Then, in the centre, are the blue points indicating ERF values > 0.85 obtained from the MFL-DEF pipeline measurement, which is considered as the reference survey. Below these are the green points indicating the location of anomalies detected by the acoustic emission survey in a limited 150 m section, which did not cover the entire section surveyed by other methods. At the bottom, the locations of measured voltage gradient values recorded using the Direct Current Voltage Gradient DCVG measurement method are marked in grey and red. This graph is further used to analyse the correlation of test results obtained by different methods along the gas pipeline route.

The research leading to these results has received funding from Horizon 2020, the European Union's Framework Programme for Research and Innovation (H2020) under grant agreement n° 101111888.

6 Comparison of the tested NDT methods.

The study's conclusions are divided into three parts. The first compares the results of various methods for detecting flaws in steel natural gas pipelines. The second part presents the advantages, disadvantages, and limitations of each method, including limitations on the types and sizes of potential flaws or damage and stress levels encountered in the pipelines, depending on the technical capabilities of the methods studied. The third part determines the suitability of alternative methods for non-pig pipelines and analyses the suitability of each method for inspecting steel natural gas pipelines carrying hydrogen, including the ability to detect material flaws associated with the negative effects of hydrogen, such as reduced fracture toughness, increased fatigue crack growth rate (FCGR), and reduced ductility of the steel pipe material.

6.1 Comparison of test results using different methods of detecting defects in a steel pipeline.

Testing of the individual methods used in the investigations was conducted on a section of a DN 700 high-pressure natural gas steel pipeline that had been subjected to MFL and DEF inspection the previous year to detect pipeline material defects. Defects detected during this pipeline inspection were expressed as ERFs according to ASME B31G, including defects with an ERF value greater than 0.85. In one location, the MFL inspection revealed a defect with an ERF value ≥ 1. The defect location was excavated by the pipeline operator and verified using non-destructive radiographic testing (RT). This direct inspection correlated well with the MFL test results, with the depth of material loss indicated by the MFL test slightly overestimating the radiographic RT test results. MFL and DEF pipeline inspection is established and widely used testing technique. The investigation and direct field verification of the identified defect after its exposure confirmed the effectiveness of this method. The method is based on direct measurement of magnetic field leakage and provides information on pipeline material losses and the presence of pipe shape irregularities. This also allows, to some extent, the identification of other types of defects in steel pipes. The reference test results were compared with those obtained with other non-destructive testing (NDT) methods used in the project, in order to compare and establish any correlations between the measurement results.

The acoustic emission test was performed using four measuring sensors placed over a 150-meter section, at equal intervals of 50 m each. The study identified three groups of defects classified based on the recorded acoustic emission signals as signals from the range of anomalies assigned to parameter 1 and parameter 2. The anomalies were classified as significant and less significant, respectively. The anomalies classified as significant located in the section from 0 to 30 m from the first sensor are consistent with the information from the MFL reference measurement, which also showed a cluster of defects at this location, including a defect with an ERF factor of ≥ 1. A good correlation with the reference survey can be found at this location. Then, in the section from 75 m to 87 m from the first sensor, signals classified as less significant defects were recorded. This group of defects does not have coverage with the reference test, which is acceptable if these are anomalies classified as less important and requiring verification. The last recorded group of signals was classified as significant anomalies located on the section from 116 m to 139 m. This group of signals has little overlap with the presence of defects identified in the reference survey. The acoustic emission (AE) test anomalies gave a clear signal, while the MFL reference test showed single defects with coefficients in the range of 0.85 < ERF < 1.0. There is no clustering of defects in this location as was the case in the first compared section, where the compilation of results gave greater consistency. To interpret the acoustic emission (AE) survey results, signals in two main parameters were used: signal strength and ASL signals. The recorded signals were then filtered using a database of reference signals, which allowed for the isolation and identification of anomalies.

A study involving the measurement of the magnetic memory of metal, here the measurements used are called Stress Concentration Tomography (SCT), resulted in the plotting of two curves. The first one informs about the presence of stress caused by the presence of material anomalies, the second one informs about the presence of stress resulting from the impact of the terrain in which the gas pipeline is located, deflections of the gas pipeline in the terrain resulting from changes in the pipeline direction vertically and horizontally, changes in the stability of the pipeline support, the impact of external factors on the pipeline structure, and others. This measurement does not include the section to which there was no access during the pedestrian measurement, the device was carried over the terrain by a single person performing the measurement, and the section where the pipeline crossed a drainage ditch and the device could not be stably moved over this terrain obstacle.

The research leading to these results has received funding from Horizon 2020, the European Union's Framework Programme for Research and Innovation (H2020) under grant agreement n° 101111888.

Comparing the curve determined from the SCT test with the reference test does not provide a clear correlation. In the section from 0 to 30 m there is a good correlation between both methods because the reference test shows that in this section there is a group of material defects with coefficients in the range of 0.85 < ERF < 1.0, including a single defect with ERF ≥ 1. In this location, the SCT test shows increased values on the curve informing about material anomalies. In the section between 100 and 175 m, where the reference test provided information on single defects with coefficients in the range of 0.85 < ERF < 1.0, increased values on the material anomaly curve from the SCT test are observed. A certain correlation of the results can be observed in the location from 275 m to 300 m and then from 340 m to 360 m, however, there are shifts between the results obtained from both measurements performed using different methods, reaching up to 20 m. In the section from 375 m to 1000 m, i.e. until the end of the measurement (excluding two sections excluded from the analysis), the SCT test provides information about the presence of material anomalies, however, the increase in values on the curve informing about the presence of stress caused by the presence of material anomalies does not have exact convergence with the reference test. Material defects indicating certain material losses are distributed with varying intensity throughout this section, in places grouping into larger clusters. In these places one would expect a correlation in the form of increased SCT values, however this is not the case and the increased SCT values occur in different places on this section in such a way that no clear correlation between the results of both compared inspection methods could be found. No such clear correlation was observed between SCT and AE on the section of the pipeline where the acoustic emission (AE) test was performed.).

A test involving the detection of defects in the external insulation of the gas pipeline's protective coating using the Direct Voltage Gradient (DCVG) method revealed a total of 21 insulation coating defects with gradient values ranging from 0.4 to 40 mV. Defects detected in the 175-225 m section of the test dominating the test, but there is no correlation with the reference MFL test. Therefore, it can be concluded that there are no material defects in this section resulting from defects in the pipeline's external insulation. The gradient value also increases, but to a lesser extent, in the 475-500 m section of the test pipeline, where there is a correlation with the presence of defects detected in the reference test. The gradient values measured using the DCVG method are relatively low, indicating the good condition of the insulation coating and the absence of significant damage to the coating in the tested section. Therefore, it was not possible to demonstrate a correlation between the reference test on the entire tested section and the mentioned correlation in one of the places is probably accidental.

6.2 Classification of pipeline defects. Advantages, disadvantages, and limitations of the inspection methods used.

Pipeline inspection aims to identify defects and material losses. It is important to identify the types of material defects found in steel pipelines. The first group are inherent defects that arise during pipe production. During the production process, steel pipes are made from billets solidified by molten metal, and the billets contain defects. Most of these defects are removed during head and tail cutting, but a number of defects remain in the billets. These inherent defects include shrinkage cavities, hot casting cracks, air pockets, inclusions, etc. These inherent billet defects then cause defects during the steel pipe rolling process, including cracks, delamination, etc. Subsequently, the heat treatment, machining, coating, and finishing processes of rolled steel pipes also cause discontinuities on the steel pipe surface. These cracks can develop as heat treatment or coating cracks. Most of these defects occur on the surface of steel pipes. Another group consists of welding defects, which occur during the welding process of pipes made with a seam connecting the pipe strips. Subsequently, during pipeline construction, cracks and corrosion can occur in the welds where the welded pipe segments are made. Therefore, welded joints are also subject to non-destructive testing (NDT) during their production phase. For this reason, among other things, the gas pipeline undergoes rigorous pressure testing for strength and tightness before being approved for operation.

The second cause of failure is corrosion occurring during pipeline service life. There are two types of cracks: stress corrosion cracking (SCC) and hydrogen-induced cracking (HIC). SCC is caused by the combined action of a corrosive environment and tensile stress and is considered one of the main types of damage. Factors influencing the intensity and propagation of SCC cracks include the microstructure of the pipe material, the chemical composition of the steel grade, grain boundary characteristics, residual stresses, the applied load, the ground pH, and the corrosive properties of the flowing medium inside the pipeline. HIC is a type of step crack that forms when pipelines are exposed to hydrogen-containing media. The growth and development of these

The research leading to these results has received funding from Horizon 2020, the European Union's Framework Programme for Research and Innovation (H2020) under grant agreement n° 101111888.

cracks ultimately leads to structural damage to the pipeline material. Corrosion damage can finally occur on both the interior and exterior surfaces of the pipeline. Furthermore, corrosion can also be caused by defects in the external insulation coating of the steel pipeline or by malfunctioning cathodic protection. A significant type of corrosion is corrosion caused by high currents, known as stray current corrosion. These corrosion defects can occur both inside and outside pipelines and include pitting, scaling, and intergranular corrosion.

Table 17: Defects in steel pipes arising during prefabrication and their causes [source GAZ-SYSTEM]

Defect type	Location	Source of defect
casting, hot crack	internal and external	stress due to different solidification rate
inclusion	surface or near-surface	Impurities in the casting process
stoma	surface or near-surface	the gas is retained when the metal solidifies
layered	surface or near-surface	defects elongated and flattened during rolling.
cracks	surface	surface indentations, discontinuities, and elongations formed during rolling
fold	surface	excess of material covering and pressing into surface
heat treatment crack	surface	uneven heating or cooling
coating crack	surface	residual stress release

Table 18: Defects arising during pipeline operation and their causes [source GAZ-SYSTEM]

Defect type	Location	Source of defect
stress corrosion	surface or near-surface	impact stresses
stress corrosion	surface or near-surface	ground or embankment pressure, subsoil instability, other
corrosion	surface	influence of corrosive environment
fatigue crack	surface	long-term stress below the tensile strength of the material
stress corrosion cracking	surface	the influence of static tensile load and a corrosive environment tensile or residual stresses acting in a hydrogen environment

When comparing the non-destructive testing (NDT) methods used to inspect a steel pipeline transporting natural gas under high pressure, it should be noted that the methods cannot be compared directly because different physical phenomena are measured in the different methods used. The magnetic field leakage method adopted as a reference test provides direct information on material defects. The AE and SCT methods are indirect methods that provide information about the possible presence of material defects by detecting stress in the steel pipeline material. The DCVG method provides information only about the tightness of the

The research leading to these results has received funding from Horizon 2020, the European Union's Framework Programme for Research and Innovation (H2020) under grant agreement n° 101111888.

insulating coating, showing possible gradient changes in the event of cathodic protection current leakage into the ground medium.

Table 19: The type of physical phenomena subject to measurement and the range of defects that can be identified in individual diagnostic methods [source GAZ-SYSTEM]

Type of inspection.	Magnetic flux leakage measurement (MFL, DEF)	Acoustic emission signals measurement. (AE)	Magnetic memory of metal / Stress concentration tomography measurement (SCT)	Cathodic protection leakage current measurement (DCVG)
Phenomena subject to measurement.	Induced magnetic field interference/scatter analysis.	Analysis of acoustic waves emitted in a steel pipeline.	Measurement of the initial magnetic field distribution of the pipeline steel structure.	Measurement of the DC voltage gradient between two electrodes in the area of a pipeline with active CP.
Type of material defects detected.	Material losses (internal and external). Pipe shape deformations, ovality, and dents.	Stress within the material resulting from material and geometric defects.	Stress concentration zones resulting from deformation.	Defects in external pipeline insulation.

Table 20: The limitations of using individual diagnostic methods [source GAZ-SYSTEM]

Type of inspection.	Magnetic flux leakage measurement (MFL, DEF)	Acoustic emission signals measurement. (AE)	magnetic memory of metal / stress concentration tomography measurement (SCT)	Cathodic protection leakage current measurement (DCVG)
Strengths	Highly advanced and standardized criteria for identifying material defects. Highly automated inspection process.	It can be used to detect dynamic defects associated with stress. It can be used over long distances and is therefore suitable for building a detection system.	It can be used to detect dynamic defects related to stress. Easy field measurement, requiring no operational preparation.	Easy and direct measurement in the field, no operational preparation required.
Weaknesses and limitations	Limited crack detection efficiency. Failure to detect defects in the welded joint area. Limited applicability for thick pipe walls (*).	Lack of a system for assessing material defects. Low efficiency of detecting defects in the elastic and plastic state of the pipe material. Sensors must be installed directly on the pipeline.	No system for assessing material defects. Identification of stress growth zones rather than specific defects. Significant limitations after– ILI inspection with electro-magnetic pigs.	No defect assessment system (*). (*) This method does not address the detection of material defects.

(*) Plane defects in the form of cracks cause low magnetic flux disturbances and therefore signals from cracks on the inner surface are difficult to detect. Difficulties also arise in detecting defects in

The research leading to these results has received funding from Horizon 2020, the European Union's Framework Programme for Research and Innovation (H2020) under grant agreement n° 101111888.

the heat-affected zone of a welded joint, where the presence of circumferential welds itself causes significant disturbances in the magnetic field. As a result, only larger defects located in this area are detected. Another limitation is the inability to detect defects in the pipeline wall when cracks are located parallel to the lines of the induced magnetic field and therefore do not cause disturbances in the flow of this field. It is also impossible to detect internal layers (including cracks) in the wall that do not reach the surface.

6.3 H_2 management protocol & recommendations.

In recent years, many companies have made significant progress in the research and development of instruments and devices. For example, the introduction of the spiral magnetic flux leak detector, which addresses the shortcomings of uniaxial magnetic fields by enabling the detection of flat defects (oriented parallel to the pipe axis) such as delamination and lamination. Detecting material defects such as weld cracks, identifying good fusion, detecting hydrogen induced cracks (HIC), circumferential cracks, fatigue cracks, shrinkage cracks, cavity cracks, and stress corrosion cracks (SCC) requires more advanced pipeline inspection techniques using measuring pigs. An example would be a tool using a combination of electromagnetic and acoustic transduction technology (EMAT). Such a sensor generates ultrasonic waves inside the pipe wall by combining Lorentz and magnetostriction forces, regardless of the presence of the medium in the pipe. The material being tested is its own transducer, which eliminates the need for a liquid coupling medium required in traditional UT methods and is therefore a good solution for gas pipelines in operation. An electromagnetic acoustic transducer (EMAT) is placed in the magnetic field and controlled by a short tone pulse of adjustable frequency. Guided waves generated by the transducer propagate between the outer and inner surfaces of the steel pipe. The presence of stress disrupts the guided wave, while a change in the waveguide dimensions, for example, caused by a crack, will reflect the wave and create an echo, which can then be detected.

The assumption that a gas pipeline can be tested with measuring pigs is not sufficient to confirm the possibility of hydrogen addition transport in the gas network. The range of material defects detected by available measuring pig instrumentation is important. Currently, MFL measuring pigs are widely used and are sufficient for a wide range of defects present in steel natural gas pipelines. A permanent magnet circuit based on the popular MFL diagnostic tool generates a magnetic field axially oriented in the plane of the steel pipeline wall, limiting the detection of a significant range of defects present in the pipeline wall cross-section. Important details regarding the limitations of MFL technology in detecting planar defects and material defects in welded joint areas, including the heat-affected zone, are included in the POF520 In-line inspection tool readiness for hydrogen pipelines document [43].

The transported hydrogen addition requires the identification of defects generated by increased fatigue crack growth rate (FCGR) and decreased plasticity of the steel pipe material. These defects usually take the form of cracks. The measurements carried out identified methods complementing the testing of steel gas pipelines, allowing the identification of material defects characteristic of hydrogen corrosion. However, to be useful for the pipeline operator, supplementary methods require the development of reliable methods for evaluating test results.

6.4 Results from the deliverable 3.1

The deliverable 3.1 contains a comprehensive analysis of the impact of hydrogen on the strength of materials and components used in natural gas transmission and distribution infrastruckture. It analyses the types of damage caused by hydrogen and the mechanisms of degradation of metallic and non-metallic materials under the influence of hydrogen. The report contains experimental data from scientific research, project results and relevant standards, which are used to assess the behaviour of materials in hydrogen-containing environments, especially in the context of hydrogen blending in the gas network. This deliverable also considers the compatibility of materials with hydrogen, providing information needed to make decisions about the safe integration of hydrogen into existing gas infrastructure.

Based on the research results provided, an analysis of existing available steel pipeline inspection techniques was carried out in this project. The available inspection techniques were analysed in two groups, i.e. techniques based on commonly used ILI inspections, taking into account the necessary modifications and extensions of

The research leading to these results has received funding from Horizon 2020, the European Union's Framework Programme for Research and Innovation (H2020) under grant agreement n° 101111888.

measurement capabilities appropriate to ensure the safety and integrity of steel pipelines for transporting hydrogen additives to natural gas, and alternative techniques that allow measurable results to be obtained in the identification of defects and anomalies characteristic of hydrogen. The complementary techniques were verified for their suitability in this project, taking into account their effectiveness in relation to MFL tool tests used in conjunction with steel pipeline geometry tests. The results of the comparison aim to indicate the basis and directions for future research, testing, and operational practices to support the transition to hydrogen-enriched energy systems.

The analysis conducted as part of the project assumed that issues related to hydrogen embrittlement, (HE) and hydrogen-induced cracking (HIC) are relevant in the context of assessing the susceptibility of steel pipe materials to hydrogen exposure and are carried out through appropriate analyses and material testing.

HE is the loss of ductility and fracture resistance, along with increased susceptibility to fracture, which occurs when diffusible atomic hydrogen is present in metal during deformation and fracture. The two most widely accepted mechanisms for HE. Hydrogen-enhanced local plasticity (HELP), which assumes that hydrogen facilitates grain dislocation movement and localises slip near the fracture tip. Hydrogen-enhanced decohesion (HEDE), which assumes that hydrogen reduces the cohesive strength at phase boundaries (crystal lattice, grain boundaries or inclusions), promoting quasi-cleavage or intergranular separation. Adsorption-induced dislocation emission (AIDE) also causes brittle fracture, but is associated with local dislocation activity at the crack tip rather than pure bond breaking. The severity of HE in a pressurised pipeline will depend on the pressure of the medium in the pipeline and therefore also on the pressure of hydrogen (fugacity), the current stress/strain concentration characteristics (e.g. local corrosion pits, grooves, dents), the cyclic rate/ frequency of deformation changes generating stress, temperature, material microstructure (e.g. existing ferrite/pearlite fractions, existing segregation bands, inclusions), weld hardness taking into account heat-affected zones (HAZ), residual stresses and surface condition. In practice, the risk of HE necessitates the inspection of steel pipelines using methods that allow for the identification of the indicated types of material defects. Risk management requires the implementation of more stringent operating conditions compared to the transport of natural gas alone.

HIC is an internal, flat type of cracking that occurs in susceptible low or medium strength steels, without external stress when hydrogen is generated on the steel surface as a result of corrosion in environments containing aqueous H_2S. Hydrogen atoms enter the steel, accumulate in traps (e.g., inclusions, voids) and can form blisters; the gradual joining of these elements causes cracking throughout the thickness. When tensile stresses (induced or residual) promote the joining, the damage is referred to as stress oriented HIC (SOHIC). In H_2S solutions, sulphide ions inhibit the recombination of adsorbed hydrogen atoms in H_2 on the surface, so more hydrogen remains available to diffuse into the steel. Increasing the concentration below the surface and the risk of cracking. The internal pressure model, hydrogen molecules exerting pressure on cavities in inclusions is often used to rationalise blistering and HIC. It is assumed that this process will not be active in the transport of natural gas that meets quality standards and does not contain sulphur or H_2S. In dry gas, H_2 does not cause HIC, but HE/HAF will be significant effecnt.

Under cyclic loading, hydrogen in gaseous form significantly accelerates the rate of fatigue crack growth (FCGR) compared to air or natura gas, often by orders of magnitude in the typical Paris law regime for ferritic steels, which are commonly used in steel pipelines for natural gas transport. Fatigue crack growth tends to increase with ΔK, i.e. the change in stress intensity factor, and is typically stronger at lower cycle frequencies due to the longer time required for hydrogen to reach the crack tip. It also depends on the stress ratio (R). The base metal, weld metal and heat-affected zone (HAZ) metal may exhibit different sensitivities. Another recognised effect of hydrogen is to lower the fatigue crack growth thresholds (ΔKth). This threshold indicates the smallest ΔK at which a fatigue crack will propagate. A lower ΔKth in hydrogen means that cracks can grow under smaller cyclic driving forces than in air or natural gas. The technical basis and principles for the susceptibility of ferritic pipeline steels to FCGR in hydrogen, calibrated from data from multiple laboratories and expressed in exponential form taking into account environmental factors, are contained in ASME B31.12. On this basis, it is possible to assess damage resistance and plan inspections of pipelines transporting hydrogen added to natural gas or hydrogen alone.

Risk management and the necessary assessment of the condition of pipeline infrastructure will require the evaluation of hydrogen-assisted fatigue (HAF), which must be monitored during operation as it can cause flat

The research leading to these results has received funding from Horizon 2020, the European Union's Framework Programme for Research and Innovation (H2020) under grant agreement n° 101111888.

damage in the form of cracks and delamination. Methods for estimating fatigue cycles during the service life of a steel pipeline will need to be verified in practice based on established methods for diagnosing steel pipelines, enabling the detection of material defects characteristic of HE and FCGR processes. The project verified existing methods and identified and tested alternative methods to ILI testing using measuring pigs. The tested methods aim to detect the presence of additional stresses in the pipeline that affect FE and FCGR phenomena, generating additional operational risks caused by the blending of hydrogen and natural gas.

7 Conclusions

As part of the project, existing methods were verified and alternative methods for testing ILI using measuring pigs were identified and tested. The tested methods are designed to detect additional stresses in the pipeline that affect FE and FCGR phenomena, generating additional operational risks caused by the mixing of hydrogen and natural gas. Ensuring safety in the process of blending natural gas and hydrogen requires the implementation of appropriate pipeline inspection techniques in order to manage risk at the required level. Current steel pipeline inspection techniques focus on detecting material loss and pipeline shape defects such as dents. MFL pigs assisted by geometry measurement pigs are commonly used for this purpose, and in recent years they have been supplemented by tools that detect geometry changes based on the position of the pipeline in space and terrain by integrating measuring pistons with inertial navigation systems (IMUs). This approach, widely used by gas system operators, is appropriate for natural gas, for which the risk of fatigue corrosion during operation is relatively low.

In the case of hydrogen, which will be transported as an additive to natural gas or on its own, the adverse effects of hydrogen must be considered. In the context of assessing the susceptibility of steel pipe materials to hydrogen, issues related to hydrogen embrittlement (HE) and hydrogen-induced cracking (HIC) of ferritic steels used in the construction of pipelines, including natural gas pipelines, are important. Although the effect of HIC can be considered less significant if the presence of sulphur and H_2S is eliminated, phenomena related to FCGR must be taken intoconsideredagement and the necessary assessment of the condition of pipeline infrastructure will require the evaluation of hydrogen-assisted fatigue (HAF), which must be monitored during operation as it can cause flat damage in the form of cracks and delamination. Hydrogen in gaseous form significantly accelerates the growth rate of fatigue cracks (FCGR) compared to air or natural gas, often by orders of magnitude in a typical Paris law regime for ferritic steels, which are commonly used in steel pipelines for natural gas transport. Furthermore, it should be noted that the base metal, weld metal, and heat-affected zone (HAZ) metal may exhibit different sensitivities. This is important in the context of the limited detection capabilities of commonly used MFL diagnostics pigs due to magnetic field interference in the weld area. Then, diagnostic tests were carried out using alternative methods on a selected section of the gas pipeline with a nominal diameter of DN 700. It should be noted that this section had previously been checked using MFL and geometric pigs, which were accepted as reference tests for checking other alternative diagnostic methods tested within the project. It should be noted that the alternative diagnostic methods used consisted of checking for the presence of additional stresses in the pipeline. These stresses may be the result of external influences or primary and secondary material defects, including flat cracks and weld defects, which are relevant in the process of identifying hydrogen-assisted fatigue (HAF).

The assumption that gas pipelines can be tested with measuring pigs, as stated in general terms, e.g. in the requirements of ASME B31.12, is not sufficient to confirm the possibility of transporting hydrogen in the gas network. The range of material defects that can be detected with the available measuring pig equipment is important.

The assumption that gas pipelines can be tested with measuring pistons, as stated in general terms, e.g. in the requirements of ASME B31.12, is not sufficient to confirm the possibility of transporting hydrogen in the gas network. The range of material defects that can be detected with the available measuring piston equipment is important.

The potential complementary methods for testing steel gas pipelines have been identified in the projekct, allowing for the identification of material defects characteristic of hydrogen corrosion. However, in order for

The research leading to these results has received funding from Horizon 2020, the European Union's Framework Programme for Research and Innovation (H2020) under grant agreement n° 101111888.

the complementary methods used to be useful for gas pipeline operators, reliable methods for evaluating test results need to be developed.

Ensuring safety should be a priority in standard operation and implementation of work.

The work carried out as part of the research project on the possibility of blending hydrogen into natural gas is important for overcoming existing technological barriers. The analyses carried out have identified gaps in the area of existing measurement techniques. The project tested alternative methods to those used in measurement pigs. However, suppliers of measuring pigs already provide many modifications to existing diagnostic tools, thus allowing the spectrum of material defects tested to be expanded to include the necessary identification of defects characteristic of hydrogen corrosion. Modifications are being made to the type of sensors used, the spatial configuration of the sensors, and the frequency of the induced magnetic field, up to and including the introduction of solutions using new technologies. An example of this is the implementation of E-MAT technology, which uses magnetic field induction to generate forces that deform the steel walls of pipes, resulting in the propagation of ultrasonic waves. This solution allows for the detection of corrosion and stress cracks, as well as delamination and lamination. It is therefore reasonable to continue research and analysis on advanced methods of detecting material defects in steel pipelines operating under pressure as part of new research and development projects.

The research leading to these results has received funding from Horizon 2020, the European Union's Framework Programme for Research and Innovation (H2020) under grant agreement n° 101111888.

8 References

[1] Geng, L.; Dong, S.; Qian, W.; Peng, D. Image Classification Method Based on Improved Deep Convolutional Neural Networks for the Magnetic Flux Leakage (MFL) Signal of Girth Welds in Long-Distance Pipelines. *Sustainability* 2022, *14*, 12102. https://doi.org/10.3390/su141912102.

[2] Macro Defects in Steel; [Online] https://www.steeldata.info/macro/demo/data/2751.html.

[3] M. Beuvink; (MFL) DATA ANALYSIS BASIC INTRODUCTION; ROSEN Group; [Online] https://pngrb.gov.in/pdf/press-note/GAIL15062022/ILI.pdf.

[4] RoCombo MFL-C/XT Service; In-line Combined Axial Feature and Geometry Analysis; https://contenthub.rosen-group.com/api/public/content/4f34c472ae3741fb8e93770cc275cac5?v=0c98e53a.

[5] T.D. Williamson; SpirALL® Magnetic Flux Leakage Technology; https://www.tdwilliamson.com/resources/videos/spirallr-magnetic-flux-leakage-technology.

[6] AQC Inspection - What Is Acoustic Emission Testing? - https://aqcinspection.com/what-is-acoustic-emission-testing/, accessed December 9, 2025.

[7] Al-Obaidi, S. et al. - Observations of changes in acoustic emission parameters for varying corrosion defect in reciprocating compressor valves - DOI:10. 10.1016/j.asej.2019.01.003.

[8] Caro. - Czym są badania nieniszczące: metody, zastosowania i korzyści - https://richconn.com/pl/what-is-non-destructive-testing/.

[9] Xie J. et al. - Regular Detection and Intelligent Monitoring Technology of Atmospheric Storage Tank Based on Acoustic Emission and Internet of Things – DOI:10.58286/30795.

[10] Baensch F. et al. - Damage evolution detection in a pipeline segment under bending by means of acoustic emission - DOI.org/10.1016/j.ijpvp.2022.104863.

[11] Baensch F. et al. - Non-threshold acoustic emission analysis of damage evolution in pipe segments of steel S355J2H under bending load – EWGAE European Conference on Acoustic Emission Testing - Bundesanstalt für Materialforschung und Prüfung (BAM) http://www.ndt.net/?id=23599.

[12] He S. et al.- Fatigue crack extension and acoustic emission response law of 316L austenitic stainless steel by hydrogen charging - DOI:10.1016/j.tafmec.2025.104983.

[13] Reed N. et al. - Passive wall thickness monitoring using acoustic emission excitation DOI:10.1016/j.ndteint.2024.103241.

[14] Rahimi S. et al. - Coupled slow strain rate and acoustic emission tests for gaseous hydrogen embrittlement assessment of API X65 pipeline steel - DOI:10.1016/j.matlet.2024.136598.

[15] Świt G. et al. - Experimental numerical analysis of the fracture process in smooth and notched V specimens - DOI:10.30657/pea.2023.29.49.

[16] Świt g. et al. - Innovative acoustic emission method for monitoring the quality and integrity of ferritic steel gas pipelines - DOI:10.30657/pea.2024.30.22.

[17] Świt G. et al. - Identification of the Fracture Process in Gas Pipeline Steel Based on the Analysis of AE Signals - DOI:10.3390/ma15072659.

[18] Roberts T.M. et al. - Acoustic emission monitoring of fatigue crack propagation - DOI:10.1016/S0143-974X(02)00064-0.

[19] Han Z. et al. - Acoustic emission during fatigue crack propagation in a micro-alloyed steel and welds - DOI:10.1016/j.msea.2011.06.065.

The research leading to these results has received funding from Horizon 2020, the European Union's Framework Programme for Research and Innovation (H2020) under grant agreement n° 101111888.

[20] Mazal P. et al. - Use of acoustic emission method for identification of fatigue micro-cracks creation - DOI:10.1016/j.proeng.2015.12.667.

[21] Chuluunbat T. et al. - Investigation of X70 line pipe steel fracture during single edge-notched tensile testing using acoustic emission monitoring - DOI:10.1016/j.msea.2015.06.030.

[22] Merson E. et al. - Application of acoustic emission method for investigation of hydrogen embrittlement mechanism in the low-carbon steel - DOI:10.1016/j.jallcom.2014.12.083.

[23] Nohal L. et al. - Acoustic Emission Response to Erosion-Corrosion and Creep Damage in Pipeline System - DOI:10.1016/j.prostr.2020.01.091.

[24] Speir Hunter information brochure, en-SPH-brochure-2024-3.

[25] Magnetyzm w służbie gazowników. (n.d.). Wirtualne Muzeum Gazownictwa. https://wmgaz.pl/gazownictwo-dzis-i-jutro/artykul/magnetyzm-w-sluzbie-gazownikow.

[26] PN-ISO-24497-3_2009P:1-3 Non Destructive Testing Metal Magnetic Memory method.

[27] Pospisil, K.; Manychova, M.; Stryk, J.; Korenska, M.; Matula, R.; Svoboda, V. Diagnostics of Reinforcement Conditions in Concrete Structures by GPR, Impact-Echo Method and Metal Magnetic Memory Method. *Remote Sens.* 2021, *13*, 952. https://doi.org/10.3390/rs13050952.

[28] P. Paszylk; Gazociągi nietłokowalne – poszukiwanie najlepszej metody inspekcji; Nafta-Gaz; s. 545–550; 2016; DOI: 10.18668/NG.2016.07.08.

[29] A. Dubov; A. Dubov; Magnetometric Diagnostics of Gas and Oil Pipelines. Energodiagnostika Co. Ltd. Accessed January 16, 2026.

[30] A. Nowakowski and P. Paszylk, "Metal Magnetic Memory method used for analyzing high-pressure gas pipelines," AGH Drilling, Oil, Gas, vol. 32, no. 2, pp. 395–404, 2015.

[31] Wiadomości Naftowe i Gazownicze, [Online]: https://www.sitpnig.pl/_files/ugd/b2bf16_4a22ba36fc6b4ea381a67e93de7369af.pdf.

[32] Z. Masilela, J. Pereira, Using the direct current voltage gradient technology as a quality control tool during construction of new pipelines, Engineering Failure Analysis, Volume 5, 1998, Pages 99-104.

[33] "Essential Features of Implementing A DCVG (Direct Current Voltage Gradient) Survey," Velosi AIMS, Jan. 20, 2023. [Online]. Available: https://velosiaims.com/essential-features-of-implementing-a-dcvg-direct-current-voltage-gradient-survey/.

[34] R. Lindley and K. Lax, "Above Ground Data Collection and Evaluation for Pipeline Rehabilitation," Corroconsult UK Limited, Dec. 13, 2017. [Online]. Available: https://www.corroconsult.com/blog-news/above-ground-data-collection-and-evaluation-for-pipeline-rehabilitation.

[35] Rzydzik S.; System iDiaGaSys do okresowego monitorowania wycieków metanu z gazociągów na podstawie lotniczych danych obrazowych. Department of Fundamentals of Machinery Design 2025.

[36] Rzydzik S.; Timofiejczuk A.; Rozwój systemu monitorowania stanu gazociągów przesyłowych i ich otoczenia.

[37] Kastek M.; Ligienza A.; Sosnowski T.; Holewa-Rataj J.; Rataj M.; Timofiejczuk A.; Rzydzik S.; Remote detection and quantification of methane emissions based on hyperspectral data analysis. Pomiary Automatyka Robotyka 2023, 3.

[38] Internal Report on the Development of the Idiagasys System.

[39] MACAW Engineering Ltd, MACAW's Encyclopedia of Pipeline Defects, Second Edition, 2014, s. 18.

[40] https://www.corrosionalliance.com/coat/most-important-methods-to-measure-external-coating-defects-on-pipelines-without-excavation.

The research leading to these results has received funding from Horizon 2020, the European Union's Framework Programme for Research and Innovation (H2020) under grant agreement n° 101111888.

[41] Nicholson J. P., “Combined Close Interval Potential Surveys and Direct Current Voltage Surveys for Increased Pipeline Integrity.” [Online] Available: https://www.cathodicprotectiondcvginstruments.com/wp-content/uploads/2016/11/Paper-9145-Eurocorr-2010.pdf.

[42] Z. Anes-Arteche, K. Yu, U. Bharadwaj, C. Lee, B. Wang, “Challenges in the application of DCVG-survey to predict coating defect size on pipelines.” [Online] Available: https://bura.brunel.ac.uk/bitstream/2438/13586/1/Fulltext.pdf.

[43] POF520 In-line inspection tool readiness for hydrogen pipelines, white paper 2024, www.pipelineoperators.org.

The research leading to these results has received funding from Horizon 2020, the European Union's Framework Programme for Research and Innovation (H2020) under grant agreement n° 101111888.